MULTISENSOR FUSION OF GROUND-BASED AND AIRBORNE REMOTE SENSING DATA FOR CROP CONDITION ASSESSMENT

A Dissertation

by

HUIHUI ZHANG

Submitted to the Office of Graduate Studies of
Texas A&M University
in partial fulfillment of the requirements for the degree of

DOCTOR OF PHILOSOPHY

December 2010

Major Subject: Biological and Agricultural Engineering

Multisensor Fusion of Ground-based and Airborne Remote Sensing Data for Crop Condition Assessment

MULTISENSOR FUSION OF GROUND-BASED AND AIRBORNE REMOTE SENSING DATA FOR CROP CONDITION ASSESSMENT

A Dissertation

by

HUIHUI ZHANG

Submitted to the Office of Graduate Studies of
Texas A&M University
in partial fulfillment of the requirements for the degree of

DOCTOR OF PHILOSOPHY

Approved by:

Co-Chairs of Committee,	Ronald Lacey
	Yubin Lan
Committee Members,	Dirk Hays
	Clint Hoffmann
	Sorin Popescu
Head of Department,	Stephen Searcy

December 2010

Major Subject: Biological and Agricultural Engineering

ABSTRACT

Multisensor Fusion of Ground-based and Airborne Remote Sensing Data for Crop Condition Assessment. (December 2010)

Huihui Zhang, B.S., Tongji University, Shanghai;

M.S., San Francisco State University

Co-Chairs of Advisory Committee: Dr. Ronald Lacey
Dr. Yubin Lan

In this study, the performances of the optical sensors and instruments carried on both ground-based and airborne platforms were evaluated for monitoring crop growing status, detecting the vegetation response to aerial applied herbicides, and identifying crop nitrogen status. Geostatistical analysis on remotely sensed data was conducted to investigate spatial structure of crop canopy normalized difference vegetation index and multispectral imagery.

A computerized crop monitoring system was developed that combined sensors and instruments that measured crop structure and spectral data with a global positioning system. The integrated crop monitoring system was able to collect real-time, multi-source, multi-form, and crop related data simultaneously as the tractor-mounted system moved through the field.

This study firstly used remotely sensed data to evaluate glyphosate efficacy on weeds applied with conventional and emerging aerial spray nozzles. A weedy field was

set up in three blocks and four aerial spray technology treatments were tested. Spectral reflectance measurements were taken using ground-based sensors from all the plots at 1, 8, and 17 days after treatment. The results indicated that the differences among the treatments could be detected with spectral data. This study could provide applicators with guidance equipment configurations that can result in herbicide savings and optimized applications in other crops.

The main focus of this research was to apply sensor fusion technology to ground-based and airborne imagery data. Experimental plots cropped with cotton and soybean plants were set up with different nitrogen application rates. The multispectral imagery was acquired by an airborne imaging system over crop field; at the same period, leaf chlorophyll content and spectral reflectance measurements were gathered with chlorophyll meter and spectroradiometer at canopy level on the ground, respectively. Statistical analyses were applied on the data from individual sensor for discrimination with respect to the nitrogen treatment levels. Multisensor data fusion was performed at data level. The results showed that the data fusion of airborne imagery with ground-based data were capable of improving the performance of remote sensing data on detection of crop nitrogen status. The method may be extended to other types of data, and data fusion can be performed at feature or decision level.

ACKNOWLEDGEMENTS

Mine has been an exceptional journey that I had never dreamed of. It is not possible to have my research career without Dr. Yubin Lan and Dr. Ronald Lacey. I would like to express my deepest gratitude to Dr. Lan for his trust, encouragement and precious guidance throughout my Ph.D. study. There is no part of this work that has not been object of his penetrating mind. From the bottom of my heart, I thank him for the influence upon my thinking and my future career that he had made. I also would like to give my sincere gratitude to Dr. Lacey for his academic, professional, and financial support. What I have learned from him made me a good researcher with passion, discipline, self-confidence, and persistence.

I would like to say special thanks to Dr. Clint Hoffmann, for his strong support in every project. I would also like to say thanks to Dr. Dirk Hays and Dr. Sorin Popescu for teaching me valuable lessons about academia and professionalism. I have been so fortunate to have all of them in my graduate committee.

I want to extend my deepest gratitude to Shirley, for her care in any respect of my life. She deserves a “Thank-you” more than anyone else. Thanks also go to Hang and Ningye for accompanying me throughout these years. They are my sister and brother, as much as friends. Thanks Meiping and Adam for all the good time I spent with them. Thanks to Yufeng, Kaiguang and Tony for helping me work out my problems during the difficult period of the study.

Many thanks also go to Dr. John Westbrook for his generous and professional feedback on all my manuscripts; Dr. Charles Suh for his financial support; Dr. Daniel Martin, Dr. Lori Henze, Dr. Chenghai Yang, Jank Phil, Mike O'Neil, Charlie Harris, Lee Denham, Ritchie Eyster, Mann Robin, and Ester Wilson, for their help. Thanks also go to Sonya, Paula, and all the other department faculty and staff for making my time at Texas A&M University a great experience.

I would like to express my appreciation to my dear parents for their consistent love, education, understanding, unconditional support, and sacrifices throughout my life. I would like to thank my grandmother and all my relatives in China for their support. I also would like to say thanks to my husband for his love and patience. And last, I want to give my deepest regrets to my dear son for not being able to take a good care of him since I started to make the dream become true. I cannot imagine that I could have completed this work without any happiness he made me feel.

TABLE OF CONTENTS

CHAPTER Page

CHAPTER Page

LIST OF FIGURES

Page

Page

Page

Page

LIST OF TABLES

Page

CHAPTER I

GENERAL INTRODUCTION

STATEMENT OF PROBLEMS

With an increasing population and a commensurate need for increasing agricultural production, there is an urgent need to improve management of agricultural resources. In traditional crop field management, uniform input application not only does not consider the concept of spatial and temporal variability within a crop field, but also results in environmental pollution and reduction of farm profits. The need of site-specific management (SSM) or precision agriculture (PA) has been noticed by researchers, producers and farmers in the worldwide since the early 1990s. Advanced information technology that can provide quick and cost-effective ways to identify spatial variability within crop fields is the basis of precision agriculture.

Remote sensing technologies have advanced rapidly in recent years and have become effective tools for site-specific management in crop protection and production. In agricultural applications, remote sensing has been conducted from different platform, e.g. ground-based, airborne and space, to obtain spectral information on crop field. Remotely sensed data measured by various types of optical sensors characterize spectral

---

This dissertation follows the style of *Transactions of the American Society of Agricultural and Biological Engineers*.

properties of crop canopy and provide a non-destructive measurement of crop growth status. Crop is the best sensor of its own environment (Legg and Stafford, 1998). Spectral reflectance properties of crop canopy based on the absorption of light at specific wavelengths are associated with specific plant characteristics. For health crops, spectral reflectance in the visible region of the spectrum (400-700 nm) is low because of the high absorption of light energy by chlorophyll. In contrast, reflectance in the near infrared (NIR) region of the spectrum (700-1300 nm) is high because of the multiple scattering of light by different leaf tissues (Taiz and Zeiger, 2006). Extensive studies have successfully suggested that crop spectral reflectance could be used to detect environmental stress, assess plant nutrient status, estimate plant physiological and biophysical variables, monitor plant growth status and conditions, and predict crop yields, and so on.

Many optical sensors or instruments are commercial available and suitable for ground-based measurements. For example, Greenseeker® (NTech Industries, Inc., Ukiah, CA) sensor may be mounted on a tractor to map normalized difference vegetation index (NDVI) from crop canopy; an ultrasonic sensor may be mounted on a mobile vehicle to measure crop height. One may hold a chlorophyll meter to measure leaf chlorophyll content and canopy analyzer for leaf area index. Although these ground-based sensors or instruments are flexible to use and with limit effects by atmospheric and environmental factors, it is quite time-consuming to use them in large fields. It is also labor intensive if one wants to get two or more types of data simultaneously. New approaches are needed to rapidly detect, record, and process multiple forms of real time crop-related data for

use in precision agriculture. It is necessary to use sensors or instruments that can measure crop physical structure and spectral reflectance at the same time.

Agricultural aircraft offer a different view of remote sensing. Airborne remote sensing technologies have made tremendous improvement and been used in precision agricultural application (Boegh et al., 2002; Lan et al., 2007a and b; Huang et al., 2008; Huang et al., 2009; Lan et al., 2009a). Multispectral cameras typically capture imagery that can be related to relative radiance in the visible and NIR regions. Multispectral data comprise a set of optimally chosen spectral wavebands that are not contiguous. Airborne multispectral techniques are much less expensive and less data-intensive than hyerspectral imaging systems and can rapidly provide continuously remotely sensed data over a large field or region. However, all remote sensing measurements can be affected by variable ground conditions, such as plant architecture, canopy characteristics, crop row orientation and coverage, and background soil properties. Relatively low spectral resolution will limit the ability of the multispectral imagery for mapping crop conditions.

The concept of multisensor data fusion was first developed by Department of Defense (DoD) (Klein, 2004) and have been gained more attention in non-military area. In general, multisensor data fusion techniques try to combine data from multiple sensors to make better interferences, such as lower error rate or less uncertainty, regarding a physical entity, event and situation than that using individual sensor alone. In precision agricultural practice, only a few studies have investigated with multisensor data fusion. If the advantages of multisensor data fusion techniques can be realized, the efficiency of the use of remotely sensed data will be improved dramatically.

MULTISENSOR DATA FUSION OVERVIEW

Multisensor data fusion has been developed to solve a diverse set of problem having common characteristics in the past two decades. Multisensor data fusion look for a combination of data from multiple sensors or sources to perform interference that may not be possible or may not be good from a single sensor or source itself (Hall and Llinas, 1997; Hall and McMullen, 2004). Multisensor fusion techniques were firstly applied and studied in military area such as target recognition. With the advances in sensing and computing, multisensor data fusion has been widespread in not only military but also nonmilitary applications, for example, disease diagnosis in medical care, product quality evaluation, and remote sensing.

Multisensor data fusion in remote sensing includes the determination of composition of land cover, forest inventory, the location of mineral resources, climate change, and so on. Data from different sensors may include the bright values of image pixels, coordinates and elevation of locations, spectral data, LiDAR, Radar, Sona data, and so forth. In principle, fusion of multisensor data provides significant advantages over a single data source. However, there are still risks in practical application. Data fusion may bring even worse results than that obtained by a single most appropriate sensor, for instance, one attempts to combine accurate data with biased data. Therefore, fundamental issues to be addressed in building a data fusion system for a particular application include (Hall and Llinas, 1997):

1. What algorithm or techniques are appropriate and optimal?
2. What architecture should be used?

3. How should the individual sensor data be processed to extract the maximum amount of information?
4. What accuracy can be achieved by a data fusion process?
5. How does the data collection environmental affect the processing?

Data Fusion Process Model

The Joint Directors of Laboratories (JDL) Data Fusion Working Group, established in 1986, made big efforts to create a process model for data fusion. The top level of JDL data fusion process model is shown in Figure 1.1 which is adapted from Hall and Llinas (1997). At the top level of this model with a two-layer hierarchy, the data fusion process is summarized by source of information, human computer interaction, source preprocessing, Level 1 processing, Level 2 processing, Level 3 processing, and level 4 processing. Each of these is summarized below:

Sources of Information: A number of sources of information may be available as inputs including sensors or other reference information, e.g., geographical information.

Human Computer Interaction (HCI): Communicates with human input.

Source Preprocessing (Level 0 Processing): Allocates data to appropriate process and force the data fusion process to concentrate on the data most pertinent to the current situation.

Level 1 Processing (Object Refinement): Achieves refinement of individual objects by combining locational, parametric and identity information of each sensor.

Level 2 Processing (Situation Refinement): Develops a situation refinement among objects in the context of their environment.

Level 3 Processing (Threat Refinement): Draws inferences about threats, opportunities of operation by apply the current situation into the future.

Level 4 Processing (Process Refinement): Assesses, refines, modify and improve the performance of data fusion.

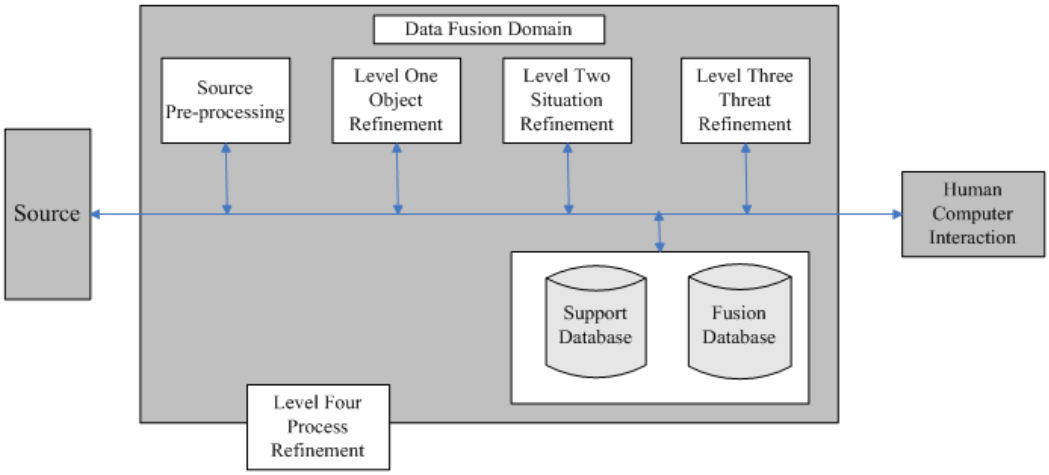

Figure 1.1. Data fusion process model (Adapted from Hall and Llinas, 1997).

Architecture for Multisensor Data Fusion

Depending on where the data fusion is happened in the data flow, for identity fusion in Level 1, there are several types of architectures can be used. Figure 1.2 shows the architecture which performs data level fusion. It combines raw data from different sensors. Subsequently, an identity declaration process is carried out by extracting a feature vector from the fused raw data and making a transformation between the feature vector and a declaration of identity. Bear in mind, the original sensor data must be commensurate in order to fuse the raw data. The advantage of raw data identity fusion

provides the most accurate results with proper sensor association and alignment. Methods for this level of fusion include neural networks, discriminant analysis, and cluster algorithm.

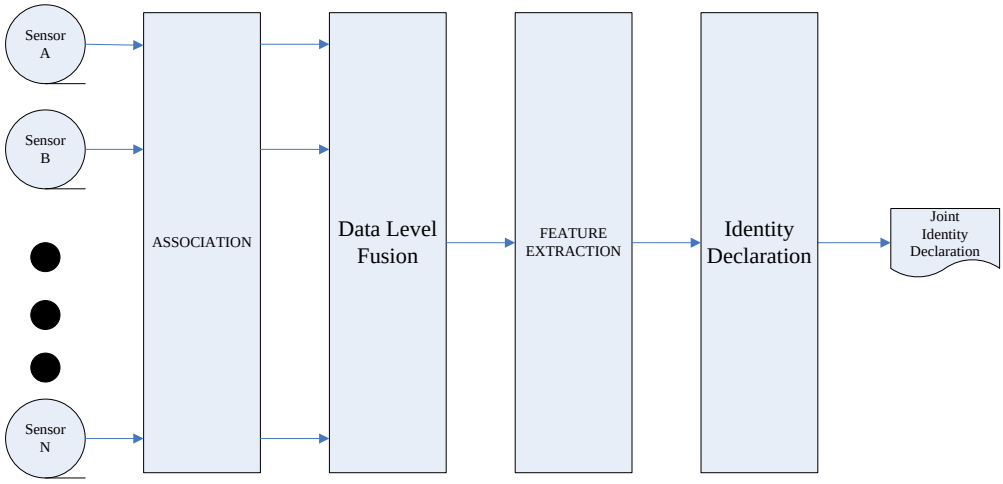

Figure 1.2. Raw data level data fusion (Adapted from Hall and Llinas, 1997).

The second architecture for identity fusion is feature level (Figure 1.3). At first, feature vectors are extracted from individual sensor. Then these feature vectors are concatenated into a single feature vector as an input into identity declaration process. Methods in this level include neural networks, and cluster algorithm.

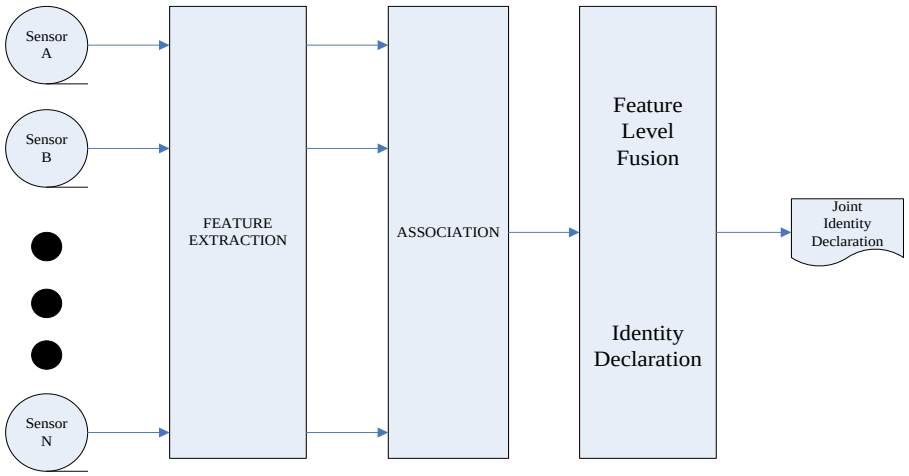

Figure 1.3. Feature level data fusion (Adapted from Hall and Llinas, 1997).

The third architecture is decision level fusion (Figure 1.4). Each sensor makes its identity declaration based on its own data source. The identity declarations made by the individual sensors then are fused by using decision level fusion techniques such as Bayesian inference.

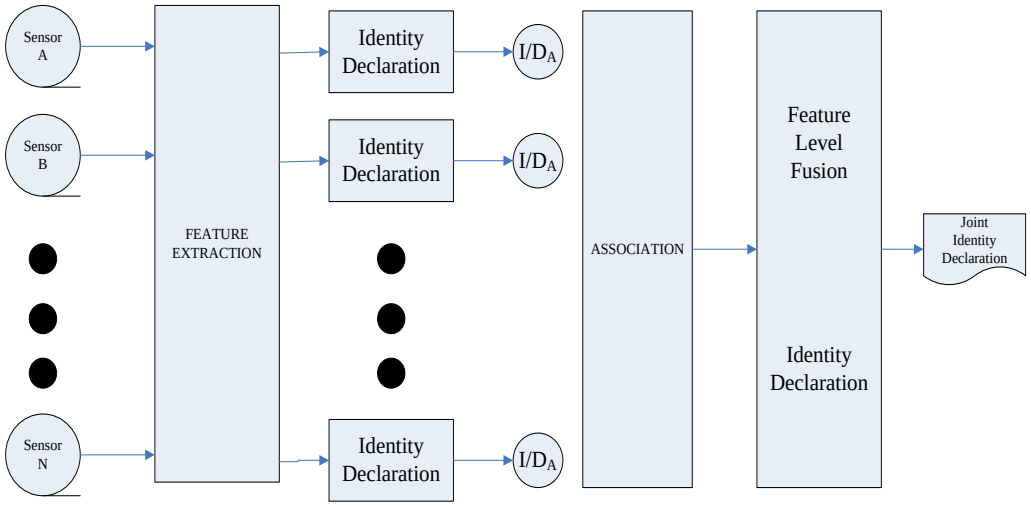

Figure 1.4. Decision level data fusion (Adapted from Hall and Llinas, 1997).

There is no universal architecture for all situations. One should select an architecture based on the capabilities of sensors, desired accuracy and available funding, etc.

OBJECTIVES OF THIS RESEARCH

Nowak (1997) distinguished ‘soft’ and ‘hard’ technologies in SSM. ‘Soft’ technologies rely more on traditional means and farmers’ experiences to acquire field information; while ‘hard’ technologies for data acquisition include remote sensing and for management include the use of statistical analysis (Plant, 2001). Whether collected from airborne multispectral imaging systems, ground-based sensors and instrumentation systems, human observations, or laboratory samples, remotely sensed data must be analyzed properly to understand cause-and-effect relationships. Multisensor data can be integrated by classical statistical methods and spatial statistics. Typically, spatial statistics may be used for analysis of data having spatial component. Many factors can contribute towards spatial variability within the field and between fields. Data from imagery, ground-based measurements, and spatial analysis together allow for a more complete understanding of a field’s spatial complexity. Farmers are able to use these data and derived information to assess the growth stage and health status of their crops and make timely crop management decisions.

This study was investigating remote sensing technologies for agricultural applications from both ground-based and airborne platforms. The specific objectives of this research were to: 1) develop a computerized crop monitoring system that combines data from a global positioning system with other instruments to measure crop condition;

2) characterize spectral properties of various crop varieties at their different growth stages; 3) use remotely sensed data to evaluate efficacy of herbicide treatments with different aerial application technologies; 4) perform geostatistical analysis on remotely sensed data; 5) investigate the potential of multisensor data fusion of ground-based and airborne imagery data for detection of crop nitrogen stress.

STRUCTURE OF THIS DISSERTATION

This dissertation includes six individual studies which are stand-along and solve different problems. Chapter II to Chapter VII was six manuscripts.

In Chapter II, a ground-based integrated sensor and instrumentation system to monitor crop condition was developed and tested in crop field. The performance of the system and repeatability of the measurements were investigated.

In Chapter III, spectral properties of four agricultural crops were characterized by hyperspectral data at their different growth stages. The ability of hyperspectral data to separate crop types was verified and the significant wavelengths for discriminant analysis were determined.

In Chapter IV, remotely sensed data was used to evaluate efficacy of herbicide treatments with different aerial application technologies.

In Chapter V, the spatial structure of canopy NDVI within a small field with different sampling density was investigated using variogram analysis.

In Chapter VI, variogram plays a crucial role in remote sensing application and geostatistics. A study was conducted to determine the changes of variograms which were calculated with various sample sizes from a multispectral image.

In Chapter VII, multisensor fusion was applied on SPAD chlorophyll readings, hyperspectral measurements and airborne imagery in the detection of nitrogen status on crop canopy.

In Chapter VIII, conclusions and summary are made.

CHAPTER II

DEVELOPMENT OF AN INTEGRATED SENSOR AND INSTRUMENTATION SYSTEM FOR MEASURING CROP CONDITION*

OVERVIEW

The study considers the possibility of gathering spectral information by various sensors simultaneously at field level to evaluate crop growth status. A ground-based integrated sensor and instrumentation system was developed to measure real-time crop conditions including normalized difference vegetation index (NDVI), crop canopy structure, and crop height. The integration system consists of a NDVI sensor, a spectroradiometer, a crop canopy analyzer for leaf area index, a crop height sensor, a multispectral camera, and a DGPS receiver to geo-reference data collected while the tractor which sensors were mounted was driven through the field. During the 2008 growing season, field tests were conducted twice to evaluate the performance of the proposed sensing system on collecting crop-related data from cotton and soybean that

---

*Reprinted with permission from "Development of an integrated sensor and instrumentation system for measuring crop condition" by Y. Lan, H. Zhang, R. Lacey, W. C. Hoffmann, W. Wu, 2009. Agricultural Engineering International: The CIGR Ejournal. Manuscript IT 08 1115.Vol XI, Copyright [2010] by CIGR.

were under normal growing process. Two rows were chosen within each field. Measurements repeatability was investigated by driving through the same row three times. Two runs were in the same direction, and the other was in the reverse direction. The results show that the integration sensor and instrumentation system supports multi-source information acquisition at field level. Spectral information, NDVI and spectral reflectance measurements, images, and crop height were able to be obtained by the proposed sensing system simultaneously from crop canopy with better measurement repeatability.

INTRODUCTION

Accurate and reliable information technology is the basis of precision agriculture. Remote sensing has been widely used to obtain and map temporal and spatial variability of crops in fields. Information on crop condition can be used to assess and monitor crop growth status, predict crop yield, or develop program for optimizing application of nitrogen fertilizer, fungicide, growth regulator, and other chemical inputs in order to reduce the impact on environment.

Successful information acquisition is relied on the ability of sensor and instrument in detecting crop canopy variables, which are indicative of crop growth (Goel et al. 2003b). The normalized difference vegetative index (NDVI) is a commonly used measurement of crop health in agricultural applications. NDVI is calculated as: NDVI= (NIR – Red)/ (NIR + Red), where NIR and Red represent the reflectance values at the near infrared (NIR) and red regions of the spectrum, respectively. Healthier crop canopy will absorb more red and reflect more NIR light, and consequently has a higher NDVI

value. Jones et al. (2007a) used GreenSeeker® sensor (NTech Industries, Inc., CA.) to measure NDVI and there was strong correlation between NDVI and chlorophyll content per plant of spinach ($R^2 = 0.91$). NDVI was also found to be closely correlated with leaf area index (Bechtel et al., 1997; Aparicio et al., 2002; Leon et al., 2003). Leaf area index (LAI) is an important structural property of crop canopy. LAI is defined as the ratio of total upper leaf surface of vegetation divided by the surface area of the land on which the vegetation grows. High correlations were found between reflectance factor and LAI and biomass by Ahlrichs et al. (1983).

Many researchers have used spectral reflectance techniques for monitoring nitrogen and chlorophyll status in different crops (Haboudane et al., 2002; Tumbo et al, 2002; Goel et al., 2003a; Xue et al., 2004; El-Shikha et al., 2007; Jones et al., 2007a). Strong correlations between the spectral data from crops and various characteristics of crops have been elucidated in numerous studies (Yoder et al., 1995; Serrano et al., 2000; Goel et al., 2003b; Lee et al., 2004). Laudien et al. (2003) explained the contrast between healthy and diseased sugar beets by using a hyperspectral radiometer. Thenkabail et al. (2000) used a hand held spectral radiometer to obtain the correlation between spectral observations with crop parameters of cotton.

Darvishzadeh et al. (2008) examined the utility of hyperspectral remote sensing in predicting canopy characteristics by using a spectral radiometer. Among the various investigated models, they found that canopy chlorophyll content was estimated with the highest accuracy. Some studies used multispectral image senor system to measure crop canopy characteristics. Jones et al. (2007b) estimated biomass based on multispectral

images taken by a Duncan Tech MS 3100 multispectral camera (Auburnm Cal.). Inoue et al. (2000) successfully estimated LAI and biomass for soybean and rice by using a dirigible-mounted camera. Ultrasonic sensing technology is good for non-destructive crop canopy characterization. Kataoka et al. (2002) in Japan showed that ultrasonic sensors performed well for measuring the height of soybean and corn crops.

Many remote sensing technologies have been conducted to obtain information from different platforms, such as ground-based, airborne and space. For truth measurement, ease of availability and cost-effective, ground-based methods have been widely developed and used. Tumbo et al. (2002) constructed the on–the–go system for sensing chlorophyll status in corn. A tractor traveled at 0.6 km h^{-1} and carried with a dual fiber–optic spectrometer, an analog-to-digital (A/D) converter, a fiber–optic sensing probe, a sensing probe holder, and a computer. The fiber–optic spectrometry was used to acquire spectral response patterns. A neural network model incorporated into the mobile system showed good correlation between predicted SPAD chlorophyll readings and actual chlorophyll readings (R^2 = 0.85, RMSE = 1.82 SPAD units). Scotford et al. (2004) in European used a tractor–mounted radiometer system in parallel with an ultrasonic sensor to obtain information about crop cover and the structure of the crop canopy. The radiometer system used two radiometers. One was mounted pointing upwards to measure incoming radiation while the other pointed downwards to measure the reflectance light from the crop canopy. Reyniers et al. (2006) compared an aerial image with a measuring device on the ground platform to predict yield of winter wheat. A multi-spectral radiometer was mounted on the end of the boom on a tractor. NDVI of the

ground system was better related to yield variables at harvest compared to NDVI of the aerial system.

The data acquisition methods and information resources used in previous studies were limited. Considering precision agricultural practice, it is necessary to acquire multi-source information on crop rapidly while save the related costs. The use of a number of sensing techniques working in combination could provide a better characterization of crop canopy (Scotford et al., 2003). New approaches are needed to rapidly gather, record, and process multiple forms of crop-related data at field level.

As a preliminary study on developing a ground-based multi-source crop-related information system to map crop vigor at field level, the particular aim of this work presented here was to investigate how to properly integrate sensor and instrument, and assess the performance of the system in monitoring crop condition.

SYSTEM DESCRIPTION

Integration System

The proposed ground-based multi-source information system consists of crop height sensor, crop canopy analyzer for leaf area index, NDVI sensor, multispectral camera, and a spectroradiometer (Figure 2.1). The system was interfaced with a DGPS receiver (Thales Navigation, Santa Clara, CA) to provide spatial coordinates for measurements taken by the spectroradiometer. The goal was to collect and contrast multi-sensor data and store in spatial information and crop property information database. The components and how they were integrated are described in the following section.

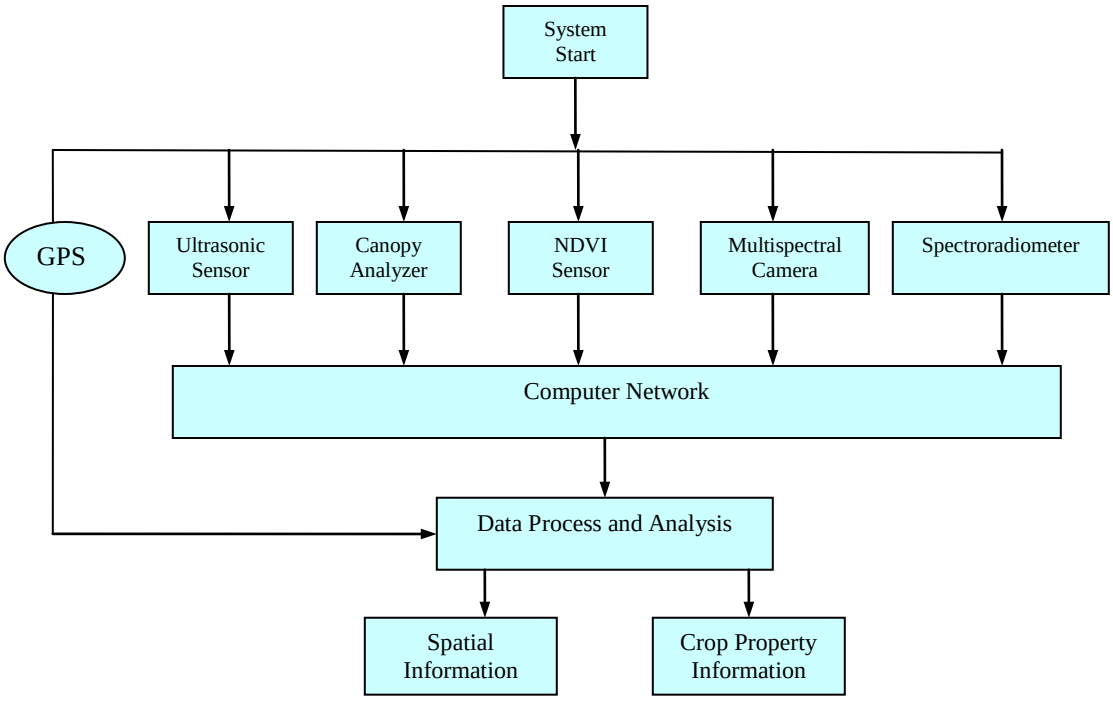

Figure 2.1. The schematic diagram: ultrasonic senor, canopy analyzer, NDVI sensor, multispectral camera and spectroradiometer.

NDVI Sensor

NDVI is a good estimate of biomass and nitrogen content in many crops. The NDVI sensor used in the system is GreenSeeker® Hand-held Data Collection and Mapping Unit Model 505 (NTech Industries, Inc., Ukiah, Cal.) (Figure 2.2).

GreenSeeker is equipped with a sensor, control box, pocket PC, and specific software for data collection. The sensor is adjustable in 15 degree increments and mounted on an adjusted-length pole to set the sensor parallel to the target canopy. The control box supplies power to the sensor and external connectors. The sensor is an active sensor, which uses light emitting diodes to generate its own red (660 ± 15 nm) and NIR

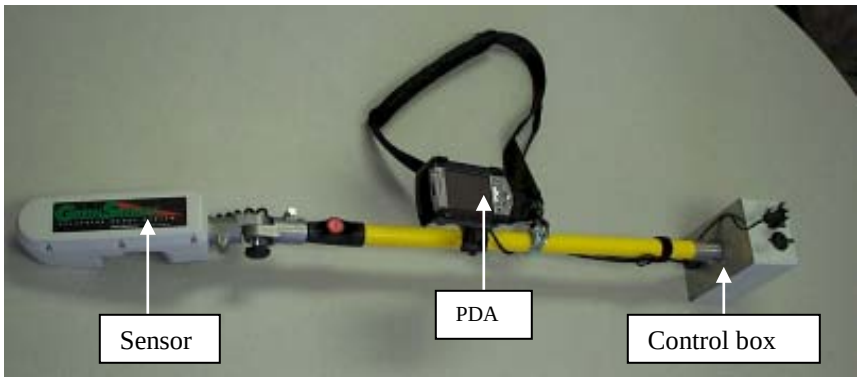

Figure 2.2. GreenSeeker hand-held data collection and mapping unit.

(770 ± 15 nm) lights. As the sensor is passed over crop surface, it measures incident and reflected light from canopy and outputs both NDVI and Red to NIR ratio. The output rate is about 10 readings per second. The illuminated area is 60 by 1 cm, with the long dimension positioned perpendicular to the direction of travel. The distance between the sensor and target can be 60 to 120 cm and NDVI readings are not affected by height variance.

LAI Canopy Analyzer

Leaf area index is a primary variable for crop monitoring. Instead of the traditional, direct and labor-consuming method in the past, the optical instrument, SunScan canopy analysis system (Delta-T, Inc.) is used. The instrument is indirectly measuring leaf area index by measuring the ratio of transmitted radiation through canopy to incident radiation. It is configured with SunScan probe, data collection terminal, and beam fraction sensor. Figure 2.3 shows SunScan probe and its data collection terminal.

Figure 2.3. SunScan canopy analyzer.

The SunScan probe has an array of 64 photosynthetic active radiation (PAR) sensors embedded in a 1 m long probe, and may be connected via an RS-232 cable to the data collection terminal or a laptop for data collection and storage. The portable and weatherproof instrument can be used in most light conditions. When a reading is taken, all sensors are scanned and the measurements transmitted to data storage unit. The average light level along the probe is calculated and canopy leaf area index is estimated. All of the individual sensor readings are available if required for detailed PAR mapping.

Spectroradiometer

Spectroradiometers can be used to quickly measure light energy over a range of wavelengths and provide spectral reflectance or transmittance information on crop canopy. FieldSpec® Handheld, a portable field spectroradiometer (FieldSpec®, Analytical Spectral Devices, Inc.) (Figure 2.4), was used in the system.

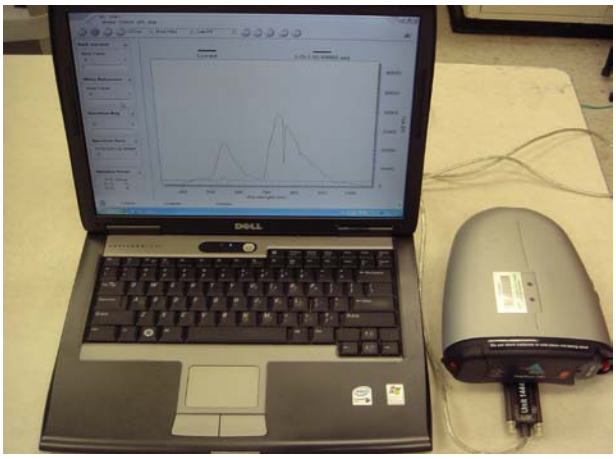

Figure 2.4. FieldSpec spectroradiometer connected to a laptop via a RS232 to USB cable.

The spectroradiometer arrives with manufacturer pre-calibrated and ready to be used. It has a 512-channel detector array and capable of measuring radiance from 325 to 1075 nm wavelengths with a sampling interval of 1.6 nm of the spectrum. The field of view of the instrument is about 25º. The reflectance of light from crop canopy is collected by the spectroradiometer and data is sent to a portable personal computer via a RS232 to USB cable. Instantaneous graphs of spectral signature are displayed. To decrease the signal to noise ratio and increase the overall accuracy, integration time needs to be changed as light conditions change, while the dark current scan is automatically taken when every reflectance scan is taken. In addition, before taking the reflectance data, it should be calibrated by taking a white reference from a white reference panel.

Multispectral Camera

The multispectral camera was a single sensor agriculture digital camera (ADC) (Teracam, Inc.) as shown in Figure 2.5. The simple and low-cost ADC camera has a resolution of 2048 × 1536 pixels per frame and able to measure visible light wavelengths longer than 520 nm and NIR wavelengths up to 920 nm. The camera is equipped with a 4.5 to 10 mm CS mount vari-focus lens. Focusing can be carried out automatically or manually. Images are stored in Teracam DCM loseless format. These DCM files are grayscale images displaying “raw” pixel values. PixelWrench2, an image editing program working with ADC camera, provides full access and control of the camera.

Figure 2.5. Multispectral ADC camera.

Ultrasonic Sensor

An ultrasonic sensor is inexpensive and accurate for detecting objects. An ultrasonic sensor can generate high frequency sound waves. When the waves strike and

bounce off an object, the sensor receives and evaluates the echo. The sensor then determines its distance from the object based on the time interval between sending the signal and receiving the echo.

Two ultrasonic sensors were tested for this system. One was a commercial ultrasonic sensor (Honeywell, Inc., NJ) (Figure 2.6 a). The sensing distance is from 20 to 200 cm. The software for automatic data acquisition from the ultrasonic sensor was programmed in Labview 8.5 (National Instruments, 2007). The other was named U.S. Distance sensor and developed by Department of Biosystems Engineering, University of Tennessee (Figure 2.6 b). It is connected to laptop with RS232 cable and communicates by hyper terminal. The operation range is from 5 to 150 cm. Both ultrasonic sensors were operated with 12 voltages DC.

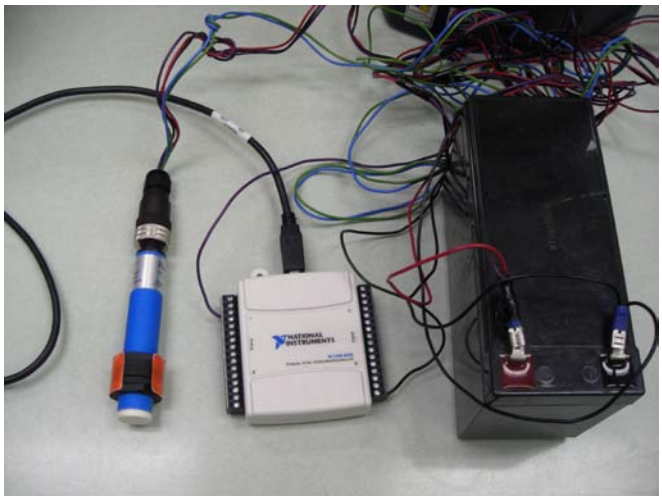

(a)

Figure 2.6. Ultrasonic sensors (a) Honeywell sensor, data logger and battery (from left to right); (b) U.S. distance sensor.

(b)

Figure 2.6. Continued.

SYSTEM REALIZATION AND DISCUSSION

Integration System Construction

System tests were conducted at the Texas A&M AgriLife Research Farm (30°31'19"N, 96°23'52"W) in College Station, Texas during the 2008 growing season. Cotton and soybean plants were grown in the field. Two sunny days was selected for field tests. Greenseeker, FieldSpec, SunScan canopy analyzer, ADC camera and the ultrasonic sensors were tested and calibrated in the lab before field tests. All the data were gathered around noon time.

The first test was on May and crops at their vegetative growth stage of development. The sensors and instruments were mounted on a metal frame that allows the distance between sensors and plants to be adjusted. The metal frame was mounted in

front of the tractor. The width of the frame could be adjusted according to the row space. Figure 2.7 shows how the system was integrated for the test in May.

Figure 2.7. The integration system construction in the first field test in May 2008.

Greenseeker and the commercial ultrasonic sensor were mounted on the right hand side of the travel direction (they measured the same row); FieldSpec, Sunscan and the U.S. Distance ultrasonic sensor were mounted on the left hand side of the travel direction. The height of Greenseeker was 60 cm above the ground and the sensor head was positioned towards the travel direction. The distance between FieldSpec and ground was 1 m. With a field-of-view of 25^{o}, it scanned about 0.154 m^2 area on the ground. The integration time was set to 217 ms. Sunscan and the commercial ultrasonic sensor were placed 20 cm above the crop canopy. FieldSpec, Sunscan and the U.S. Distance ultrasonic sensor were controlled by a laptop and all the data were stored in it for further process.

Figure 2.8 shows the system construction during the field test in July 2008. Greenseeker and FieldSpec were mounted on the right hand side of the travel direction. Sunscan, ADC camera and ultrasonic sensor were mounted on the left hand side. The height of Greenseeker was adjusted to 80 cm above the canopy. The heights of FieldSpec and ADC camera were 1 m and 1.2 m above the ground, respectively.

Figure 2.8. The integration system construction in the first field test in July 2008.

NDVI Readings

A part of NDVI readings from Greenseeker in both tests are given in Figure 2.9. As mentioned previously, Greenseeker is designed to be about 80 to 120 cm above the target. The width of sensor scanning is constant and doesn't change with the distance between the sensor and target. The average width of cotton plants was less than 25 cm in May. The Greenseeker sensor not only scanned on the green vegetation but also did on

the soil around the plants. Therefore, the NDVI dataset had a large range and high variation. The average width of cotton plants became about 51 cm in July. Consequently, the variance of NDVI readings in July was much smaller than the one in May.

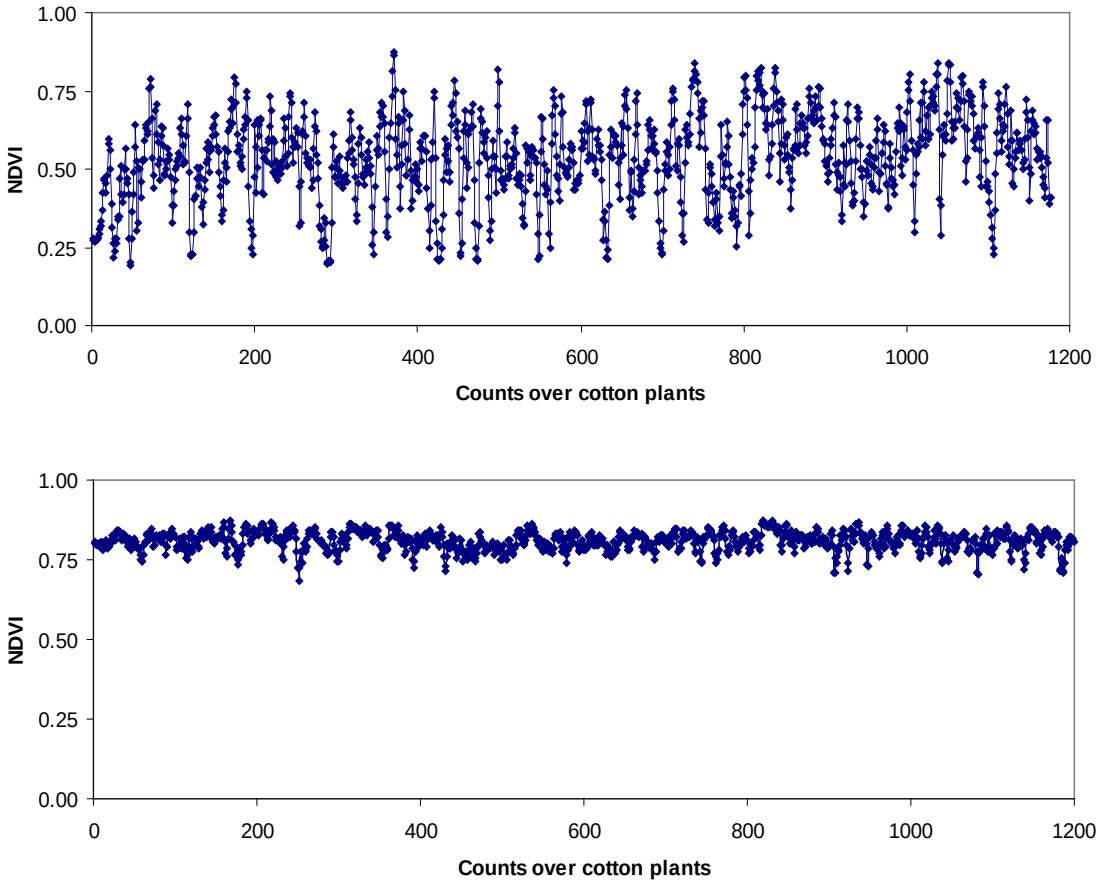

Figure 2.9. NDVI mapping in cotton field in May (above) and July (below) 2008.

The tractor was driven at a speed of 2 km h^{-1} in order to reduce its deviation from the center of the row. To test the repeatability of the measurements by the system, three runs were conducted on the same row with two runs from east to west (E-W, row

orientation) and another from west to east (W-E) in July test. The number of samples, average, standard deviation and coefficient of variation of NDVI readings for three runs are summarized in Table 2.1.

Table 2.1. Summary statistics of NDVI readings for three runs in the soybean field.

Run	No. of Sample	Avg. NDVI	SD	CV (%)
E-W	3100	0.7906	0.0635	8.03
W-E	3027	0.7807	0.0538	6.89
E-W	3150	0.7764	0.0662	8.53

The Greenseeker gives an output every 0.11 second. This means a new value is recorded every 0.0627 m. While moving through the field, 16 readings were taken per meter. By averaging 80 readings for each 5-meter long distance, a total of 33 and 40 NDVI values were gained for the two runs in the same direction on cotton and soybean rows, respectively. Figures 2.10 and 2.11 show the correlation between NDVI values measured on the same rows in the same direction for cotton and soybean, respectively.

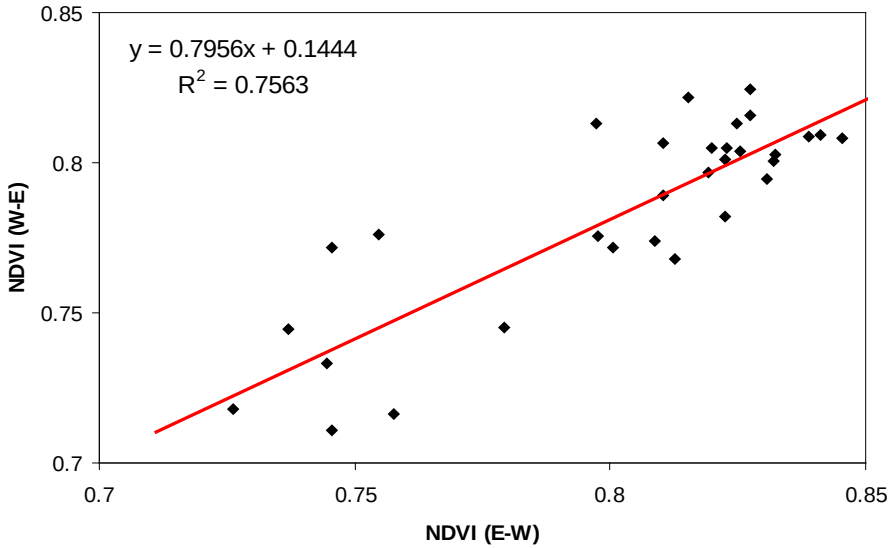

Figure 2.10. Correlation between NDVI readings of two runs on the same row of cotton plants in the same direction.

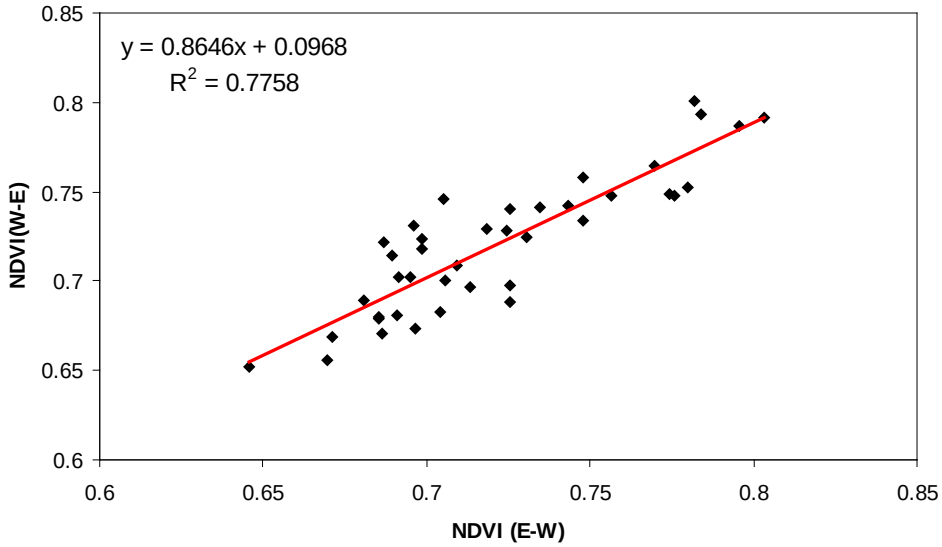

Figure 2.11. Correlation between NDVI readings of two runs on the same row of soybean plants in the same direction.

Reflectance Measurements

Reflectance data were processed by Viewspec Pro 4.05 comes with FieldSpec. Reflectance measurements for each run were averaged to one curve for cotton and soybean, respectively. The reflectance curves of both cotton and soybean were characterized by low reflectance in the blue (450-495 nm) and red (620-700 nm) regions of the spectrum. The peaks in green and high reflectance in the NIR region of the spectrum appeared. However, there were considerable noises in the near infrared region of the spectrum.

The spectra comparison and the coefficient of variation (CV) of the measurements of three runs for cotton and soybean were presented in Figures 2.12 and 2.13. For cotton, the CV of the reflectance measurements from the run in the reverse direction was higher than the other runs in the same direction. By discarding the reflectance values from 750 to 775 nm and 1000 to 1075 nm where the noises appeared, the analysis of variance test was applied on the CV of the reflectance measurements from three runs. The CV of the reverse direction run was significantly different from the two other runs on the row in the same direction (*p-value* < 0.001). The reflectance measurements of the three runs in soybean field were not comparable. The CV of the reflectance data for the second run in the same direction was higher than those for the first run. The tendencies of the CV values in these two were similar from the lower visible to higher NIR wavelengths.

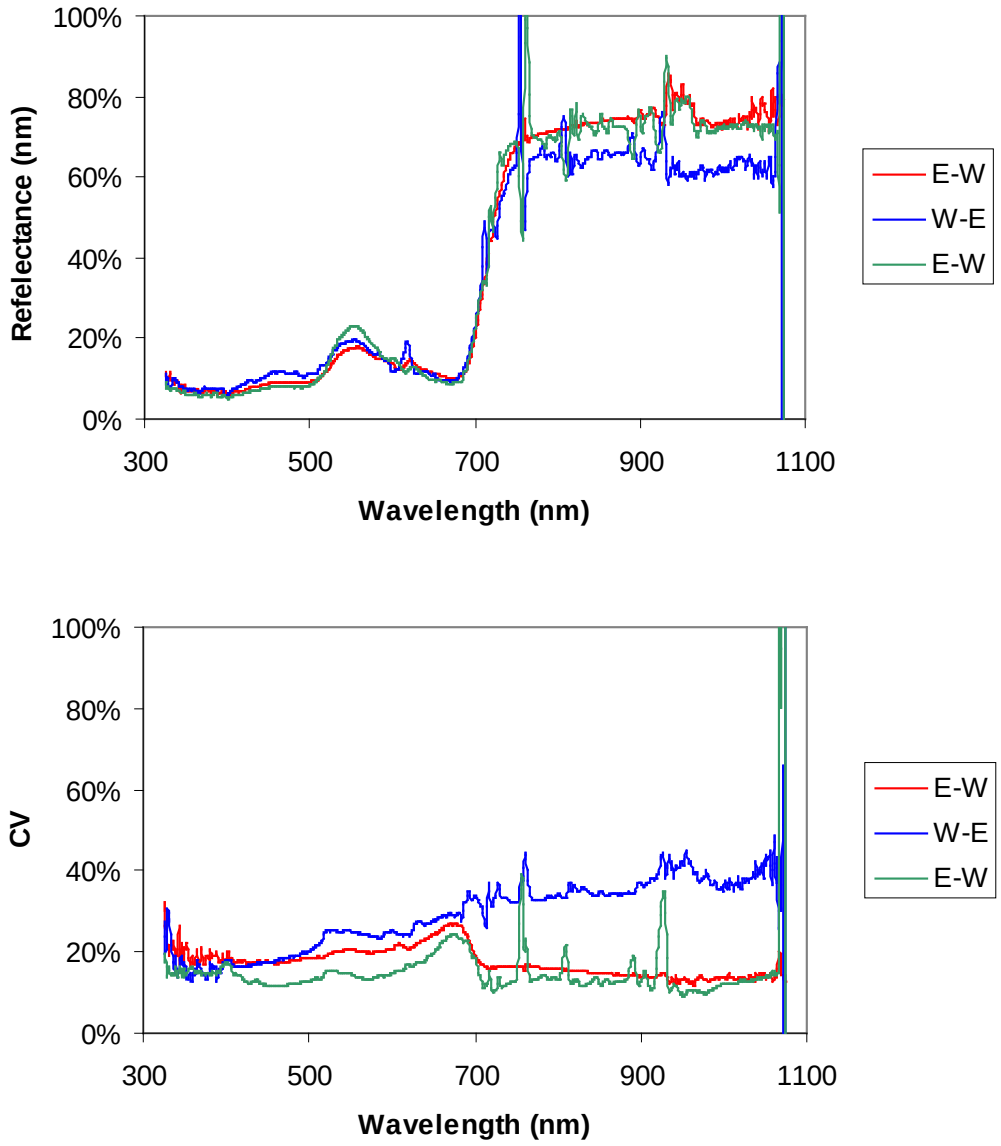

Figure 2.12. The reflectance spectra of three runs for cotton (above) and coefficient of variation (CV) of the spectral data (below).

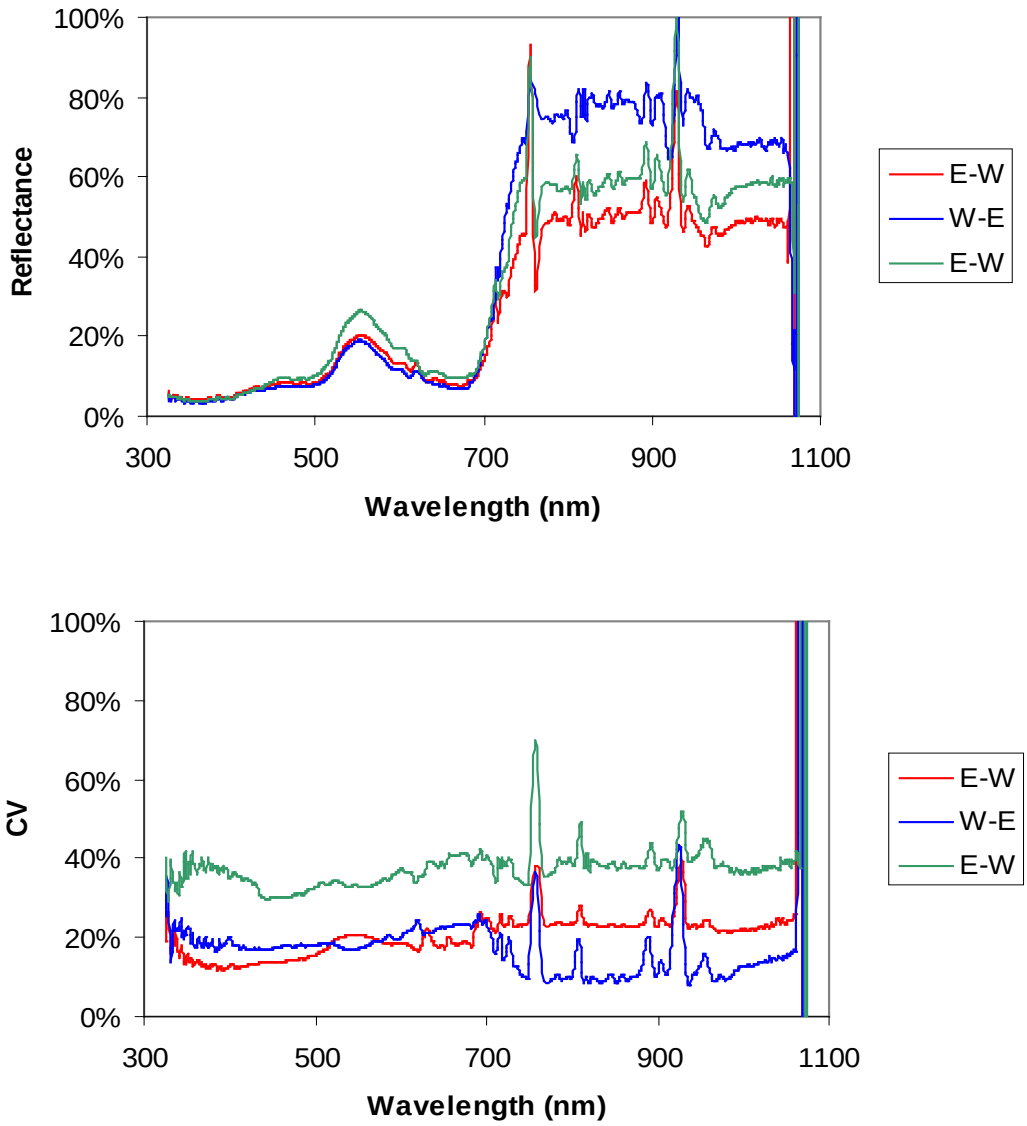

Figure 2.13. The reflectance spectra of three runs for soybean (above) and coefficient of variation (CV) of the spectral data (below).

Crop Height Measurements

The data of U.S. Distance ultrasonic sensor for three runs in the soybean field is plotted in Figure 2.14 and the summary statistics is reported in Table 2.2.

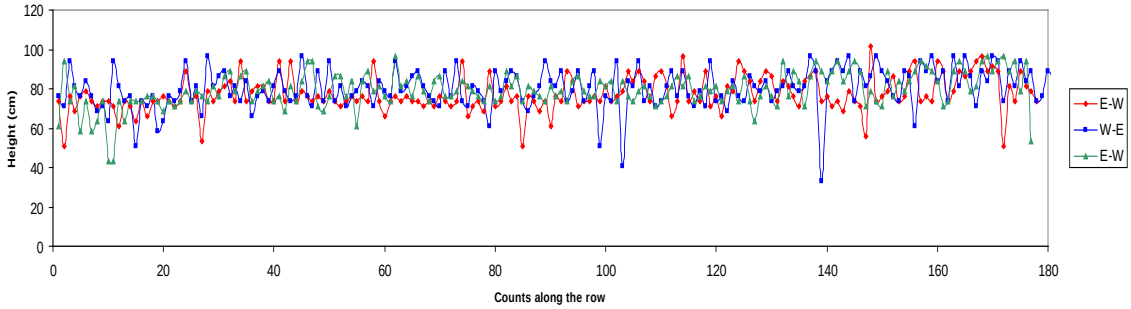

Figure 2.14. Map of the crop height data by the U.S. Distance ultrasonic sensor.

Table 2.2. Summary statistics of ultrasonic crop height for three runs in the soybean field.

Run	No. of Sample	Avg. Height (cm)	SD	CV (%)
E-W	178	77.3	8.71	11.28
W-E	180	80.1	10.0	12.48
E-W	177	79.4	8.93	11.24

Greenseeker NDVI vs. Height

The U.S. distance sensor gives an output every second. The every five measurements were averaged to represent the mean crop height within the 5-meter long distance. The correlation between crop height measurements and Greenseeker NVDI were investigated. Figure 2.15 gives the correlation for the data taken from soybean. The

correlation was only 0.2387. The correlation for the data taken from cotton by these two sensors was even lower.

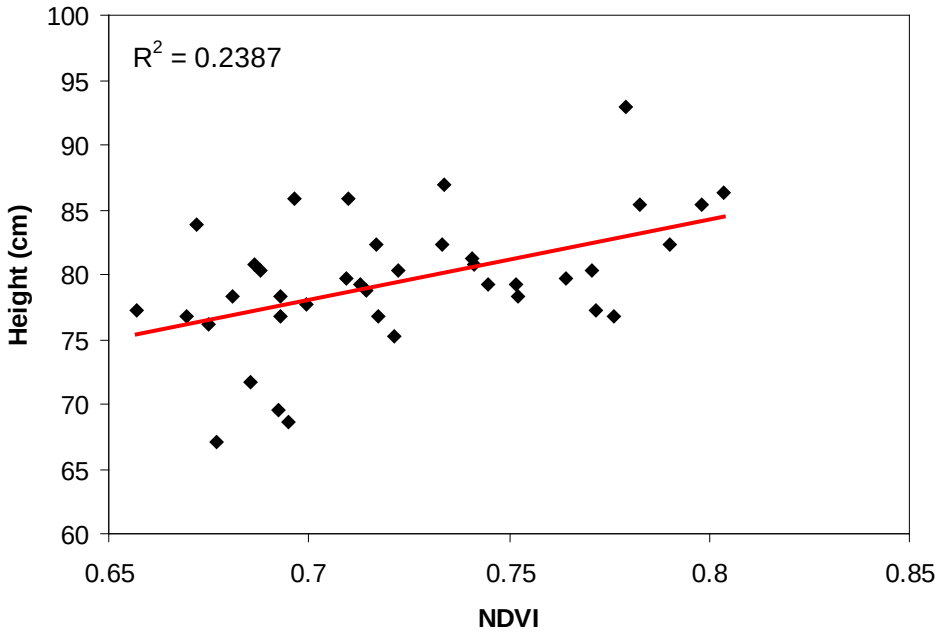

Figure 2.15. Correlation between Greenseeker NDVI and the crop height measured by the U.S. distance sensor.

Multispectral Images

Figure 2.16 shows one of the images was taken by ADC camera when the tractor was driving through the soybean field. Only a few good quality images could be acquired by the ADC camera during the field tests. Some images were blurted or over exposure like the extremely bright part marked with a circle in Figure 2.16.

Figure 2.16. Multispectral image taken by ADC camera from soybean canopy.

CONCLUSIONS

Spectral information on field crop, such as NDVI, reflectance measurements, multispectral images, and crop height, has been acquired by the integration system. The authors did not get meaningful LAI data during two field tests. This preliminary work indicates that the potential of the integration sensor and instrument system to realize multi-source information acquisition at field level. Two rows were chosen within cotton and soybean crop field, respectively. Measurements repeatability was investigated by driving through the same row three times. Two runs were in the same direction, and the other was in the reverse direction. Spectral information, NDVI and spectral reflectance measurements, images, and crop height were able to be obtained by the proposed sensing system simultaneously from crop canopy with good measurement repeatability. The

reflectance data taken by spectroradiometer in the reverse direction were significantly different from the data taken in the same direction. These factors may influence the acquisition of reflectance data, for example, the time of the data being taken, solar zenith angle at the time, clear sky, need to be paid more attention for field data collection in the future.

CHAPTER III

CHARACTERIZE SPECTRAL PROPERTY AND DISCRIMINANT ANALYSIS OF AGRICULTURAL CROPS AT DIFFERENT GROWTH STAGES WITH HYPERSPECTRAL DATA

OVERVIEW

The spectral reflectance properties of cotton (*Gossypium hirsutum* L.), corn (*Zea mays* L.), soybean [*Glycine max* (L.)], and sorghum [*Sorghum bicolor* (L.)] crops during their different growth stages of development were examined to determine whether the spectral properties of plants could be used to distinguish cotton from other crops. Two field blocks with two different soil types (Belk clay (BaA) and Ships clay (ShA)) were set up with cotton, corn, soybean and sorghum in each block using conventional production practices for the area. Spectral information was collected from all crops at different growth stages from May to July 2009. Reflectance spectra and the first derivative of the spectra were analyzed to characterize the spectral properties of crop varieties and to compare the crops grown in different soil types. The red-edge positions were shown differences among cotton, corn, soybean and sorghum among crops at the vegetative growth stage, and soybean and sorghum at the reproductive

growth stage. The red-edge points of cotton, soybean and sorghum shifted with the growth stages of development. Principal component analyses were successful in reducing the dimensionality of hyperspectral data and identifying significant features from original data. Most significant wavelengths selected were among 548-556 nm, 679-682 nm, 756-764 nm, and 928-940 nm regions of the spectrum. The discriminant analysis method was found to be able to differentiate crop types at four critical growth stages with 100 % accuracy of classification for all four days data, except for 1.32 % misclassification rate in cross-validation for the dataset from the early vegetative stage.

INTRODUCTION

The need to minimize populations of overwintering boll weevils, *Anthonomus grandis* Boheman, is widely recognized by eradication programs. One tactic to reduce overwintering survival of boll weevils is timely post-harvest stalk destruction. Even where cotton plants, *Gossypium hirsutum* L., are destroyed after harvest, regrowth from stalks or growth of volunteer plants from unharvested seed can occur when environmental conditions permit. Occurrence of regrowth or volunteer cotton, particularly fruiting plants, is a major concern of the Texas Boll Weevil Eradication Foundation (TBWEF) because such plants extend the opportunity for weevils to reproduce and/or acquire the necessary fat reserves to overwinter.

Presently, regulations established by the Texas Department of Agriculture (TDA) permit the existence of regrowth or volunteer plants beyond the crop destruction deadline as long as plants do not possess fruiting structures. TDA is solely responsible for monitoring fields and administering fees for non-compliance, but limited resources

restrict the frequency and coverage of field inspections. Detecting volunteer cotton in other crops or uncultivated habitats is also problematic because these plants are usually hidden by the surrounding vegetation. Thus, there is a need to develop or identify technologies that can be used to efficiently detect regrowth and volunteer plants in both cultivated and uncultivated habitats. One potential method may involve remote sensing with multispectral and hyperspectral sensors.

During the past decade, hyperspectral and multispectral sensors have shown considerable promise as tools for efficiently detecting stressed plants in localized areas of fields. Spectral reflectance properties based on the absorption of light at a specific wavelength are associated with specific plant characteristics. For healthy crops, spectral reflectance in the visible region (400-700 nm) of the spectrum is low because of the high absorption of light energy by chlorophyll. In contrast, reflectance in the near infrared (NIR) region (700-1300 nm) of the spectrum is high because of the multiple scattering of light by different leaf tissues (Taiz and Zeiger, 2006). Reflectance in the green region is also higher than that in the blue and red regions of the spectrum. Stress or damage to crops can cause a decrease in chlorophyll content and change internal leaf structure (Curran, 1989). As a result, the reflectance in the green and NIR regions of the spectrum will decrease. Reflectance at the boundary between the visible and NIR region of the spectrum is called the “red-edge” region. The red-edge point is defined as the absolute maximum of the first derivative in the range 690-750 nm and can be found by plotting the first derivative of the reflectance spectrum, and then identifying the highest peak manually (Horler et al., 1983; Fillella and Peñuelas, 1994). Demetriades-Shah et al.

(1990) proposed the use of first and second derivative spectra in canopy measurements since these essentially eliminate the effects of soil background. Many researchers also have related the red-edge position to chlorophyll concentration, biomass and leaf area index estimation (Curran et al., 1991; Danson and Plummer, 1995; Mutanga and Skidmore**,** 2007).

Several studies have used hyperspectral measurements in support of crop management, such as crop type identification, plant nutrition deficiency assessment, crop stress or damage, yield estimation and growth status evaluation. Thenkabail et al. (2000) used narrow-band spectral data between 350 and 1050 nm to determine appropriate bands for characterizing biophysical variables of various crops, including corn, soybean and cotton. Zhao et al. (2005a) evaluated the hyperspectral vegetative indices for discrimination of cotton nitrogen stress and growth stage. Zhao et al. (2005b) investigated the effects of nitrogen deficiency on grain sorghum growth and leaf hyperspectral reflectance properties. They reported that nitrogen deficiency increased leaf reflectance at 555 nm and 715 nm, but their experiments were conducted under outdoor pot-culture condition. Plant et al. (2000) investigated the relationships between remotely sensed reflectance data and cotton growth and yield. Muhammed (2005) used hyperspectral data to discriminate between healthy and diseased plants in a spring wheat crop which suffered from fungal infestation. Koger et al. (2003) determined the potential for wavelet-based analysis of hyperspectral reflectance signals for detecting the presence of early-season pitted morning glory when intermixed with soybean and soil. Hyperspectral reflectance data were analyzed with a variety of methods for

differentiating soybean, soil, and six weed species commonly found in Mississippi agricultural fields (Gray et al., 2009).

In this study, four common agricultural crops, cotton (*Gossypium hirsutum* L.), corn (*Zea mays* L.), soybean [*Glycine max* (L.)], and sorghum [*Sorghum bicolor* (L.)], were planted in two blocks with different types of soil. The objective of this study was to investigate the spectral properties of four crop types at different growth stages under different types of soil and distinguish crop types at different growth stages with hyperspectral data.

MATERIALS AND METHODS

Study Site

The study site was located at the Texas A&M AgriLife Research Farm (30°31'19"N, 96°23'52"W) in Burleson County, Texas. Dominant soil types in the field include a Belky clay (fine, mixed, active, thermic Entic Hapluderts) and a Ships clay (very-fine, mixed, active, thermic Chromic Hapluderts). The field was divided into two blocks, which were called block BaA and block ShA. Four agricultural crops, cotton, corn, soybean, and grain sorghum were planted and managed in each block during 2009 using conventional production practices for the area (Table 3.1). Within each block, there were six rows of each crop with a row spacing of 1 m and rows oriented in the east-west direction.

Table 3.1. Crop varieties with respective planting dates in 2009, Texas A&M AgriLife Research Farm, Burleson Co., TX.

Agricultural crop	Variety	Planting date
Corn	Integra INT9673VT3	March 24
Cotton	Deltapine DP174RF	April 16
Sorghum	DynaGro DG771B	April 15
Soybean	Asgrow O361380	March 24

Spectral Measurements and Analysis

Hyperspectral measurements were carried out from May to July during 2009 growing season. Plant canopy spectra were collected with an ASD FieldSpec® Handheld spectroradiometer (Analytical Spectral Devices, Inc., Boulder, CO). Sunny days were chosen for the field tests and all data were collected around solar noon time. The instrument optimization and white reference measurements were performed prior to taking measurements (Castro-Esau et al., 2006). Reflectance was calculated as the ratio between the reflected radiation from the canopy and the incident energy on the white reference panel ($BaSO_4$). The spectroradiometer was adjusted to 10 scans per dark current and the integration time was set at 217 ms. Spectral reflectance data, which were uncorrected for sun angle or atmospheric effects, were used for analysis in this study since the data were taken at field level and at noon time. The spectroradiometer was mounted on a tractor with a nadir-looking view at the top of plant canopies. Because the field-of-view (FOV) of the sensor is an important factor in determining how much of the

canopy will be viewed, the mounted height of the spectroradiometer was adjusted to maximize plant coverage and subsequently minimize soil background effects. For example, the average width of the cotton plants at May 27 was 35.7 cm, so the sensor was placed about 80 cm above the canopy with a 25^{o} FOV. Measurements were taken at about a 4-m interval from the two middle rows for each crop. An average of 18-20 readings was taken for crop within block BaA and 10 readings for crop within block ShA (The block ShA was about half size of the block BaA). The average reflectance of these readings was used to represent the spectral reflectance signature of each crop variety within the block.

The spectral data ranged from a wavelength of 325 to 1075 nm with a sampling interval of 1.6 nm. The spectroradiometer outputs 512 continuous data points with each sample. The ViewSpec Pro® software supplied by ASD was used to interpolate each sample into 1-nm intervals. This resulted in 751 individual wavebands for each sample. All 751 wavebands were presented as spectral signatures of crop varieties at different growth stages. According to the previous study and other studies (Thenkabail et al., 2000, 2002), spectral data in 325-395 nm and 1000-1075 nm had significant noise problems. Therefore, except for spectral signature comparison, all the further analyses were only based on spectral data from 400-1000 nm.

The data collection day and the corresponding growth stages are summarized in Table 3.2.

Table 3. 2. Hyperspectral measurement dates, days after planted (DAP) and respective stages of plant development designation in parentheses, 2009 growing season.

Crop	May 7 [DAP]	May 27 [DAP]	June 11 [DAP]	July 16 [DAP]
Cotton	Early vegetative (EV) [21]	Early squaring [41]	Squaring (SQ) [56]	Bolls & Blooming (Boll/BM) [91]
Corn	Early vegetative (EV/V) [44]	Vegetative / Ear developing (V/E) [64]	Dough stage (DS) [79]	Hard dent (HD) [114]
Soybean	Early vegetative (EV/V) [44]	Pod developing (POD) [64]	Pod 3/16 inch at one of four upper nodes (PF) [79]	Seeding/full seed (SD) [91]
Sorghum	Early vegetative (EV) [22]	Vegetative (V) [42]	Boot (head surrounded by flag leaf) (BT) [57]	Black layer/mature (BL) [92]

Data Analysis

The spectral reflectance values at each of the 1-nm wavebands were analyzed with principal component analysis (PCA) to extract features prior to processing by discriminant analysis (DA). PCA is a multivariate technique used as a tool for reducing high dimensional data. The information content contained in original variables is projected onto a smaller number of principal components (PCs) which are linear combinations of those variables. The process of PCA returns PCA scores which are the estimated values for each principal component and PCA loadings. The PCA score plot can present the clustering of the data and the PCA loading plot can be used to investigate the contribution of each variable. In this case, PCA was used to reduce the dimension of the hyperspectral data to a few bands that explain most of the variation among the original data. PCA was performed using PRINCOMP procedure in SAS (SAS Institute,

Cary, NC) in which a new principal component was created for each wavelength variable in the original data.

The DISCRIM procedures in SAS were applied on various numbers of derived PCs for classification. The parameters being used to develop discriminant function were pooled covariance matrix and prior probability of the groups. The DISCRIM procedure divided the data into two subsets. One subset was used to develop calibration model and the other was used to validate the model. Leave-one-out method was used for cross-validation in this procedure. The output matrix provided the misclassification rate of calibration and cross-validation.

RESULTS AND DISCUSSION

Reflectance Spectra

The average height of corn plants was more than 2.7 m on DAP 79, which exceeded the height of the frame of the ground-based system described in Chapter II (Lan et al., 2009b). Consequently, the reflectance spectra of corn plants were only available at their early vegetative and vegetative growth stages.

Figures 3.1 (a) and (b) shows the mean spectral reflectance characteristics across the 325 to 1075 nm wavelength for these four crops in two blocks at their early vegetative, vegetative, reproductive and late growth stages of development. At the early vegetative stage, all the spectra had two peaks at the green and NIR regions except for cotton and sorghum. The maximum contrast of the reflectance value of cotton to those of other crops was around the 680 nm wavelength. The highest reflectance in the NIR region was observed at the reproductive stage, which was cotton at “squaring”, soybean at “pod formation” and sorghum at “boot”. There was considerable variation in the reflectance spectra of sorghum during the late growth stage. Contributing factors could be the leaf and canopy structures of the sorghum plants and the considerable movement of the plant canopies when the tractor was driving through the rows. Moreover, the seeds of sorghum plants were fully mature, and it is likely that the sensor measured reflectance not only from leaves but dark kernels.

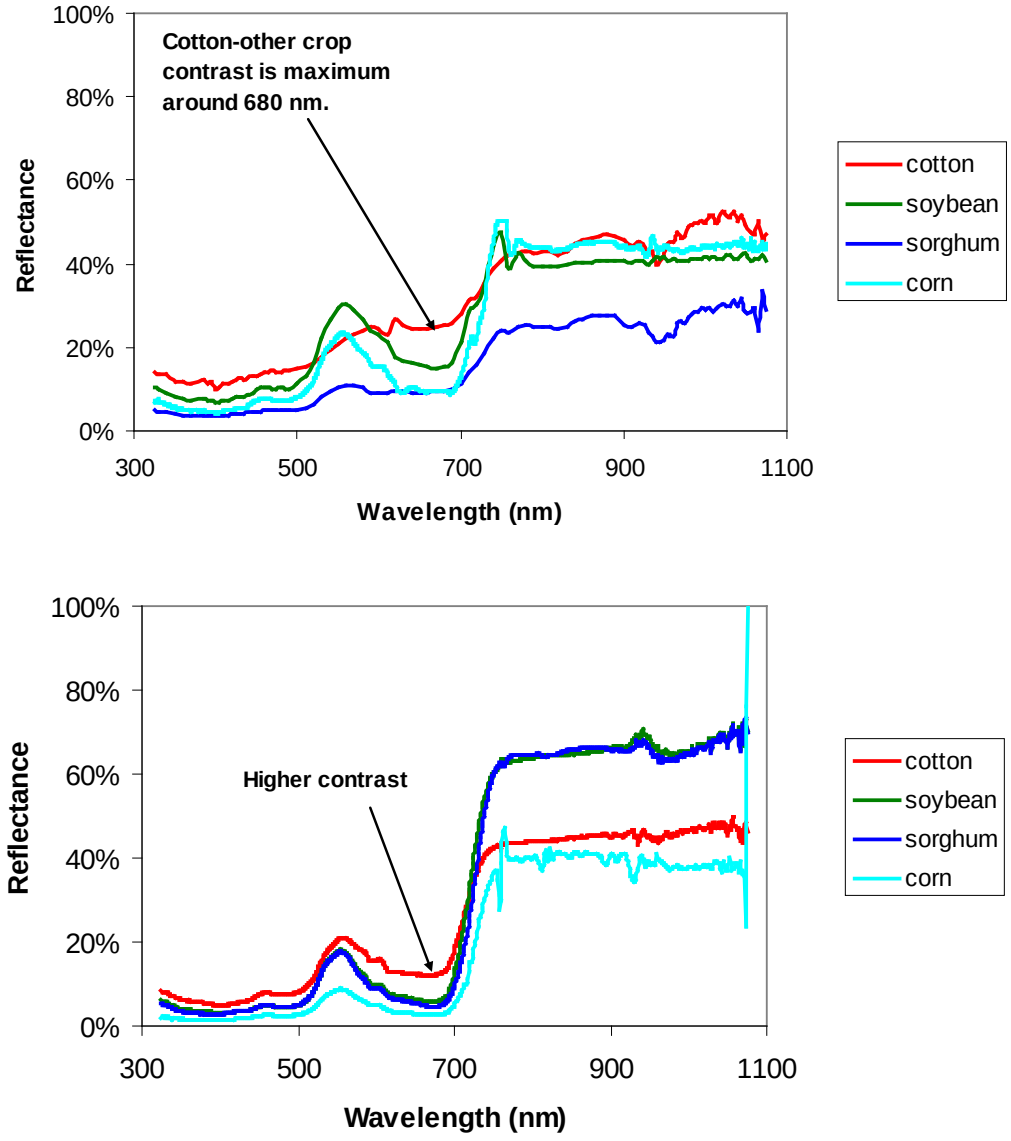

Figure 3.1. The mean spectral reflectance of cotton, soybean and sorghum measured at four growth stages and corn at early vegetative and vegetative stages. (a) block BaA (b) block ShA.

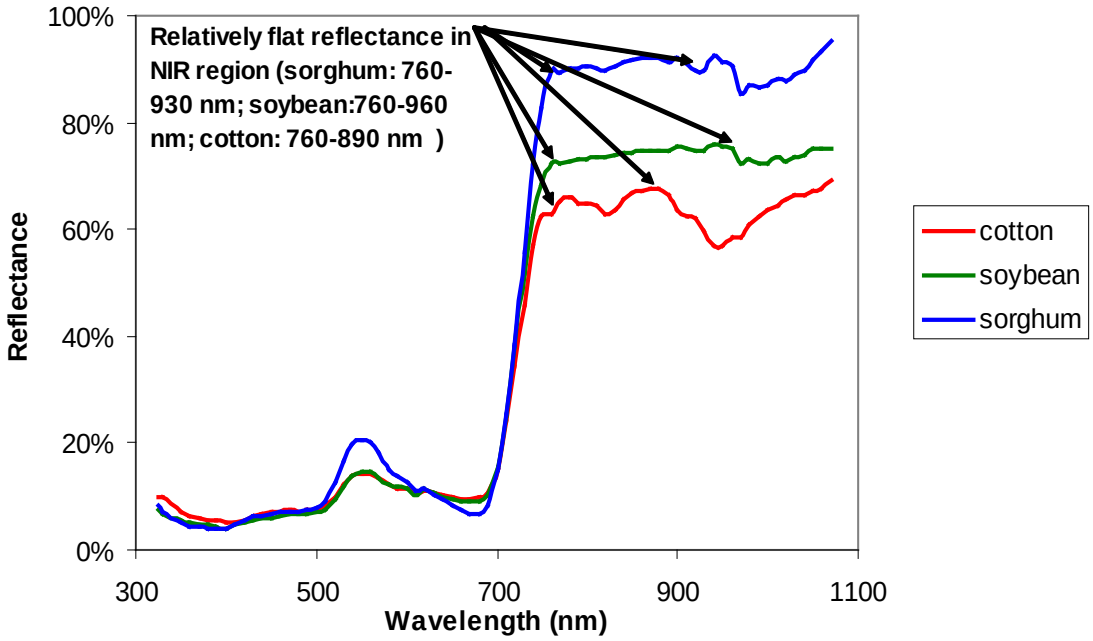

(a) BaA.

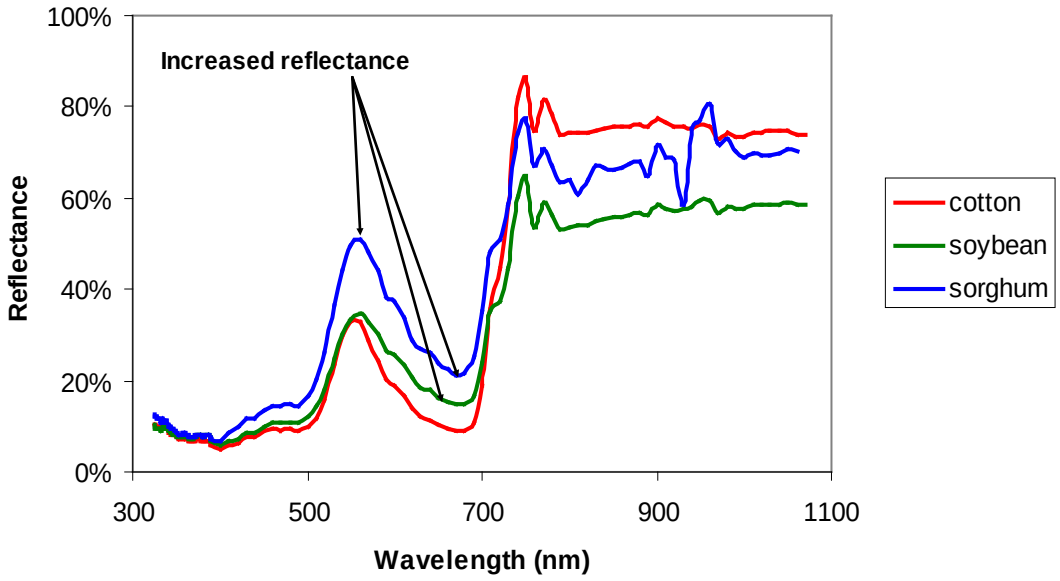

(a) BaA.

Figure 3.1. Continued.

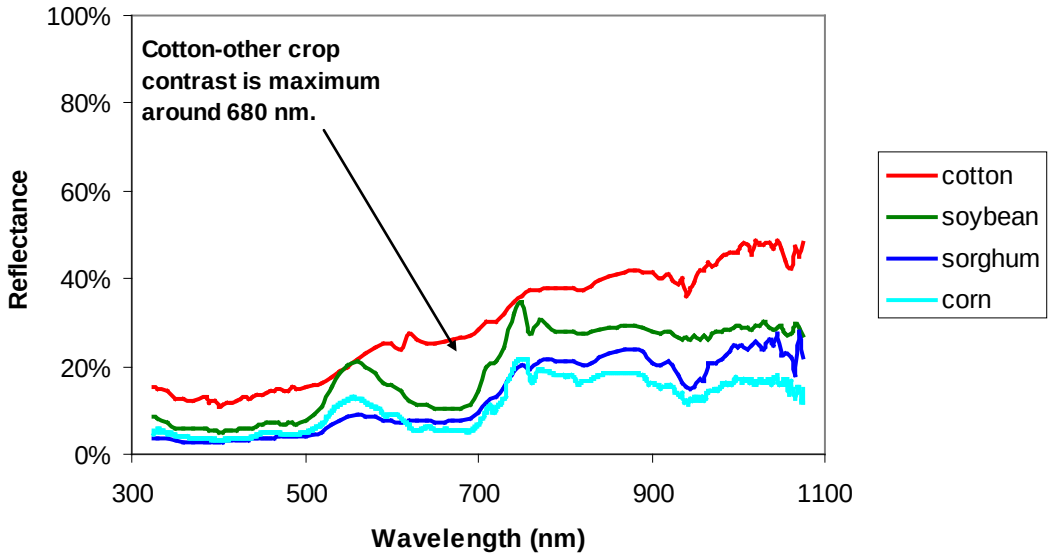
100%
80%
60%
40%
20%
0%
Reflectance
Cotton-other crop
contrast is maximum
around 680 nm.
300
500
700
900
1100
Wavelength (nm)
cotton
soybean
sorghum
corn

(b) ShA.

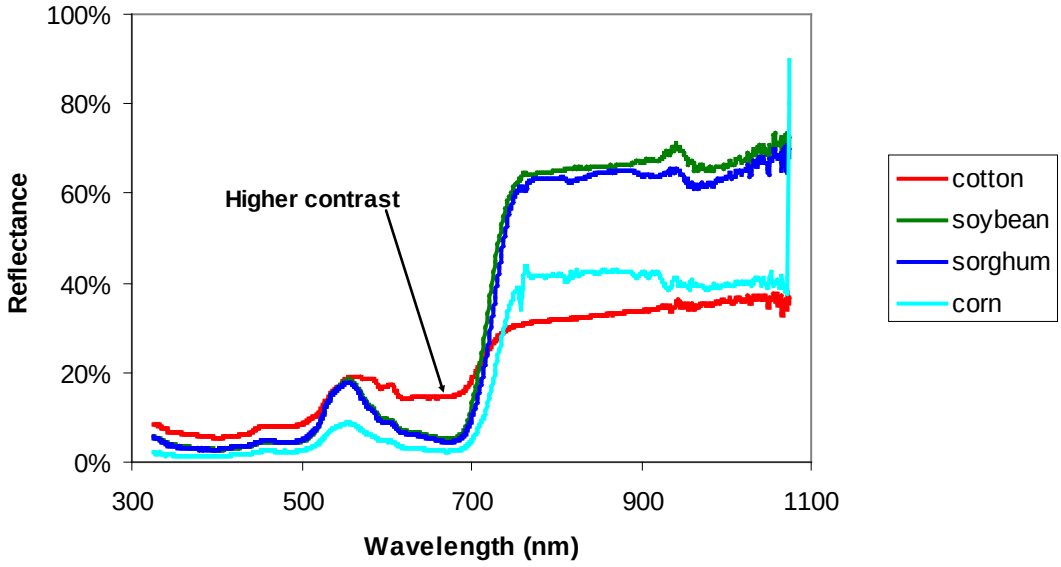
100%
80%
60%
40%
20%
0%
Reflectance
Higher contrast
300
500
700
900
1100
Wavelength (nm)
cotton
soybean
sorghum
corn

(b) ShA.

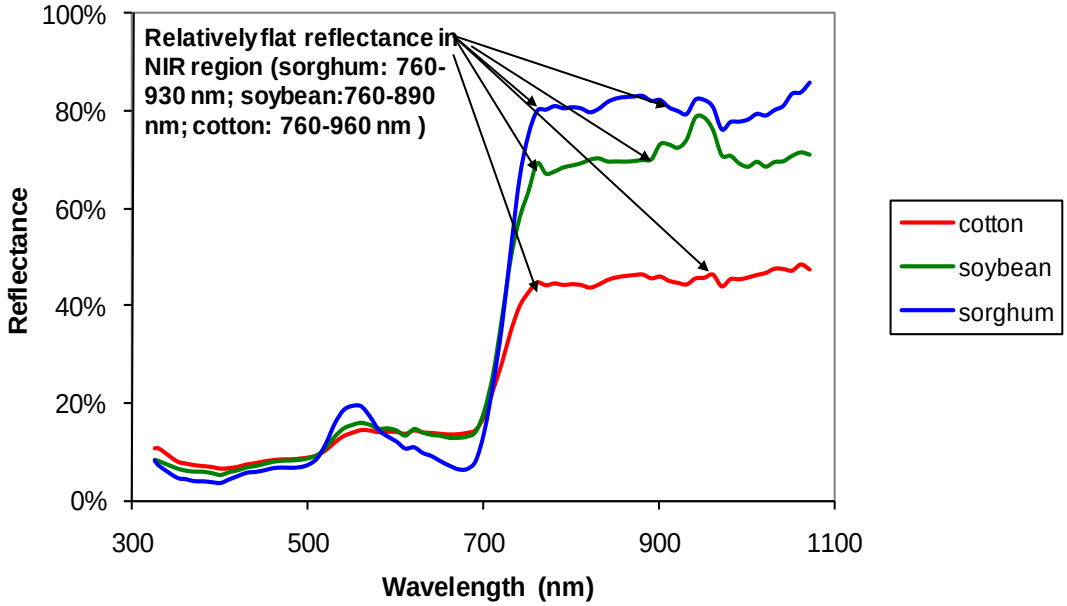

(b) ShA.

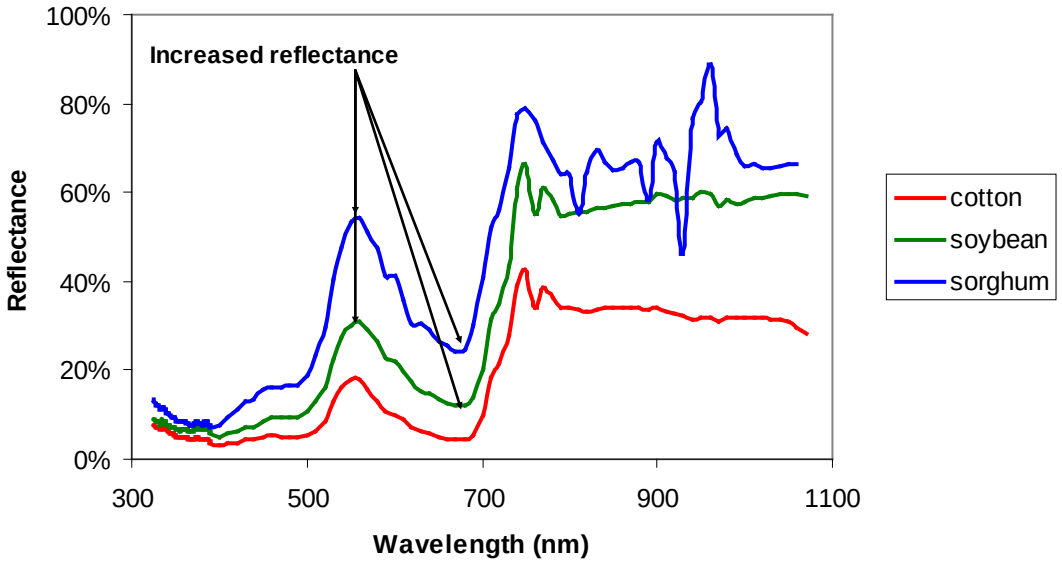

(b) ShA.

Figure 3.1. Continued.

Figures 3.2 (a) to (d) illustrate the mean spectral reflectance of each crop in two blocks at four growth stages, respectively. Each spectrum curve represents the average of all the measurements for each crop at the certain stage. The average reflectance of each crop in block BaA was higher than those in block ShA. The reflectance spectra of corn at the vegetative stage, soybean and sorghum at the vegetative and late stages in both blocks were similar to each other. In other cases, the spectral reflectance values of crops in block BaA were higher than those in block ShA. We also noticed that the reflectance of sorghum in the green and red regions increased at the late growth stage.

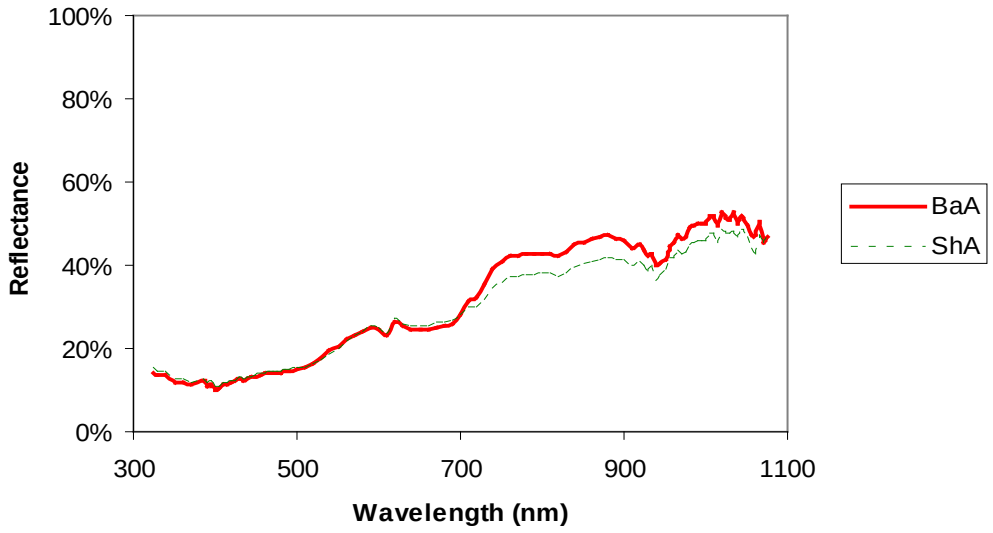

(a) Cotton.

Figure 3.2. The mean spectral reflectance of cotton (a), corn (b), soybean (c) andsorghum (d) measured in block BaA and ShA at early vegetative stage, vegetative stage, reproductive stage, and late stage.

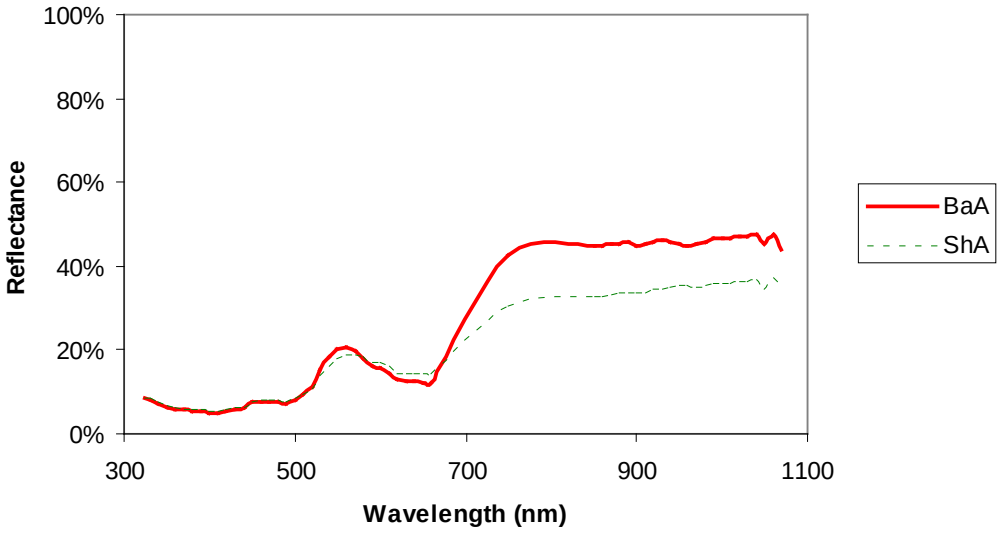

(a) Cotton.

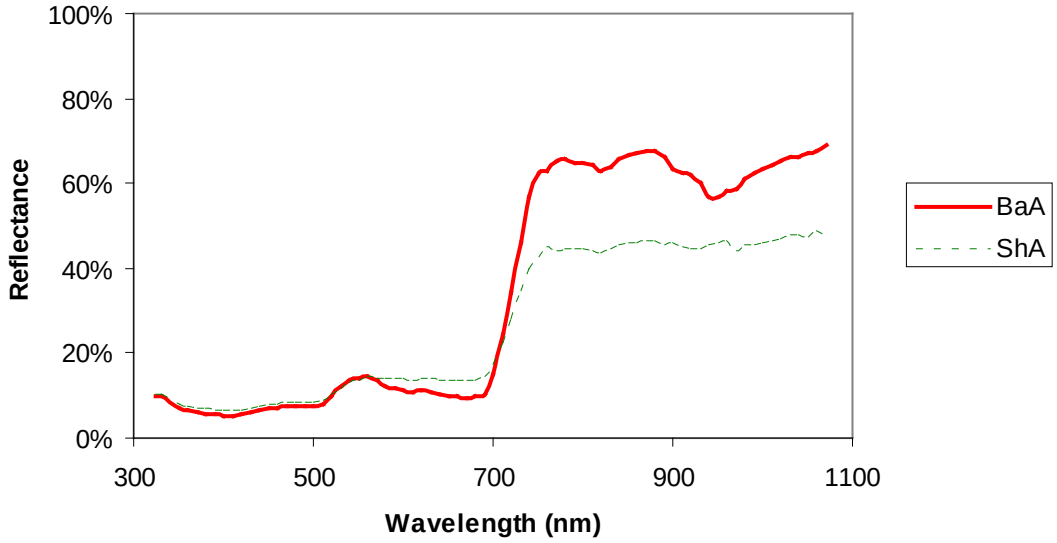

(a) Cotton.

Figure 3.2. Continued.

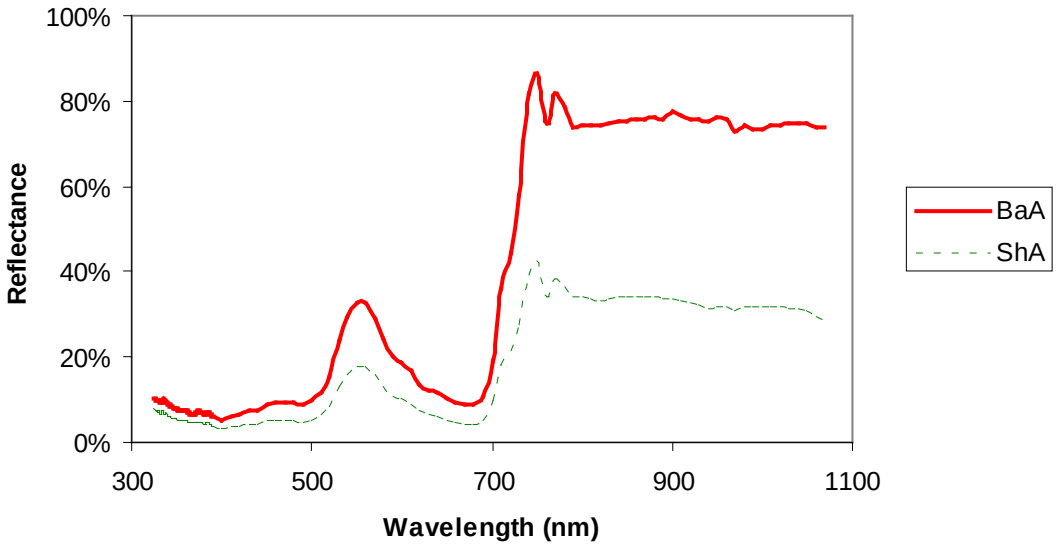

(a) Cotton.

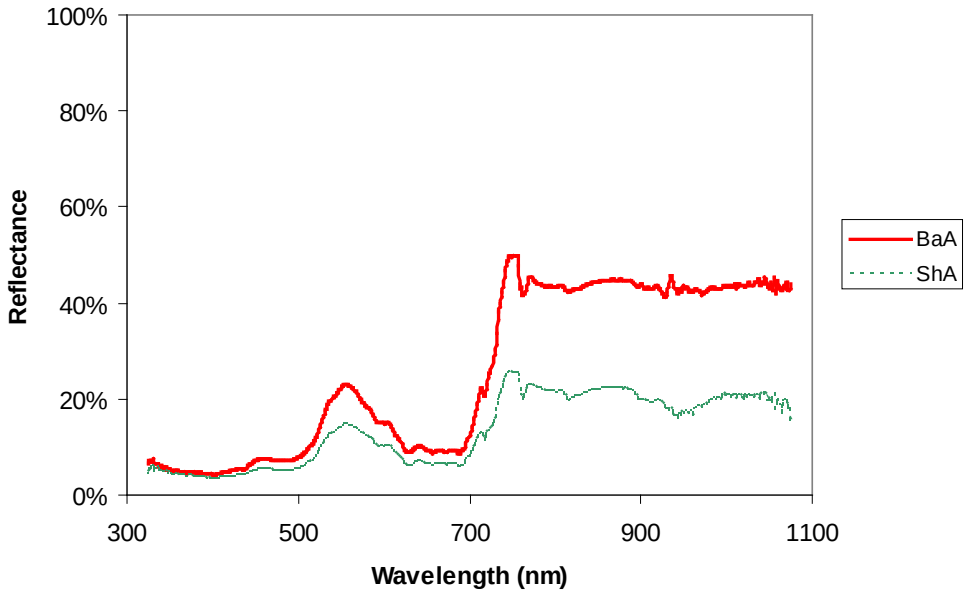

(b) Corn.

Figure 3.2. Continued.

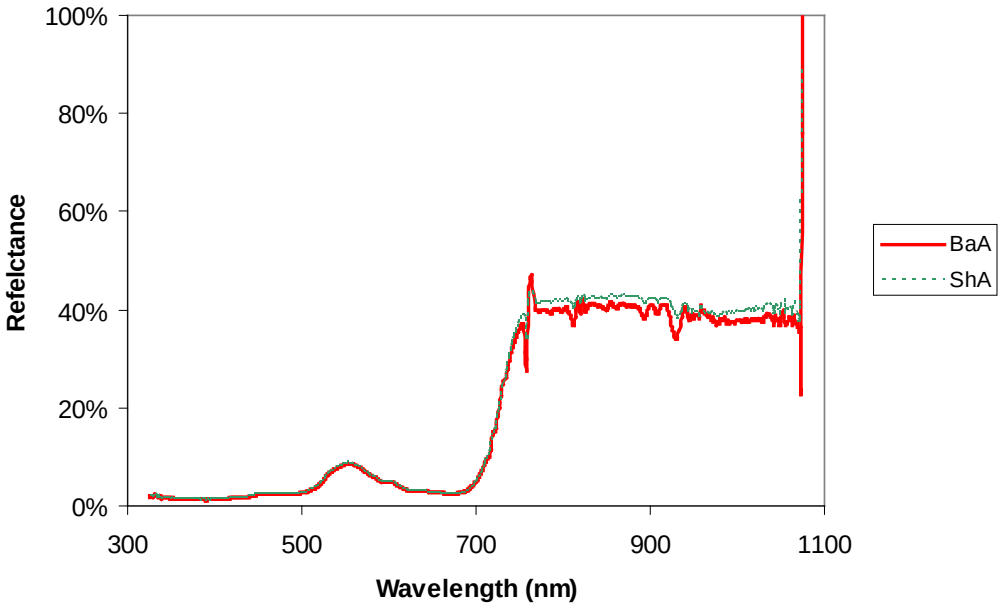

(b) Corn.

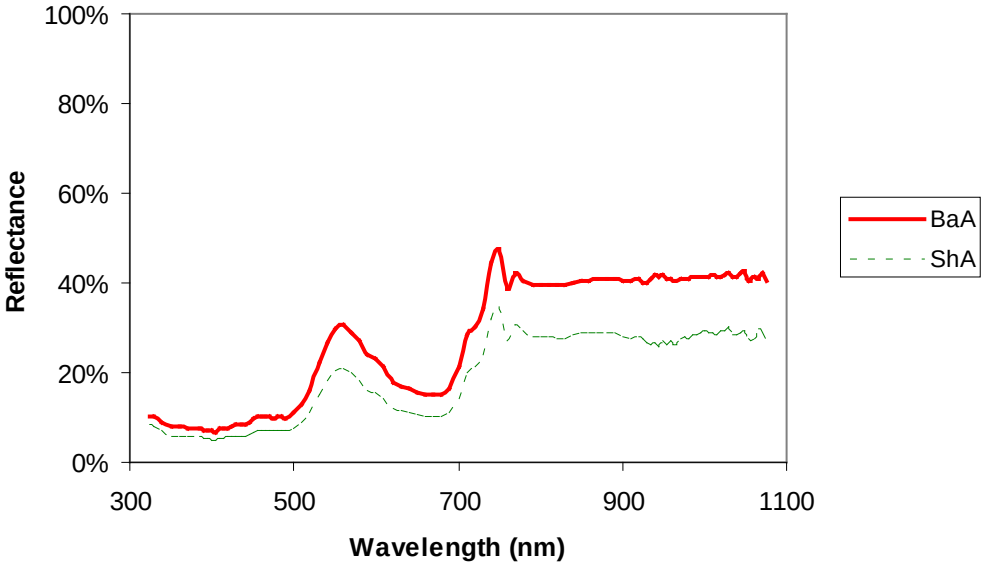

(c) Soybean.

Figure 3.2. Continued.

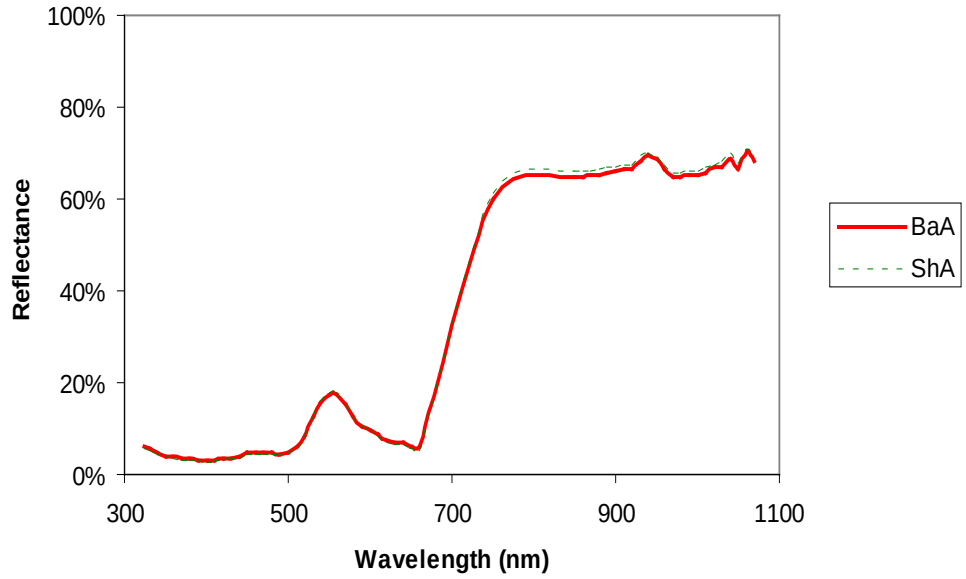

(c) Soybean.

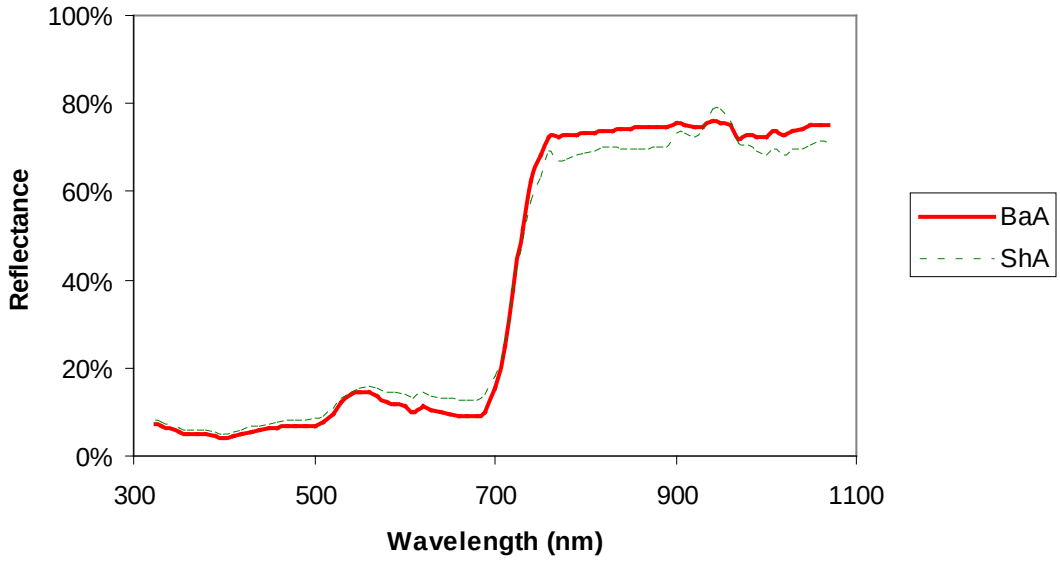

(c) Soybean.

Figure 3.2. Continued.

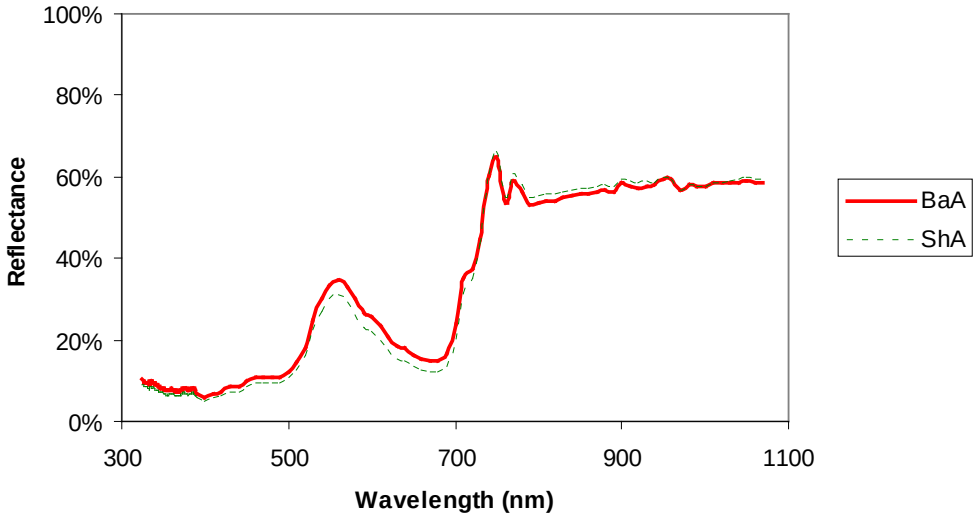

(c) Soybean.

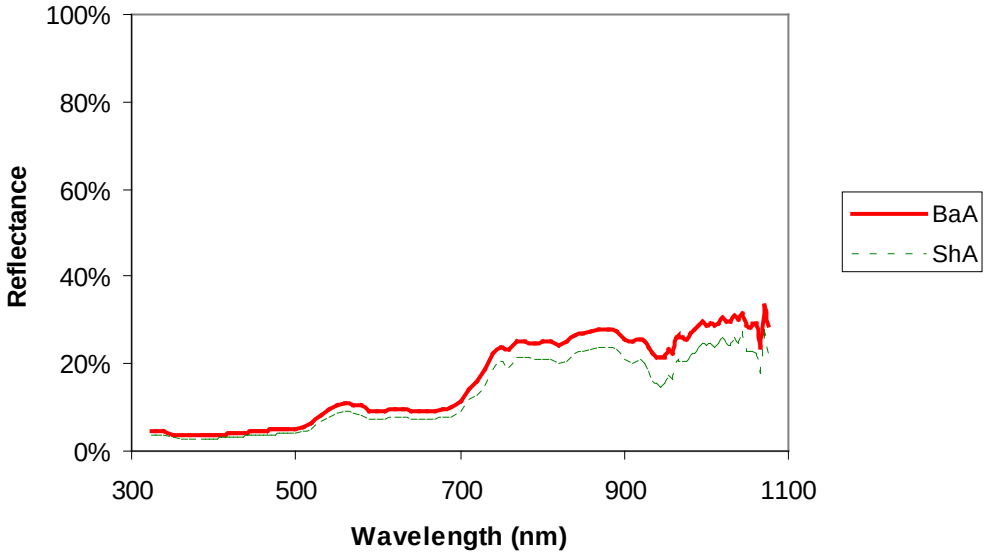

(d) Sorghum.

Figure 3.2. Continued.

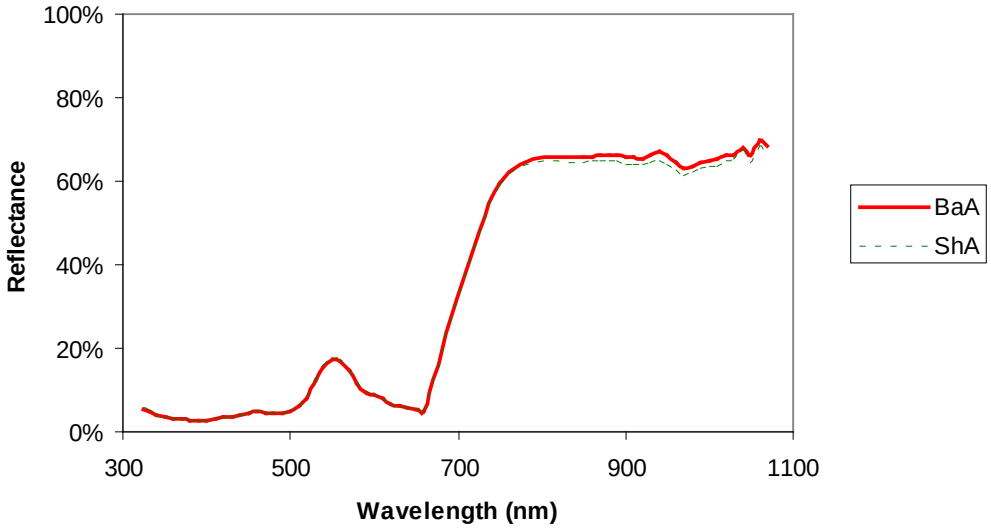

(d) Sorghum.

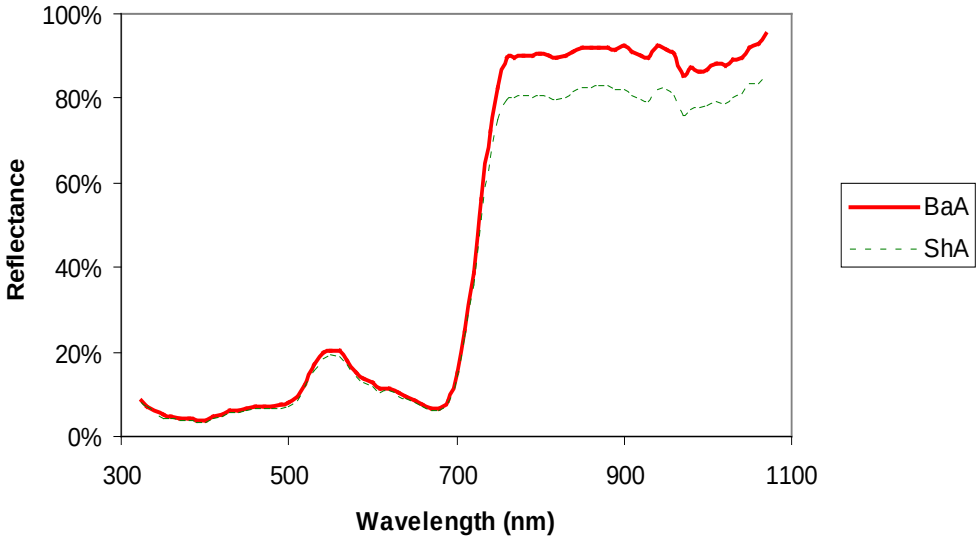

(d) Sorghum.

Figure 3.2. Continued.

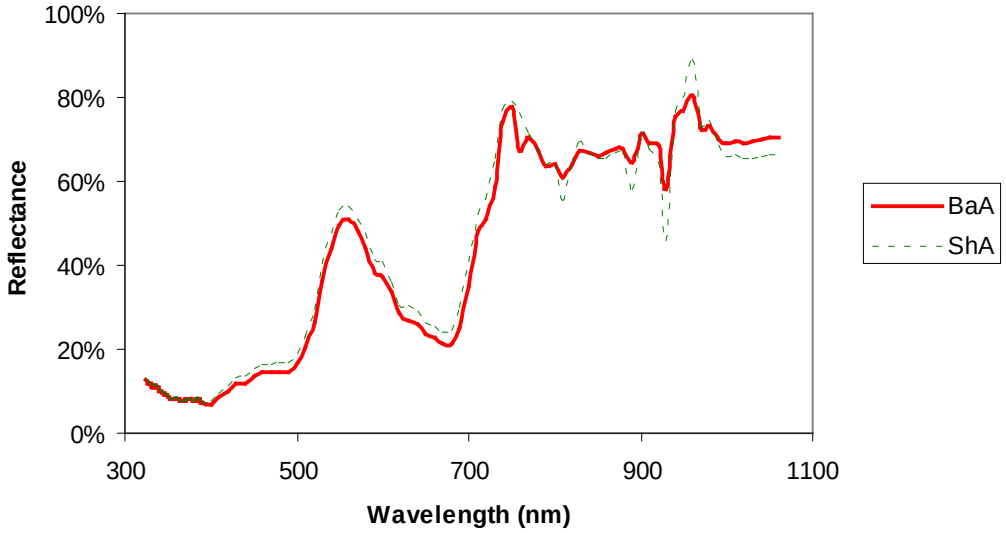

(d) Sorghum.

Figure 3.2. Continued.

1st Derivative of Reflectance Spectra

Figure 3.3 represents the first derivative of reflectance spectra of cotton, soybean and sorghum in two blocks at the vegetative, reproductive and late stages, respectively. The first derivative of reflectance spectra of corn is only available for the vegetative stage and is not plotted in the figure.

Cotton, soybean and sorghum could be distinguished from each other by the red-edge points of the spectra at the vegetative and reproductive growth stages of development. In block BaA, the red-edge points were found at 710 nm, 726 nm, 720 nm, and 728 nm for cotton, corn, soybean and sorghum respectively at vegetative stage; the red-edge points were found at 718 nm, 721 nm, and 730 nm for cotton, soybean and sorghum, respectively, at the reproductive stage. The same wavelengths were found in

block ShA except that 714 nm was found for cotton at the vegetative stage. The red-edge positions were shifted to longer wavelengths with later crop development. This result is consistent with the findings by Railyan and Korobov (1993) that studied the red-edge structure of canopy reflectance spectra of Triticale and concluded that the red-edge position varied according to the plant growth stage.

Two or more peaks were identified in the red-edge region at late stage. The maxima were at 704 and 732 nm, and 702 and 732 nm for cotton in blocks BaA and ShA, respectively; 704 and 735 nm for soybean in both blocks; and 700 and 732 nm for sorghum in both blocks. Horler et al. (1983) reported that the first peak was attributed to the chlorophyll content in the leaves and the second was attributed to cellular scattering in the leaves. In our case, the reflectance spectra were measured at the plant canopy scale instead of individual leaves. The soybean plants were at seeding/full seed stage, and the leaves had started senescence. For sorghum plants, aside from the noise of the raw reflectance spectra, other factors which may cause more peaks in the red edge region need to be investigated in a future study.

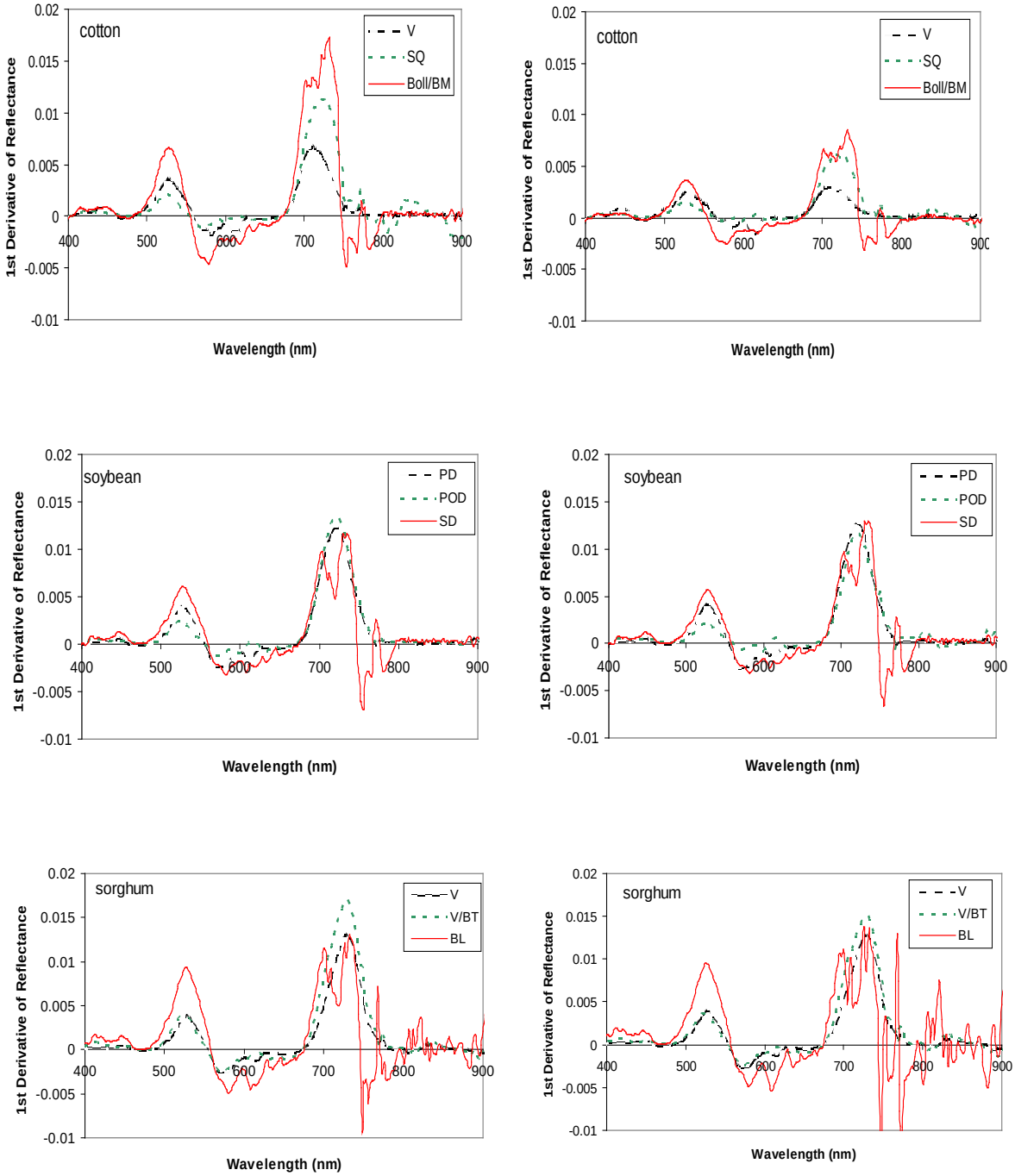

(a) (b)

Figure 3.3. First derivative of the spectra of cotton, soybean and sorghum at different stages in block BaA (a) and block ShA (b).

PCA Feature Extraction

PCA procedures were undertaken on the spectral measurements for crops in block BaA. There were a total of four spectral datasets for four test days. Figure 3.4 gives the first three principal components which explained 99% of the variation from PCA for dataset on May 7, 2009. The corresponding wavelengths could be selected based on the minimum and maximum of PC loadings in the different regions of spectrum. For example, PC3 had peaks at the wavelengths of 557 nm and 747 nm.

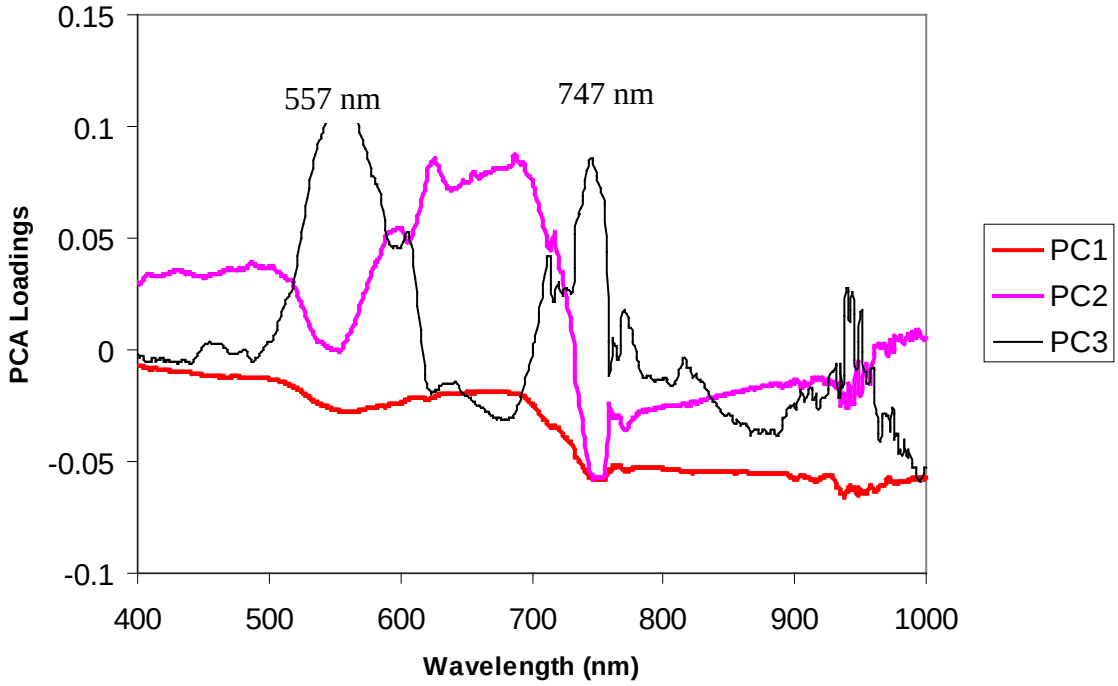

Figure 3.4. The PC loadings of the first three principal components for spectral data on May 7.

The selected wavelengths based on their PC loadings for all datasets and the proportion of variation explain by each principal component are summarized in Table 3.3. The wavelengths picked up by PCs varied for four datasets, but most of them were between 548-556 nm, 679-682 nm, 756-764 nm, and 928-940 nm. These wavelengths carried significant information on the discrimination of crop types.

Table 3.3. Selected wavelengths by principal component analysis.

Test Date	Principal Components	Selected Wavelengths (nm)	Explained Variation (%)
May 7, 2009	PC1	554, 680	86.32
	PC2	516, 540, 688, 757	10.38
	PC3	557, 684, 747, 940	2.72
	PC4	607, 625, 759, 940	0.29
	PC5	556, 680, 720, 756, 940	0.18
	PC6	607, 625, 718, 892	0.02
May 27, 2009	PC1	550, 680, 758	90.93
	PC2	710, 754, 758, 764, 928	8.36
	PC3	516, 686, 728, 758, 764, 932	0.32
June 11, 2009	PC1	549, 550, 700, 760	93.72
	PC2	548, 690, 720, 780, 818, 872, 943	3.83
	PC3	549, 721, 762, 946, 818	1.65
	PC4	555, 679, 730, 816, 868, 928	0.55
	PC5	552, 682, 730, 928	0.13
	PC6	624, 759, 762, 778, 817, 867, 927, 936	0.04
July 6, 2009	PC1	552, 757, 762, 928, 960	76.9
	PC2	581, 695, 757, 762, 928, 960	20.79
	PC3	545, 621, 755, 762, 928, 960	1.63
	PC4	553, 710, 715, 753, 759, 919, 932	0.26

Discriminant Analysis

The classification results for four datasets are reported in Table 3.4. For four days, the DISCRIM procedure was able to identify the crop varieties during the calibration step

Table 3.4. Summary of misclassification matrices obtained from DISCRIM procedure.

Test Date	No. of Principal Components	Calibration (%)	Cross-Validation (%)	Misclassification
May 7, 2009	1	36.84	51.32	
	2	21.05	22.37	
	3	2.63	3.95	
	4	1.32	2.63	
	5	2.63	2.63	
	6	0	1.32	corn vs. soybean
May 27, 2009	1	35.29	38.24	
	2	5.05	1.47	soybean vs. sorghum
	3	0	0	
June 11, 2009	1	33.33	33.33	
	2	12.5	14.58	
	3	10.42	16.7	
	4	0	4.17	
	5	0	2.08	soybean vs. sorghum
	6	0	0	
July 6, 2009	1	3.17	4.76	
	2	1.59	1.59	
	3	0	1.59	cotton vs. soybean
	4	0	0	

with different numbers of PCs. For May 27 and July 6 datasets, the accuracy of classification was 100 % with three or four PCs for both calibration and cross-validation steps. For June 11 dataset, six PCs were used to get 100 % accuracy of classification in

both calibration and cross-validation steps. Only May 7 dataset gained a misclassification rate of 1.32 % in cross-validation. The misclassified crop types from four days datasets were corn vs. soybean on May 7; soybean vs. sorghum on May 27 and June 11; cotton vs. soybean on July 6. Generally speaking, the discriminant analysis was able to differentiate cotton from corn, soybean and sorghum.

CONCLUSIONS

Field tests were carried out to investigate the spectral properties of cotton, corn, soybean and grain sorghum crops at their different growth stages of development during the growing season in 2009. Four crops were grown in two blocks with different soil types, Belk clay and Ships clay. Hyperspectral data was collected from crop canopies at the early vegetative, vegetative, reproductive and late growth stages of development. The spectral characteristics of crops at different growth stages were compared. Using the first derivative of the spectral data, the red-edge position of cotton crop was at the shorter wavelength than those of corn, soybean and sorghum at the vegetative stage and soybean and sorghum at the reproductive stage. The red-edge points of cotton, soybean and sorghum shifted about 4 nm, 1 nm, and 2 nm, respectively, from the vegetative stage to the reproductive stage. Two or more peaks were observed from the first derivative of spectra, and the maxima were at 732 and 735 nm wavelengths.

Principal component analyses were successful in reducing the dimensionality of hyperspectral data and identifying significant features from original data. The discriminant analysis method was found to be able to differentiate crop types at four critical growth stages with 100 % accuracy of classification for all four days data, except

for 1.32 % misclassification rate in cross-validation for the dataset from early vegetative stage.

In light of our findings, the spectral properties of plants shows considerable promise as method for discriminating among crop types and continued investigation of this technology is warranted.

CHAPTER IV

GROUND-BASED SPECTRAL REFLECTANCE MEASUREMENTS FOR EVALUATING THE EFFICACY OF AERIALLY-APPLIED GLYPHOSATE TREATMENTS*

OVERVIEW

Aerial application of herbicides is a common tool in agricultural field management. The objective of this study was to evaluate the efficacy of glyphosate herbicide applied using aircraft fitted with both conventional and emerging aerial nozzle technologies. A weedy field was set up in a randomized complete block experimental design using three replicates. Four aerial spray technology treatments, electrostatic nozzles with charging off, electrostatic nozzles with charging on, conventional flat-fan hydraulic nozzles and rotary atomisers, were tested. To evaluate the glyphosate efficacy and performance of aerial spray technologies, spectral reflectance measurements were acquired using a ground-based sensing system for all treatment plots. Three

---

*Reprinted with permission from "Ground-based spectral reflectance measurements for evaluating the efficacy of aerially-applied glyphosate treatments" by H. Zhang, Y. Lan, R. Lacey, W. C. Hoffmann, D. E. Martin, B. Fritz, J. Lopez Jr., 2010. Biosystems Engineering, Vol. 107, Page 10-15, Copyright [2010] by Elsevier.

measurements were taken at 1, 8, and 17 days after treatment (DAT). The statistical analyses indicated that glyphosate applied with different methods killed the weeds effectively compared to untreated areas at 17 DAT. Conventional flat-fan nozzles and rotary atomisers performed better than the electrostatic nozzles with charging off. There was no evidence to show that the electrostatic nozzle performed better with charging on or charging off. The results could provide applicators with guidance equipment configurations that can result in herbicide savings and optimized applications in other crops.

INTRODUCTION

Glyphosate, a non-selective contact herbicide, is used extensively for weed control in agricultural production systems. Use of glyphosate has increased dramatically due to the introduction of transgenic crop varieties that tolerate over-the-top or directed applications during some growth phases without significant impact on yield. It has also increased because of the increase in reduced-tillage or no-tillage farming systems. Jordan et al. (1981) evaluated the efficacy of glyphosate alone and in combination with other herbicides, but their work was limited to ground applications. Specialised agricultural aircraft have developed largely as a result of convenience as they allow for better timing of and greater efficiency in application treatments. Aircraft are able to apply agricultural products, such as fertilizers and pesticides, in a timely manner over large areas. Aerial applications of glyphosate have increased with the requirement for more effective weed management prior to planting spring-seeded crops. Many studies have been conducted to evaluate the performance of aerial spray technologies. For the

most part these studies have indicated that optimum spray rate and droplet size combinations vary with pesticide product, pest, and specific crop (Bouse et al., 1992, Hoffmann et al., 1998, and Kirk et al., 1992, 1998 and 2001). Latheef et al. (2009) investigated the efficacy of different insecticides applied with aerial electrostatic-charged sprays and conventional sprays and found comparable deposition and insect control between both electrostatic and conventional flat fan nozzles.

Spectral reflectance properties based on the absorption of light at a specific wavelength are associated with specific plant characteristics. The spectral reflectance in the visible wavelengths (400-700 nm) is low because of the high absorption of light energy by chlorophyll. Reflectance of the near infrared (NIR) wavelengths (700-1300 nm) is high because of the multiple scattering of light by different leaf tissues (Taiz and Zeiger, 2006). For example, plant stress usually results in an increase in visible reflectance and a decrease in NIR reflectance. Lamb and Brown (2001) suggested that differences in spectral reflectance between weeds and their background could be used to remotely sense weeds. Detecting weeds against a soil background on fallow ground is a straightforward process as the weeds and soil have significantly different spectral reflectance characteristics in the Red and NIR wavelength bands. It is also well known that the normalized difference vegetative index (NDVI) is a good indicator of vegetation, crop biomass and health in agricultural applications (Rouse et al., 1973; Tuker, 1979; Sembiring et al., 1998). NDVI is calculated by: NDVI= (NIR – Red) / (NIR + Red), where Red and NIR are the spectral reflectance measurements acquired in the red and near-infrared regions, respectively. Healthier crop canopies will absorb more red and

reflect more near infrared light than stressed or unhealthy canopies, and consequently have a higher NDVI value.

Many on-the-go, ground-based sensors are available for collecting real time spectral reflectance data and calculating NDVI. The Greenseeker has been widely used for mapping NDVI in a variety of different crops. Martin et al. (2005 and 2007) used this sensor to collect NDVI data at multiple growth stages during the life cycle of maize and evaluate the relationship between NDVI and maize grain yields. Jones et al. (2007a) estimated chlorophyll yield and concentration in spinach by using NDVI values from a Greenseeker sensor and a multispectral imaging system. Freeman et al. (2007) collected Greenseeker sensor NDVI values and plant height measurements on individual corn plants at various growth stages and related them to individual plant biomass, forage yield and nitrogen (N) uptake. Flynn et al. (2008) evaluated spatial properties of grassland biomass with Greenseeker sensor NDVI data. A spectroradiometer is also a useful tool for the detection and monitoring crop growing status. Bronson et al. (2005) used Greenseeker NDVI to compare to NDVI values taken by a spectroradiometer to determine which device better estimated in-season plant N status. Darvishzadeh et al. (2008) examined the utility of hyperspectral remote sensing in predicting canopy characteristics by using a spectroradiometer. Zhang et al. (2009) characterised the spatial variation of NDVI derived from spectral reflectance measurements with a FieldSpec® (Analytical Spectral Devices, Inc., Boulder, CO, USA) spectroradiometer.

At the time this study was conducted, there were no other studies involved in evaluating aerial application of glyphosate using remotely sensed data. The objective

was to characterise the glyphosate efficacy applied with conventional and emerging aerial spray nozzles using ground-based spectral reflectance data.

MATERIALS AND METHODS

Study Site

The field used for this study was located in Burleson County, TX, USA (30°31’28”N, 96°24’25”W) and was treated with glyphosate on Mar 2, 2009. The field had been left fallow for the previous eight months and thus, was inundated with both broadleaf and grass weeds. Figure 4.1 is the photo of the study weedy field which was taken on Feb 24, 2009. The soil type of the study area, ShA, was Ships clay, 0 to 1 % slope, and rarely flooded (http://websoilsurvey.nrcs.usda.gov/app/WebSoilSurvey).

Figure 4.1. The photo of the study site taken on Feb 24, 2009.

Treatment Protocol

Treatments were applied in randomized complete blocks with three replications (Figure 4.1). Each replicate block was subdivided into five unique randomized treatments. This design strategy improved the accuracy of the comparisons among nozzle technologies by eliminating the variability among the replicates with a block, the order in which the five treatments were tested was randomly determined. Each treatment plot was three swaths wide (59 m) and (183 m) long and was delineated with a disked strip of soil (Figures 4.1 and 4.2).

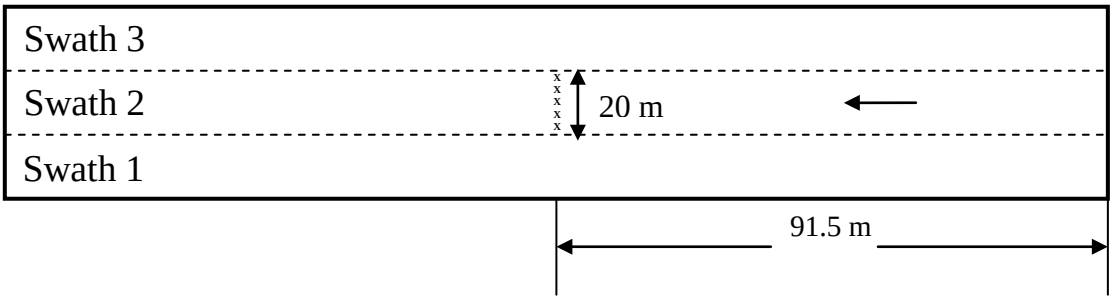

Figure 4.2. Sampling locations layout within each treatment plot.

A turbine-powered Air Tractor AT-402B agricultural aircraft (Air Tractor, Inc., Olney, TX, USA) was used to make all applications. Treatments were made with aerial electrostatic nozzles (Spectrum Electrostatic Sprayers Inc, Houston, TX, USA), CP-11TT 4015 hydraulic flat-fan nozzles (CP Products, Tempe, AZ, USA) and AU-5000 windmill-driven rotary atomisers (Micron Sprayers Ltd., Bromyard, Herefordshire, UK). Table 4.1 shows aircraft and nozzle settings for each treatment. The droplet $D_{V0.5}$ (or Volume Median Diameter (VMD)) is the diameter of droplet such that 50 % of the total

volume of droplets is in droplets of smaller diameter. The VMD values were determined using the USDA-ARS Spray Quality models (Kirk, 2007) using the nozzle and aircraft operating parameters, including spray pressure, nozzle type and deflection, and airspeed. The aircraft approached the field from the northwest and three passes (swaths) were required to apply chemical over one experimental plot. The spray height was 3 m.

Table 4.1. Spray treatment setups and droplet size information.

Treatment	Nozzle	Number of Nozzles	Rate (l ha^{-1})	Orifice	Deflection (degrees)	Pressure (kPa)	Airspeed (km h^{-1})	Target VMD[a] (µm)
1	Electrostatic Off	100	9.4	TXVK-8	0	483	209	200
2	Electrostatic On	100	9.4	TXVK-8	0	483	209	200
3	CP-11TT	39	28.1	15	0	241	210	350
4	AU-5000	8	28.1	VRU=Max[b]	Blade-65	241	177	350
5	Untreated Check	N/A	N/A	N/A	N/A	N/A	N/A	N/A

[a] VMD or $D_{V0.5}$ is the volume median diameter which is the diameter of droplet such that 50% of the total volume of droplets is in droplets of smaller diameter; values were estimated using the USDA-ARS Spray Quality model (Kirk 2007) [b] VRU is the variable rate unit for the Micronair AU5000 and is used to adjust flowrate to the nozzle. Max is the full open setting.

All treatments were made with Helosate Plus™ (Helm Agro US, Inc., Memphis, TN, USA) at 1168 ml ha^{-1} and 0.5 % v/v R-11 non-ionic surfactant (Wilbur-Ellis Co., Fresno, CA, USA). Helosate Plus contains 41% glyphosate (n-(phosphonomethyl) glycine), in the form of its isopropyl amine salt. The spray mixture also contained Caracid Brilliant Flavine fluorescent dye at a rate of 37 g ha^{-1}.

Sensing System

A sensing system (Lan et al., 2009b) was assembled using a Greenseeker® hand-held data collecting and mapping unit (NTech Industries, Inc., Ukiah, CA, USA) and a FieldSpec® (Analytical Spectral Devices, Inc., Boulder, CO, USA) handheld spectroradiometer. The Greenseeker and FieldSpec sensors were mounted on a tractor at the height of 1 m above the ground. Sampling was carried out as the tractor was driven along the strips which were marked in the centre of each treatment plot (Figures 4.1 and 4.2). The spectral data collection in the centre swath was used for statistical analyses to avoid the effects of cross contamination between treatments.

As the Greenseeker sensor moved over the field, it measured incident and reflectance light from the target and outputted NDVI readings. Weeds within each plot responded in a similar manner to treatments, so the NDVI data of the centre swath of each treatment plot were averaged to give a single value for each treatment. The analysis of variance (ANOVA) was carried out based on the experimental data using R statistics software (http://cran.r-project.org). Treatment variables were considered fixed and variations in experimental treatments were considered random.

The FieldSpec, with an angular field-of-view of 25^{o}, scanned approximately 0.154 m^2 of weedy field. The spectroradiometer collected spectral data from the ground ranging from a wavelength of 325 nm to 1075 nm with a sampling interval of 1.6 nm. The spectroradiometer produced 512 continuous data points with each reading. Ten spectral measurements were taken from each treatment plot. By averaging these ten measurements, a single reflectance measurement was obtained for each treatment plot,

thereby, minimising measurement noise. The instrument optimisation and white reference measurements were performed prior to each treatment plot measurements according to Castro-Esau et al. (2006). The spectroradiometer was adjusted to 10 scans per dark current and the integration time was set at 217 ms. The reflectance values at the 680 nm wavelength in the red region and the 800 nm wavelength in the NIR region were used to calculate the narrowband NDVI for each spectral measurement (Castro-Esau et al., 2006). ANOVA test was also carried out based on the NDVI data measured with the FieldSpec. All the field tests were conducted between 12:00 and 14:00 at 1, 8, and 17 days following aerial treatment (DAT).

RESULTS AND DISCUSSION

Greenseeker NDVI

The ANOVA test results on DAT 1 and DAT 8 did not show any difference among treatment means. The ANOVA test on DAT 17 is shown in Table 4.2. Nozzle type had a significant effect on glyphosate efficacy ($p = 0.0315$ at $\alpha = 0.05$). The normal plot of residuals and the residuals versus predicted value plot were checked and there was no severe indication of non-normality, nor was there any evidence pointing to possible outliers.

The analysis indicated a significant difference in treatment means, so the comparisons between paired treatments were conducted using Tukey's HSD (Honestly Significant Difference) in R (Table 4.3). Only treatment 3 was significantly different from treatment 5 at $\alpha = 0.1$ level. There was no significant difference between the other two treatments.

Table 4.2. Analysis of variance test result on DAT 17 (Greenseeker data).

Source	Degree of freedom	F-Value	P-value (Prob > F)	
Block	2			
Model	4	4.62	0.0315	significant
A-Treatment	*4*	*4.62*	*0.0315*	
Residual	8			
Cor Total	14			
Std. Dev.	0.036	R^2	0.6981	
Mean	0.26	R^2_{adj}	0.5471	

Table 4.3. Tukey's HSD (Greenseeker data).

Treatment[a]	Mean Difference	d.f.	Standard Error	t for H0 Coeff=0	Prob > |t|
1 vs 2	0.066	1	0.029	2.26	0.2505
1 vs 3	0.083	1	0.029	2.87	0.1117
1 vs 4	0.065	1	0.029	2.24	0.2579
1 vs 5	-0.015	1	0.029	-0.53	0.9821
2 vs 3	0.018	1	0.029	0.61	0.9698
2 vs 4	-6.667E-004	1	0.029	-0.023	0.9999
2 vs 5	-0.081	1	0.029	-2.78	0.1250
3 vs 4	-0.018	1	0.029	-0.63	0.9657
3 vs 5	-0.099	1	0.029	-3.39	**0.0545***
4 vs 5	-0.080	1	0.029	-2.76	0.1289

[a] Treatment 1: electrostatic (off); treatment2: electrostatic (on); treatment 3: CP-11TT; Treatment 4: AU-5000; treatment 5: control

*Significant at α=0.1 level

FieldSpec Spectral Reflectance

The ANOVA test results for DAT 1 and DAT 8 did not show any difference among treatment means. The ANOVA test results on DAT 17 are presented in Table 4.4. Nozzle type had a significant effect on glyphosate efficacy (p = 0.0002 at α = 0.01 level). The result of Tukey's HSD (Table 4.5) reported that treatment 2, 3 and 4 were

significantly different from treatment 5 at α = 0.01 level; treatment 1 was significantly different from treatment 3 and 5 at α = 0.05 level; and treatment 1 was significantly different from treatment 4 at α = 0.1 level. The result did not show any difference

Table 4.4. Analysis of variance test result on DAT 17 (FieldSpec data)

Source	**Degree of freedom**	**F-Value**	**P-value (Prob > F)**	
Block	2			
Model	4	21.38	0.0002	significant
A-Treatment	*4*	*21.38*	*0.0002*	
Residual	8			
Cor Total	14			
Std. Dev.	0.029	R^2	0.9145	
Mean	0.17	R^2_{adj}	0.8717	

Table 4.5. Tukey's HSD (FieldSpec data).

Treatment[a]	**Mean Difference**	**df**	**Standard Error**	**t for H0 Coeff=0**	**Prob > |t|**
1 vs 2	0.044	1	0.024	1.86	0.4046
1 vs 3	0.098	1	0.024	4.15	0.0198**
1 vs 4	0.076	1	0.024	3.22	0.0690*
1 vs 5	-0.097	1	0.024	-4.12	0.0206**
2 vs 3	0.054	1	0.024	2.28	0.2427
2 vs 4	0.032	1	0.024	1.36	0.6685
2 vs 5	-0.14	1	0.024	-5.98	0.0022***
3 vs 4	-0.022	1	0.024	-0.93	0.8784
3 vs 5	-0.19	1	0.024	-8.27	0.0002***
4 vs 5	-0.17	1	0.024	-7.34	0.0005***

[a] Treatment 1: electrostatic (off); treatment2: electrostatic (on); treatment 3: CP-11TT; Treatment 4: AU-5000; treatment 5: untreated check

* Significant at α=0.1 level

** Significant at α=0.05 level

*** Significant at α=0.01 level

between treatments 1 and 2, 2 and 3, 2 and 4, and 3 and 4. Therefore, conventional flat-fan nozzles and rotary atomizers had better performance than the electrostatic nozzles with charging off. There was no evidence that the electrostatic nozzle with charging on was better than the electrostatic nozzles with charging off.

The average spectral reflectance values obtained by the FieldSpec spectroradiometer for each treatment plot from three replicates at DAT 1, DAT 8 and DAT 17 are shown in Figure 4.3, Figure 4.4 and Figure 4.5, respectively. Overall changes within the study field were observed from the shapes of the reflectance curves. Overall decreases in healthy weed area due to herbicidal control resulted in an increase in the blue and red reflectance and a decrease in the NIR reflectance. Since the soil type of the study field was the same, the effect of soil property was not a factor. As shown in Figure 4.3, the spectral reflectance responses from five treatment plots were similar at DAT 1. Treatment 3 had higher reflectance both in the visible and NIR wavelength regions at DAT 8 (Figure 4.4). At 17 days after treatment, there was a significant increase in the visible reflectance under treatment 3 (Figure 4.5). Compared to DAT 1, the reflectance at DAT 17 increased from about 8 % to 20 % in the blue region, 15 % to 38 % in the green region, and 15 % to 30 % in the red region. Basically, changes in the reflectance in the NIR region were not significant. Treatment 2 and 4 were comparable. It should be noted that at DAT 17, the untreated control (TRT5) had the smallest reflectance in the visible region but the largest reflectance in the NIR. It was concluded that the glyphosate herbicide efficacy under different aerial spray treatments could be differentiated from spectral responses over the visible and NIR spectrum regions.

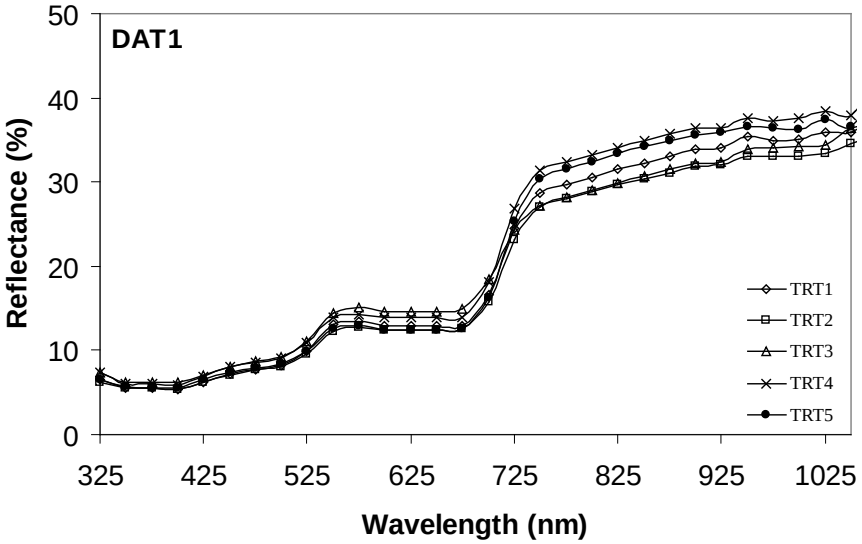

Figure 4.3. Average spectral reflectance curves for each treatment plot from three replicates at DAT 1.

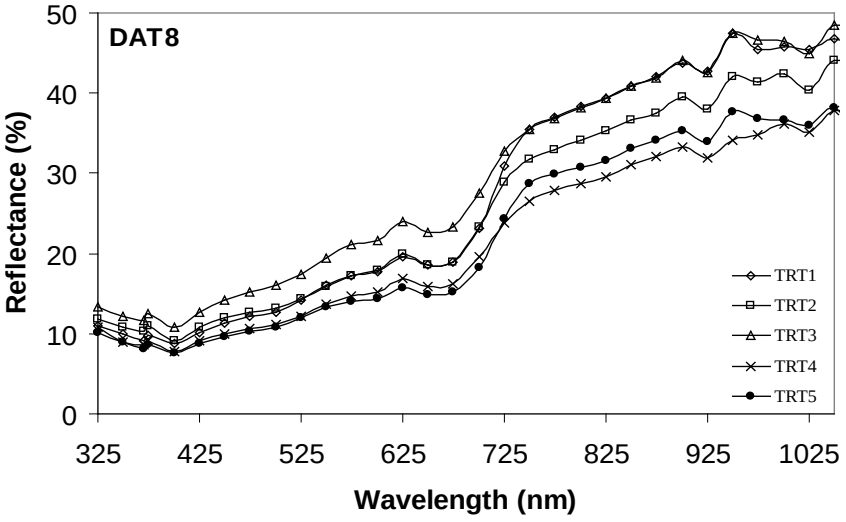

Figure 4.4. Average spectral reflectance curves for each treatment plot from three replicates at DAT 8.

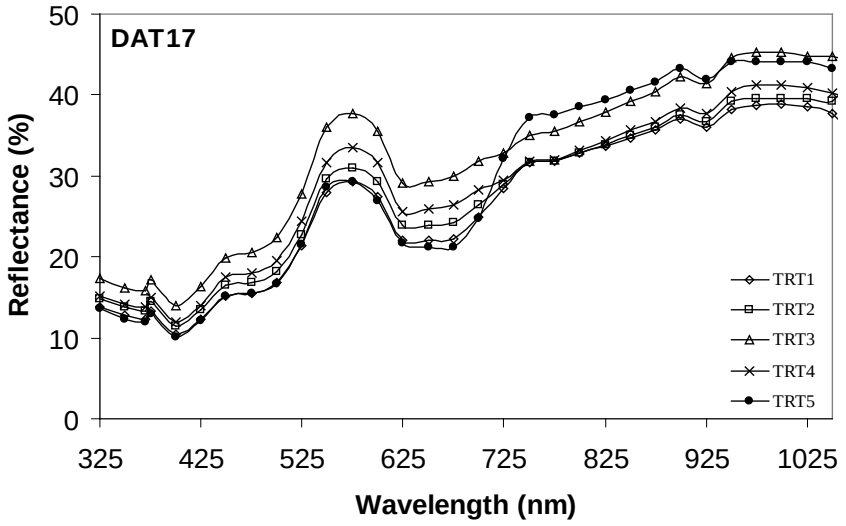

Figure 4.5. Average spectral reflectance curves for each treatment plot from three replicates at DAT 17.

CONCLUSIONS

The analysis of variance test results of NDVI measurements from the Greenseeker and FieldSpec collected data on DAT 1 and DAT 8 did not show any difference among treatments; however, a significant difference among treatment means on DAT 17 was observed. All the glyphosate application treatments provided effective weeds control as compared to untreated areas at DAT 17. The Tukey's HSD result of the Greenseeker data shows that there was no significant difference between any other two treatments except for treatment 3 and untreated area. The Tukey's HSD test result of NDVI measurements from the FieldSpec shows that applications using CP-11TT flat-fan nozzles and AU-5000 rotary atomisers were more efficacious in controlling weed populations than the electrostatic nozzles with charging off; but no evidence was

available to show that electrostatic nozzles with charging on was better than the electrostatic nozzles with charging off. Based on the analysis of spectral reflectance measurements with the FieldSpec spectroradiometer, the overall changes within the study field were observed from the shapes of the reflectance curves. Glyphosate herbicidal efficacy under different aerial spray treatments could be differentiated from spectral responses over the visible and NIR spectrum regions. At DAT 17, treatment 3 had the highest spectral reflectance in the visible wavelength bands.

Overall, the ground-based spectral reflectance data could be used to assess the glyphosate efficacy applied with different aerial spray technologies. This research showed that reflectance data obtained from ground based platform can be used to compare treatment performance for aerial herbicide application using different nozzle technologies. For this study, aerial herbicide applications performed within product label recommendations and were efficacious, regardless of the nozzle technology employed.

CHAPTER V

SPATIAL ANALYSIS OF NDVI READINGS WITH DIFFERENT SAMPLING DENSITY

OVERVIEW

Advanced remote sensing technologies provide researchers an innovative way to collect spatial data in precision agriculture. Sensor information and spatial analysis together allow for a detailed understanding of the spatial complexity of a field and its crop. The objective of the study was to describe field variability in the normalized difference vegetative index (NDVI) and characterize the spatial structure of NDVI data by geostatistical variogram analysis. Data sets at three different sampling densities were investigated and compared to characterize NDVI variation within the specified study area. Variograms were computed by Matheron's method of moments (MoM) estimator and fitted by theoretical models. The fitted spherical model was determined to be the best model for the data analysis in the study. The range of spatial dependence of the NDVI data was 40 m for sampling area of 4x3 m^2. Knowing the amount of remotely sensed data needed to characterize the spatial variation of the field with NDVI allows us to save sampling costs and prescribe nitrogen and other agrichemical applications.

INTRODUCTION

Advanced remote sensing technologies provide researchers an innovative way to collect spatial data in precision agriculture. Many commercially available sensors or optical instruments provide the capability of acquiring real time spectral information from vegetation. Studies have suggested that crop spectral reflectance can be used to assess plant nutrient and pigment status (Goel et al., 2003a; Osborne et al., 2002), monitor plant conditions at various scales (Blackmer et al., 1994; Plant et al., 2001), and crop biophysical variables (Thenkabail et al., 2000; Goel et al., 2003b).

Canopy spectral reflectance properties based on the absorption of light at a specific wavelength are associated with specific plant characteristics. The spectral reflectance in the visible wavelengths (400-700 nm) is low because of the high absorption of light energy by chlorophyll. The reflectance in the near infrared (NIR) wavelengths (700-1300 nm) is high because of the multiple scattering of light by different leaf tissues (Taiz and Zeiger, 2006). Vegetation indices have been developed with the reflectance data from red and NIR wavelengths and are often used to monitor crop growth conditions. The normalized difference vegetative index (NDVI) is a good indicator of vegetation, crop biomass and health in agricultural applications (Rouse et al., 1973; Tuker, 1979). NDVI is calculated as: NDVI= (NIR – Red) / (NIR + Red), where Red and NIR stand for the spectral reflectance measurements acquired in the red and near-infrared regions, respectively. Healthier crop canopies will absorb more red and reflect more near infrared light than stressed or unhealthy canopies, and consequently have a higher NDVI value. Sembiring et al. (1998) found that NDVI was a good

indicator of nitrogen (N) uptake of winter wheat. Freeman et al. (2007) collected NDVI with Greenseeker® (NTech Industries, Inc., Ukiah, Cal.) handheld sensor and plant height measurements on individual corn plants at various growth stages and related them to individual plant biomass, forage yield and N uptake. Bronson et al. (2005) used NDVI collected from different sensors to give a better estimation of in-season plant N status.

Remotely sensed data and spatial analysis together allow for a detailed understanding of the spatial complexity of a field and its crop. Determination of the spatial variability of field parameters is usually based on the concept that sampled values at nearby locations are more similar than those farther apart. Measurements from the field are usually gathered as point data, such as samples from an individual plant. Spatial analysis methods can be used to interpolate measurements to create a continuous surface map or to describe its spatial pattern (Cressie, 1993). As a powerful tool in geostatistics, variograms (also referred to as semivariograms) characterize the spatial dependence of data and give the range of spatial correlation, within which the values are correlated with each other and beyond which they become independent. The parameters of the best fitted model for a variogram can be used for kriging (Matheron, 1963; Stein and Corsten, 1991). Kriging has been recommended as the best method to interpolate point data since it minimizes the error variance using a weighted linear combination of the data (Panagopoulos et al., 2006). There are also numerous studies demonstrating the benefits of the geostatistical analysis techniques to agricultural management. Heisel et al. (1996) used kriging to map the density of weeds in winter wheat. Stewart et al. (2002) had used geostatistical methods to interpolate the data and produce maps of the field representing

the spatial variability of all the soil and wheat properties. With the aid of these maps and empirical modeling techniques, relationships between the wheat and soil factors were determined. Yamagishi et al. (2003) investigated the spatial variability of crop biomass and determined if site-specific management could be applied to a small field by using a variogram.

The large amount of remotely sensed data also could increase the sampling costs, provide redundant information and require complicated data analysis techniques. The issue has drawn considerable attention to specify the sampling requirements needed to accurately analyze the spatial property of an object. The objectives of this study were to describe the variability of a soybean field in NDVI, characterize the spatial structure of NDVI with different sampling data sets using variogram analysis, and determine an optimum sampling size that could adequately describe the field variation in canopy NDVI for the future studies.

MATERIALS AND METHODS

Study Site

The study site consisted of a 15 x 65-m^2 area within an approximately 1- ha soybean field near College Station, Texas (30°12’13”N, 96°12’57”W). The soybeans (Variety HBK C5025, Hornbeck Seed Co., Dewitt, AR) were planted on March 31, 2008 with a row spacing of 1 m and rows oriented in the east-west direction. Nitrogen was applied as ammonium sulfate (336 kg ha^{-1}) broadcast prior to planting and incorporated into the beds. The field was irrigated weekly as needed during the pod fill period.

Sampling Design and Data Collection

At the end of June 2008, the plants on the north side of plot reached senescence, while the other plants were growing vigorously. To assess the spatial variation of soybean plants within this area, spectral reflectance measurements were conducted along four selected rows with a FieldSpec® handheld hyperspectroradiometer (Analytical Spectral Devices, Inc., Boulder, CO). The distance between selected rows was 3 m. The sampling position along each row was marked by a 2-m. Thus, the sampling grid was 2x3-m^2. Each row comprised 32 sampling points for a total of 128 observations.

The FieldSpec handheld hyperspectroradiometer was positioned with a nadir view from a height of about 2 m above the ground. With an angular field-of-view of 25^o, it scanned approximately 0.62 m^2 of field area. The spectroradiometer collects data from the canopy ranging from a wavelength of 325 nm to 1075 nm with a sampling interval of 1.6 nm. The spectroradiometer outputs 512 continuous data points with each reading. A sunny day was chosen for the field test and all data were collected around solar noon time. The instrument optimization and white reference measurements were performed prior to sample measurements using the RS^3 software (Analytical Spectral Devices, Inc., Boulder, CO). The spectroradiometer was adjusted to 10 scans per dark current and the integration time was set at 217 ms. All the reflectance measurements taken from each rows were completed within half an hour. The reflectance values of 680 nm wavelength in the red region and 800 nm wavelength in the NIR region were chosen to calculate NDVI (Castro-Esau et al., 2006).

Statistical Analysis

Descriptive statistics for NDVI values was performed and the outliers and anomalies were examined using R-2.8.0 (R Development Core Team 2008). The autocorrelation analysis was applied to each row. The spatial structure of NDVI readings was determined by using geostatistical techniques and variogram analysis.

Variogram

Variograms were computed for three data sets, one was all the NDVI data at the 2-m sampling interval (2x3-m^2 sampling area); the second one was reduced to sampling points at a 4-m interval (4x3-m^2 sampling area); and the third one was reduced to sampling points at a 6-m interval (6x3-m^2 sampling area). This resulted in 128, 64 and 40 measurements being used for the 2-, 4-, and 6-m spatial analysis, respectively. The procedures for detecting trend and anisotropy were performed.

The experimental variogram was computed by Matheron's (Matheron, 1965) method of moments (MoM) estimator. The equation is given by equation:

$$\hat{\gamma}(h) = \frac{1}{2m(h)} \sum_{i=1}^{m(h)} [z(x_i) - z(x_i + h)]^2 \qquad (5.1)$$

where $\hat{\gamma}(h)$ is an unbiased estimate of the variance of these *m(h)* pairs of NDVI readings; $m(h)$ is the number of sampling pairs separated by a lag h for i=1, 2, . . ., $m(h)$; $z(x_i)$ and $z(x_i+h)$ are the NDVI values at locations x_i and (x_i+h), respectively.

Theoretical Models

The experimental variograms were fitted (based on a weighted least squares approximation) with theoretical models that provide three key parameters: the nugget variance, the sill variance, and the range of spatial dependence. These model parameters described the spatial structure of NDVI readings. With sample sizes of 128 and 64 in this study, it satisfied the requirement of acquiring reliable estimation of a variogram by MoM (Webster and Oliver 1992; Kerry and Oliver 2007). Therefore, the spherical and exponential models were fitted to the variogram computed from the 2-m interval and 4-m interval data sets. For the 6-m interval data set, the variogram was estimated by the maximum likelihood (ML) approach and compared to those estimated by MoM (Lark 2000). On the basis of the least Sum of Squares or Akaike information criterion (AIC) (Akaike, 1973), a good fit model was chosen and the parameters of the model were used for kriging. Overall, the model with a smaller nugget and lower nugget to sill ratio will be chosen.

The spherical model is one of the most commonly used models for experimental data (Webster and Oliver, 2007) and expressed as:

$$\gamma(h) = \begin{cases} c_o & \text{when } h = \varepsilon \text{ (a very small lag)} \\ c_0 + \mathrm{c}\left(\dfrac{3h}{2a} - \dfrac{1}{2}\left(\dfrac{h}{a}\right)^3\right) & \text{when } 0 < h \le a \\ c_0 + \mathrm{c} & \text{when } h > a \end{cases} \qquad (5.2)$$

where c_o is the nugget variance, c is the sill, h is the lag and a is the range. All variograms computed in this study are all fitted with spherical model.

The exponential model has been used commonly because of its generality. In the isotropic case it is given by equation:

$$\gamma(h) = \begin{cases} c_0 + c(1 - \exp(h/r)) & \text{for } h > 0 \\ 0 & \text{for } h = 0 \end{cases} \qquad (5.3)$$

The non-linear parameter r defines the spatial scale of the variation. The sill is approached asymptotically. For practical purposes $a = 3r$ is regarded as the effective range of the exponential model, which is the lag at which the sill reaches approximately $c_0 + 0.95c$ **(**Webster and Oliver, 2007). The variogram analyses, experimental variogram computing, model fitting and kriging were performed with the geoR package in R software.

RESULTS AND DISCUSSION

Descriptive Statistics

For the four rows, NDVI data were plotted (Figure 5.1) and descriptive statistics of NDVI data at three sampling intervals were calculated (Table 5.1). Mean, median, and standard deviation of three data sets were similar. Student t-tests were performed for three data sets and there was no significantly difference among means. In other words, the decrease in the sampling density did not affect the properties of NDVI data. No transformation of the data was necessary for geostatistical analysis.

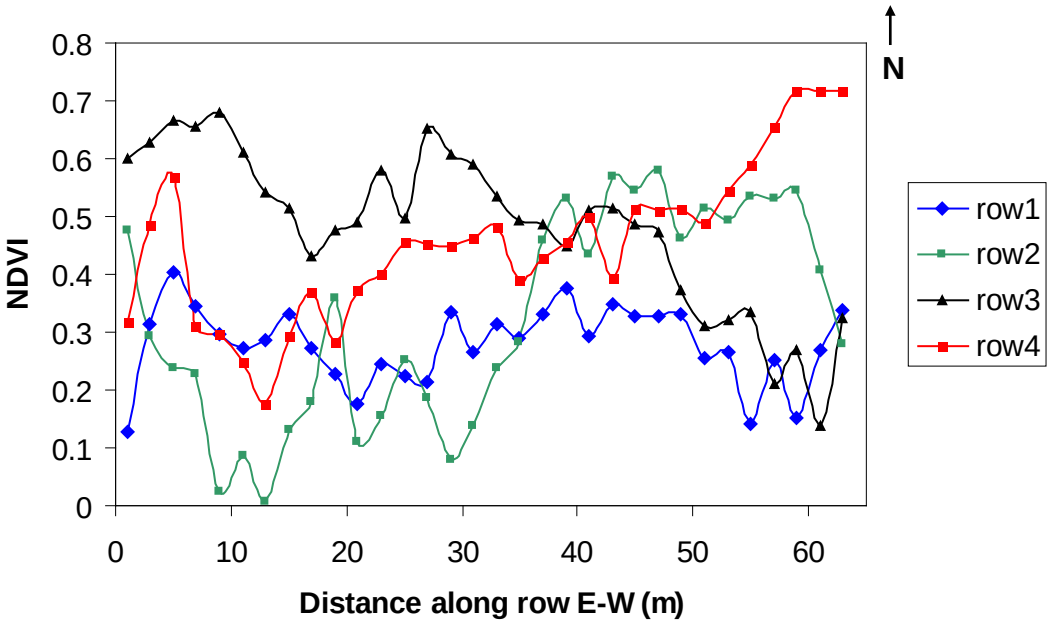

Figure 5.1. NDVI data for four rows.

Table 5.1. Descriptive statistics of NDVI for three data sets in the study area.

Parameter	2m data set	4m data set	6m data set
Mean	0.3850	0.3810	0.3780
Median	0.3721	0.3876	0.3653
SD	0.1601	0.1640	0.1589
Skewness	-0.0198	-0.19	-0.097
CV (%)	41.59	43.08	42.04
Count	128	64	44

Geostatistical Analysis

The existence of anisotropy was assessed first. Anisotropy was tested in four directions. The direction of the maximum continuity was found along rows and the direction of the minimum continuity was perpendicular to rows. The calculation of

semivariance was restricted to the direction of rows only. The NDVI variograms computed for 2-m interval, 4-m interval and 6-m interval data sets are shown in Figure 5.2. There were no evident differences in shape and semivariance magnitude between sample densities.

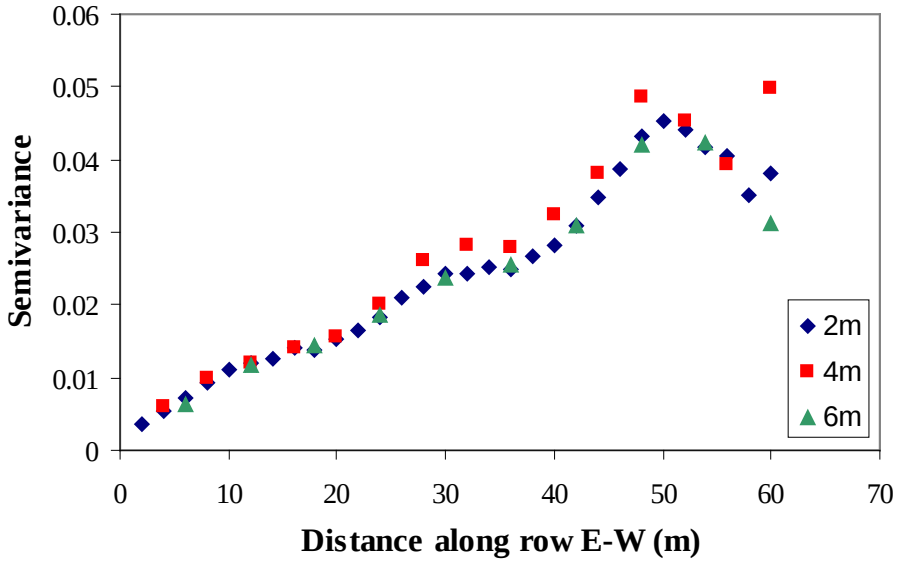

Figure 5.2. Variograms of three NDVI data sets in the study field: 2-m interval (red), 4-m interval (blue) and 6-m interval (green).

Exponential and spherical models were fitted to the variograms computed for the 2-m interval and 4-m interval data sets (Figures 5.3 and 5.4). Figure 5.5 indicated that the variogram computed for the 6-m interval data set was fitted with exponential and spherical models estimated by weighted least squares and maximum likelihood.

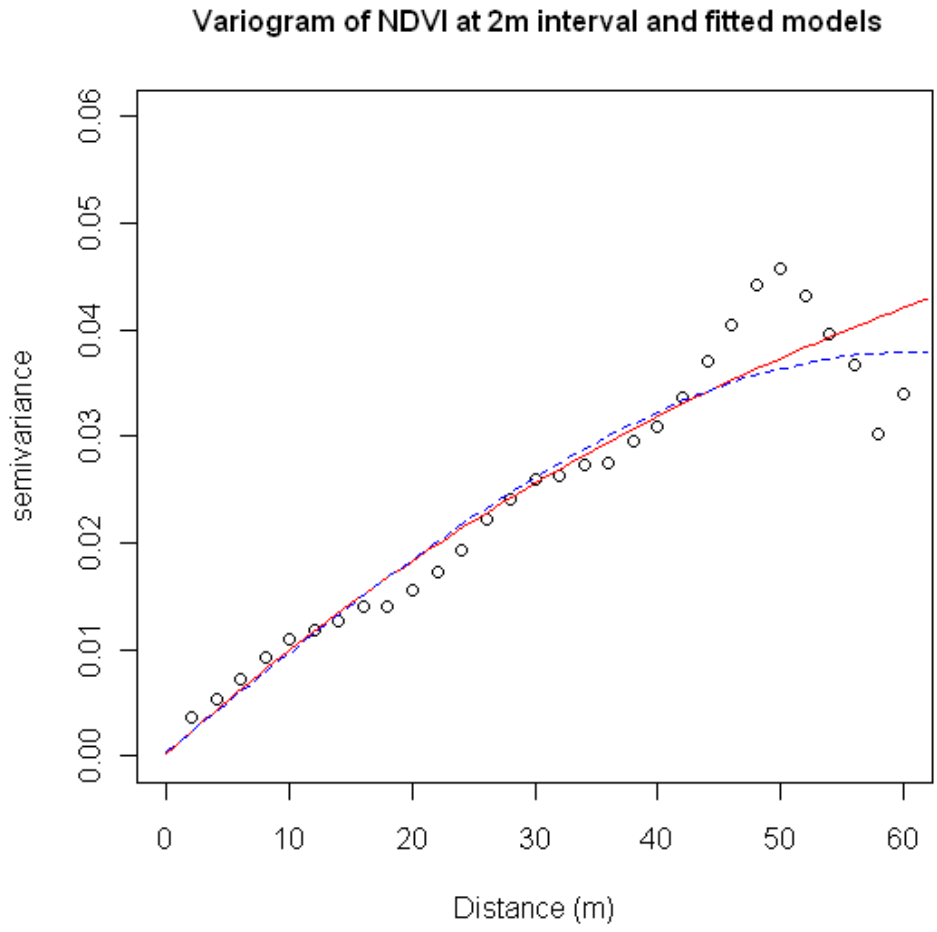

Figure 5.3. Variogram of NDVI data set (2-m interval) in the study field: experimental variogram calculated by method of moments estimator (o); exponential (red solid) and spherical (blue dashed) models fitted by weighted least squares.

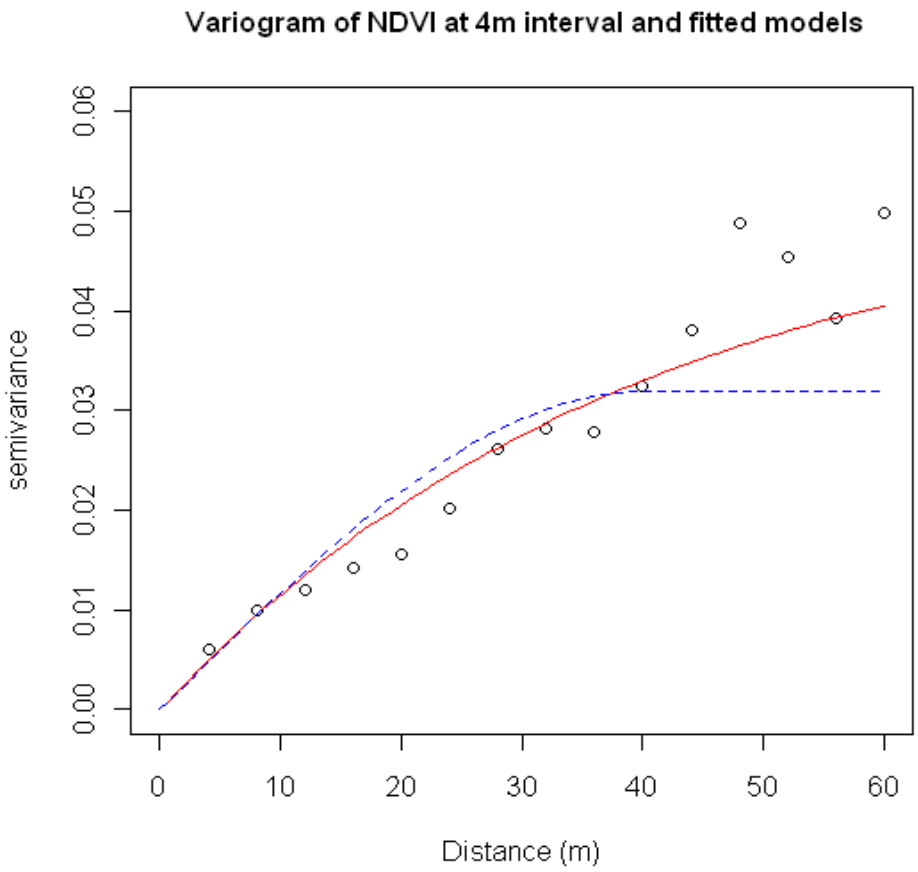

Figure 5.4. Variogram of NDVI data set (4-m interval) in the study field: experimental variogram calculated by method of moments estimator (o); exponential (red solid) and spherical (blue dashed) models fitted by weighted least squares.

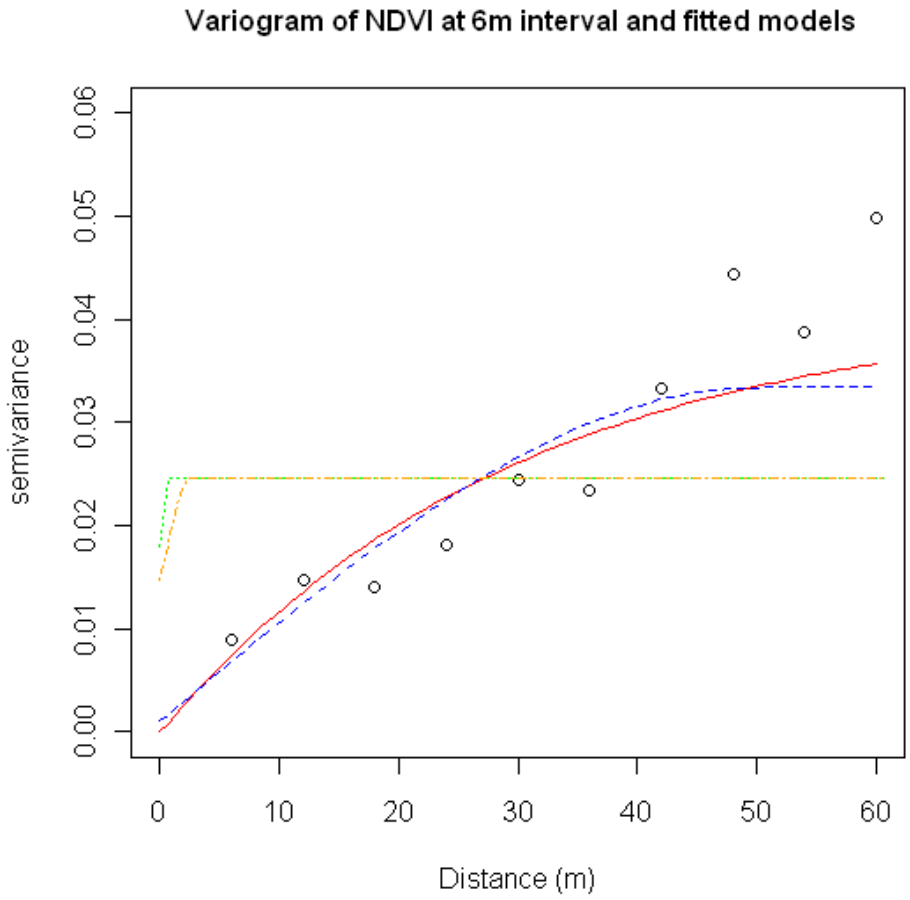

Figure 5.5. Variogram of NDVI data set (6-m interval) in the study field: experimental variogram calculated by method of moments estimator; exponential (red solid) and spherical (blue dashed) models fitted by weighted least squares and exponential (green dotted) and spherical (orange dotdash) models fitted by Maximum Likelihood.

The variogram parameters are summarized in Table 5.2. For the 2-m interval data set, the sum of squares of exponential model and spherical model were same, but the exponential model had a smaller nugget and nugget to sill ratio. For the 4-m interval data

set, both exponential and spherical models had zero nuggets. The sum of squares of spherical model was smaller than that of exponential model. Moreover, the range of the exponential model was larger than the length of the row. The range of the spherical model was 40 m, beyond which the NDVI became independent. Although the calculation of a variogram is suggested to use with maximum likelihood when the data size is less than 50, both models fitted for 6-m interval data set had high nugget to sill ratios in this case. Also from Figure 5.5, the maximum likelihood models were far away from the variogram and could not give a better fit and more information than the other two models estimated by MoM. Overall, the spherical model for 4-m interval dataset had the range of 40 m, zero nugget and nugget to sill ratio, the smallest sum of squares and good fit with visual inspection (Figure 5.4). The parameters of the spherical model for the 4-m interval data set were used for kriging and predicting of NDVI values at unsampled locations.

Table 5.2. Parameters of exponential and spherical models fitted to the experimental variogram estimated by method of moments (MoM) (n=128) and maximum likelihood (n=64) that describe the spatial structure of NDVI in the study field.

Model	Range (m)	Nugget	Sill	Nugget% [a]	Sum of Squares	AIC
2-m Interval						
Exponential	209	0.0003	0.0728	0.4	0.0108	
Spherical	60	0.0005	0.0379	1.3	0.0108	
4-m Interval						
Exponential	119	0	0.0522	0	0.0061	
Spherical	40	0	0.0319	0	0.0036	
6-m Interval						
Exponential	89	0	0.0413	0	0.0047	
Spherical	50	0.0011	0.0434	25.34	0.0051	
ML/exponential	0.15	0.018	0.0247	72.87		-30.01
ML/spherical	2.5	0.0147	0.0247	59.51		-30

a. Percentage nugget is calculated as Nugget/Sill x 100

Figure 5.6 shows the NDVI data map of the study area. The map describes the spatial variation of NDVI within the study field in a better way and adds more information and an easier understanding than the classical descriptive statistics analysis. Within the 15 x 65-m^2 area, NDVI values were very low on the northwest side, which indicated that the soybean plants were not vigorous and/or plants coverage was low. The variability perpendicular to the rows was large.

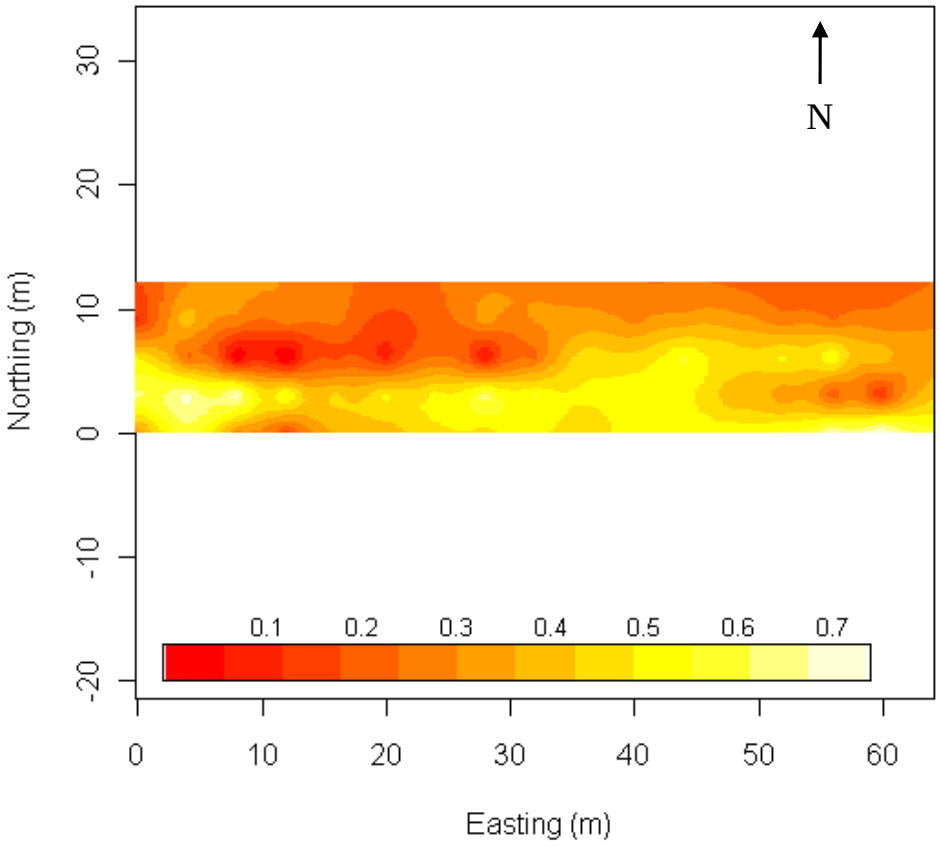

Figure 5.6. NDVI map of the study field.

CONCLUSIONS

This study revealed that the remote sensing vegetation index, NDVI, was suitable to assess crop ground cover and monitor crop growing status. NDVI data, analyzed by a geostatistical method, variogram and kriging, gave a better description of spatial variation within the field. In the study, the spatial dependence of NDVI data was 40 m with a sampling area of 4x3 m^2. Although it is possible to increase the sampling interval

to 6-m without lost spatial information, the parameters of the fitted model are not accurate enough for kriging. Compared to a sampling interval of 2 m, the use of the 4-m interval data set reduces the processing of redundant data without affecting the quality of the variation described. Knowing the amount of remotely sensed data needed to characterize the spatial variation of the field with NDVI allows us to save sampling costs and prescribe nitrogen and other agrichemical applications.

The study only considered three sampling densities for this field. The distance between rows was consistent. Different sampling area and spatial structure of other remotely sensed data will be examined in a future study.

CHAPTER VI

ANALYSIS OF VARIOGRAMS WITH VARIOUS SAMPLE SIZES FROM A MULTISPECTRAL IMAGE*

OVERVIEW

Variogram plays a crucial role in remote sensing application and geostatistics. It is very important to estimate variogram reliably from sufficient data. In this study, the analysis of variograms computed on various sample sizes of remotely sensed data was conducted. A 100 x 100 - pixel subset was chosen randomly from an aerial multispectral image which contains three wavebands, Green, Red and near infra-red (NIR). Green, Red, NIR and normalized difference vegetation index (NDVI) datasets were imported into R software for spatial analysis. Variograms of these four full image datasets and sub-samples with simple random sampling method were investigated. In this case, half size of the subset image data was enough to reliably estimate the variograms for NIR and Red wavebands. To map the variation on NDVI within the weed field, ground sampling interval should be smaller than 12 m. The information will be particularly important for kriging and also give a good guide of field sampling on our weed field in the future

---

*Reprinted with permission from "Analysis of variograms with various sample sizes from a multispectral image" by H. Zhang, Y. Lan, R. Lacey, Y. Huang, W. C. Hoffmann, D. Martin, G. C. Bora, 2009. *International Journal of Agricultural & Biological Engineering,* Vol 2, Page 62-69, Copyright [2010] by IJABE.

study.

INTRODUCTION

The techniques of spatial statistics were first developed and formalized in the 1950s. Recently, with the development of GIS, spatial statistical techniques have drawn considerable attention and have been widely applied in spatial data modeling and analysis for natural sciences such as geophysics, biology and agriculture. There are numerous studies demonstrating the benefits of the spatial analysis techniques to agricultural management (Stein et al., 1997 and Stewart et al., 2002). Geostatistics is a part of the spatial statistics. Geostatistical analysis consists of computing some function such as variogram (also referred to as semivariogram) to characterize the spatial variation in a region of interest.

The determination of the spatial variability of field parameters is usually based on the concept that sampled values at nearby locations are more similar than those from further apart. Measurements from the field are usually gathered as point data, such as an individual plant. Geostatitical analysis methods can be used to interpolate the measurements to create a continuous surface map or to describe its spatial pattern (Cressie, 1993). As a powerful tool in geostatistics, variogram describes the spatial dependence of data and gives the range of spatial correlation, within which the values are correlated with each other and beyond which they become independent. The parameters of the best fitted model for a variogram can be used for kriging (Matheron, 1963, and Stein and Corsten, 1991). Kriging has been recommended as the best method to interpolate point data since it minimizes the error variance using a weighted linear combination of the data (Panagopoulos et. al., 2006). Therefore, it is very important to

estimate variograms reliably from sufficient data and modeled properly (Oliver and Webster, 1991). The effect of sampling on the accuracy of sample variograms was studied from independently generated random fields (Webster and Oliver, 1992) and from experimental data (Van Meirvenne and Hofman, 1991). Brus and De Grunijtar (1994) concluded that design-based sampling strategies based on classical sampling theory offered unprecedented potentials for estimation of theoretical variograms. A sampling configuration, simple random sampling design, was tested for estimating the variograms of three soil properties in that study. Gascuel-Odoux and Boivin (1994) investigated the consistency of the sample variograms and spatial estimates by a sub-sampling procedure. They took five series of 20 sub-samples with different sample size of data points from the initial sample and found that the consistency of both experimental and fitted variograms increased with sample size.

Remotely sensed imagery constitutes a record of distinct spatial properties of the Earth's surface. Images can be treated as "field" data depicted by varied digital numbers (DN). These spectral values of pixels are spatially autocorrelated and their spatially dependent structures can be represented by variogram. Variogram has been estimated and investigated in a wide range of remote sensing applications (Curran, 1988; Jupp et al., 1988 a and b; Curran and Atkinson, 1998; Cohen et al., 1990; Atkinson and Curran, 1995; Oliver et al., 2000). Woodcock et al. (1988a and b) had studied the sensitivity of variogram by varying parameters of scene models in calculating explicit variograms, simulating images and real digital images. They found that the height of the variogram was affected by the density of the coverage of the objects in the scene and the range of

the variogram changed with the size of the object. They also found that when the variance in the distribution of the sizes of objects increased, the shape of the variogram curve becomes more round. Atkinson and Emery (1999) explored the relationship between wavelength and spatial structure which was summarized by the variogram. Several studies have applied the geostatistical analysis on various agricultural applications, such as soil properties (Cambardella and Karlen, 1999; Hengl et al., 2004; Iqbal et al., 2005; Ge et al., 2007), crop yield monitor data (Yang and Everitt, 2002; Dobermann and Ping, 2004; Miao et al., 2006) and crop qualities (Kravchenko and Bullock, 2002; John and Richard, 2005; Ge et al, 2008).

With advanced multispectral imaging systems, aerial images are now collected in several bands. Few studies investigated how the variogram changes with various sample sizes of data by given a certain remotely sensed imagery. The objective of the study was to explore the effect of sample size of image data on sample variogram estimation and find out how much image data could be used to estimate variogram reliably. Design-based simple random sampling was used for the sub-sampling procedure.

MATERIALS AND METHODS

The Image

The imaging system used to acquire multispectral image is TerraHawk® Aerial Imaging System. An MS4100 multi-spectral camera (Geospatial Systems, Inc., Rochester, NY) is the central component of the airborne multi-spectral imaging system. The image sensors are charge coupled device (CCD) array sensors with spectral sensitivity from 400-1000 nm and support three standard models for RGB, Color

Infrared (CIR) and RGB/CIR with blue band between 437 and 483 nm, green band between 520 and 560 nm, red band between 640 and 680 nm, and near infra-red (NIR) band between 767 and 833 nm. They approximated Landsat satellite (NASA, Washington DC and USGS, Reston, VA) bands. NIR, Red, and Green bands can be combined to make CIR image, which is often called “false-color” image. This band combination makes vegetation appear as shades of red. Brighter reds indicate more vigorously growing vegetation. Soils with no or sparse vegetation will range from white to greens or browns depending on moisture and organic matter content (Stein et al., 1999).

A CIR aerial image was obtained over the Texas AgriLife Research Farm (30.524588°N, 96.407181°W), College Station, Texas in Feb 2009. The field had been left fallow for the previous eight months and thus, was inundated with both broadleaf and grass weeds. The acquired raw image was calibrated and processed into reflectance image. A 100 x 100-pixel subset was randomly chosen from the reflectance image and highlighted in Figure 6.1.

Figure 6.1. Aerial multispectral image of Texas AgriLife Research Farm field, College Station, Texas obtained in Feb, 2009.

Variogram and Fitting Model

The sample variogram was computed by Matheron's method of moments (MoM) estimator. The spatial variance between the digital numbers of any two distinct pixels would depend on their separation distance, lag *h*. The semivariance, $\gamma(h)$, between any two pixels at a lag *h* can be expressed as:

$$\gamma(h) = \frac{1}{2} E[z(x) - z(x+h)]^2 \qquad (6.1)$$

where: $\gamma(h)$ is the semivariance at lag distance *h*, z(x) is the digital number of the pixel at location x. In the region of interest, suppose there will be *m(h)* pairs of pixels separated by a particular lag *h*. Their semivariance is given by equation:

$$\hat{\gamma}(h) = \frac{1}{2m(h)} \sum_{i=1}^{m(h)} [z(x_i) - z(x_i + h)]^2 \qquad (6.2)$$

where $\hat{\gamma}(h)$ is an unbiased estimate of the variance of these *m(h)* pairs of pixels, *m*(*h*) is the number of pairs of pixels separated by a lag h for i=1, 2, . . ., *m*(*h*), $z(x_i)$ and $z(x_i+h)$ are the digital numbers of z(x) at locations x and x+h, respectively. $\hat{\gamma}(h)$ is a useful measure of dissimilarity between spatially distributed regionalized variables. The larger $\hat{\gamma}(h)$ is, the less similar the pixels. The similarity between two pixels increases with decrease in the value of $\hat{\gamma}(h)$.

When a variogram is plotted using discrete experimental data points, it is called an experimental or sample variogram. A theoretical model can be fitted through the

experimental data points to quantify spatial patterns. The shape and description of a "classic" variogram (Curran, 1988; Curran and Aktinson, 1998) is shown in Figure 6.2.

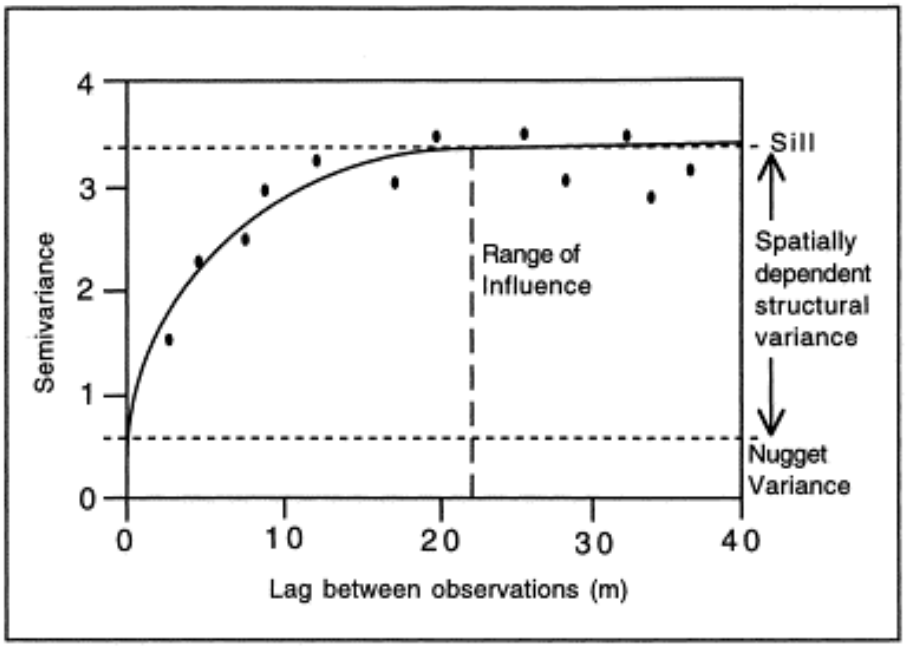

Figure 6.2. The shape and description of a "classic" variogram (Curran, 1988; Curran and Atkinson, 1998).

There are three key terms in each model, the sill, the range, and nugget variance. The sill corresponds to the overall variance in the dataset and the range is the maximum distance of spatial autocorrelation (Matheron, 1965). The nugget variance is the positive intercept of the variogram and can be caused by measurement errors or spatial sources of variation at distances smaller than the sampling interval or both.

The spherical model is the most commonly used model for experimental data (Webster and Oliver, 2007) and expressed as:

$$\gamma(h) = \begin{cases} c_o & \text{when } h = \varepsilon \text{ (a very small lag)} \\ c_0 + \mathrm{c}\left(\frac{3h}{2a} - \frac{1}{2}\left(\frac{h}{a}\right)^3\right) & \text{when } 0 < h \le a \\ c_0 + \mathrm{c} & \text{when } h > a \end{cases} \qquad (6.3)$$

where c_0 is the nugget variance, c + c_0 is sill, h is the lag and a is the range. All variograms computed in this study are all fitted with spherical model.

Data Collection and Analysis

The image was processed in the Environment for Visualizing Images (ENVI) software package (Version 4.5, ITT Visual Information Solution, www.ittvis.com). A 100 x 100-pixel subset was randomly selected from the image. The subset image and its NDVI were shown in Figure 6.3, respectively. Each subset comprised of total of 10,000 pixels. Since the spatial resolution of the image was 0.51 m, it covered 0.51 x 0.51 m^2 area of the field.

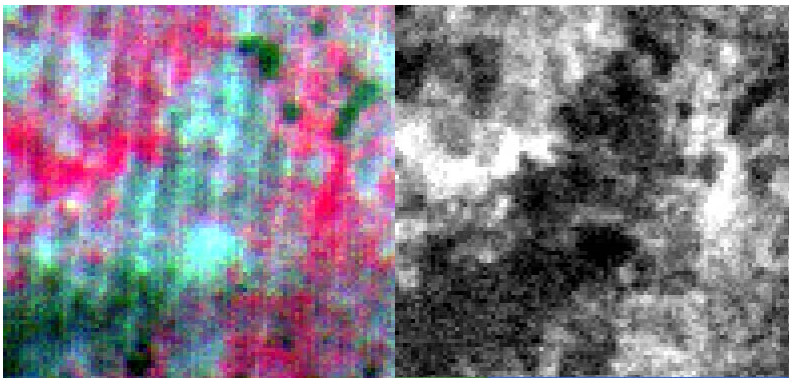

Figure 6.3. The subset image (left) and its NDVI (right).

These two datasets were exported as ASCII text files. The data file from original image contained the coordinates of the pixels and the pixel values of three wavebands, NIR, Red and Green. The data file of NDVI image contained the coordinates and the NDVI values of the pixels. These two data files were then imported into R statistical software(R 2.8.1, www.r-project.org) and converted into four geostatistical datasets, NIR, Red, Green wavebands and NDVI, with as.geodata function. Variograms were computed for each of the NIR, Red, Green wavebands and NDVI. The spherical model was fitted to those variograms and the sill, nugget and range were identified. To investigate how variograms and those parameters change with sample size, these four geodatasets were randomly sub-sampled in R. The sub-samples were taken independently from each other. For each sub-sample, locations were selected randomly and independently.

RESULTS AND DISCUSSION

Full Datasets Analysis

Geostatistical methods are optimal when data are normally distributed and stationary (mean and variance do not vary significantly in space). Significantly deviation from normality and stationarity can cause problems. The scatter plots of four geodatasets were shown in Figure 6.4. Each scatter plot consists of four subplots, which were x versus y coordinate plot, data versus y coordinate plot, x coordinate versus data plot, and the histogram plot. By looking at the histograms in the subplots of three wavebands and NDVI, severe deviation from normality was not observed. It can be noticed that there

were some hint of NW- SE trends from the subplots of data versus y coordinate for NIR and Green wavebands.

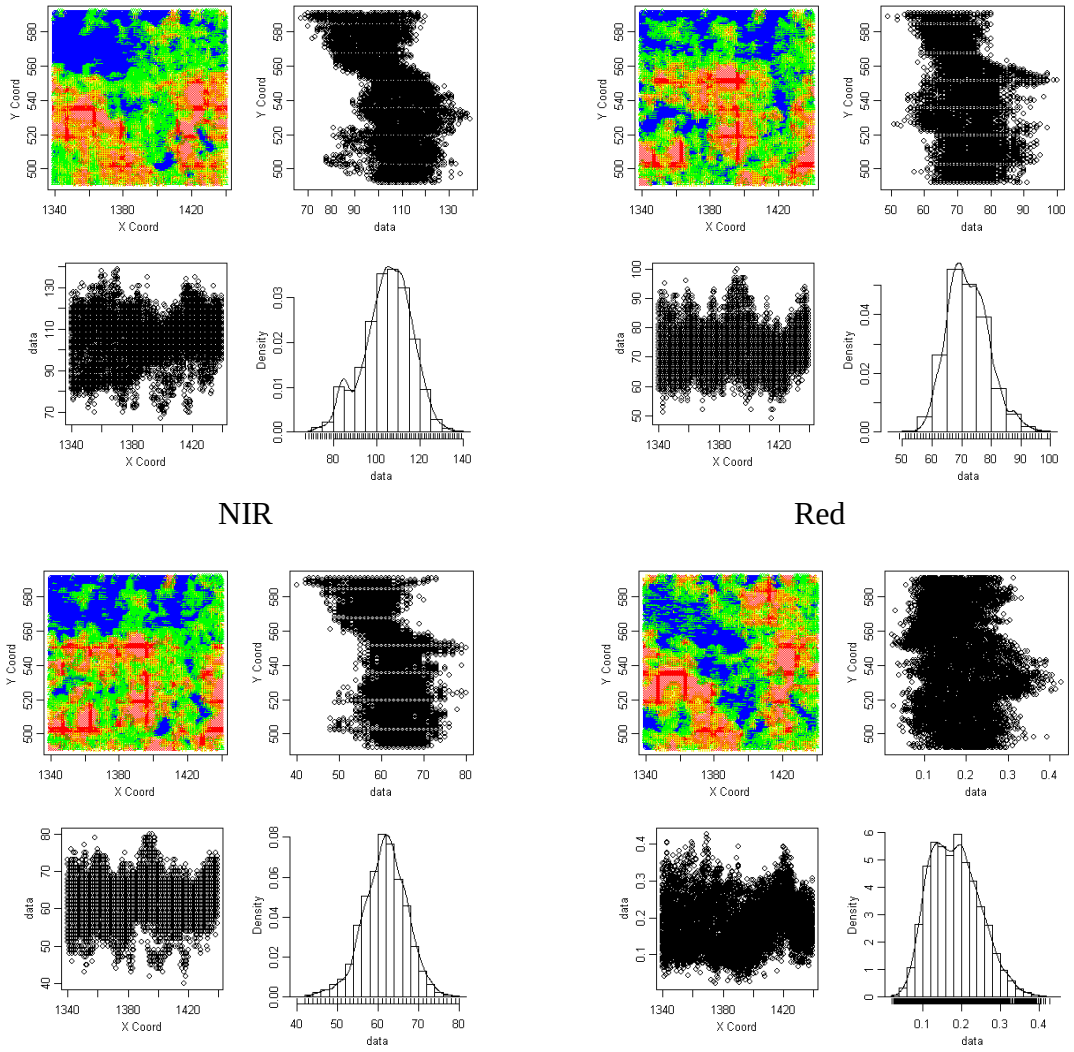

Figure 6.4. Plots of geodatasets: NIR, Red, Green, and NDVI.

Variograms were computed on them and fitted with spherical models (Figure 6.5). If the semivariance increases steadily over the separation distance, it is often

indicative of a significant spatial trend in the variable. The variograms for green waveband data indicated a significant trend. A spatial trend usually results in a negative correlation between variables separated by large lags. Trend surface fit is always needed. After trend surface fit for NIR, the range of variogram dropped from 137 to 23 pixels; the sill decreased from 141 to 41; and the nugget variance reduced from 50 to 34. For Red, detrending only reduced the range by 7 pixels but the partial sill and nugget variance

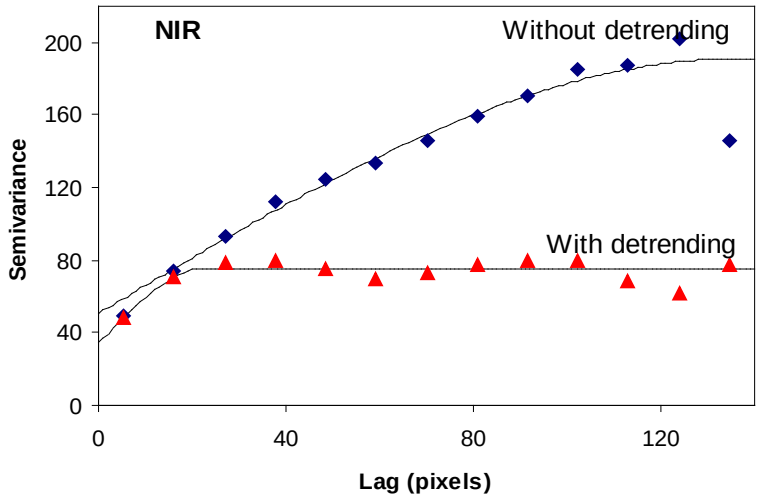

Figure 6.5. Variograms computed on NIR, Red, Green wavebands and NDVI with and without detrending.

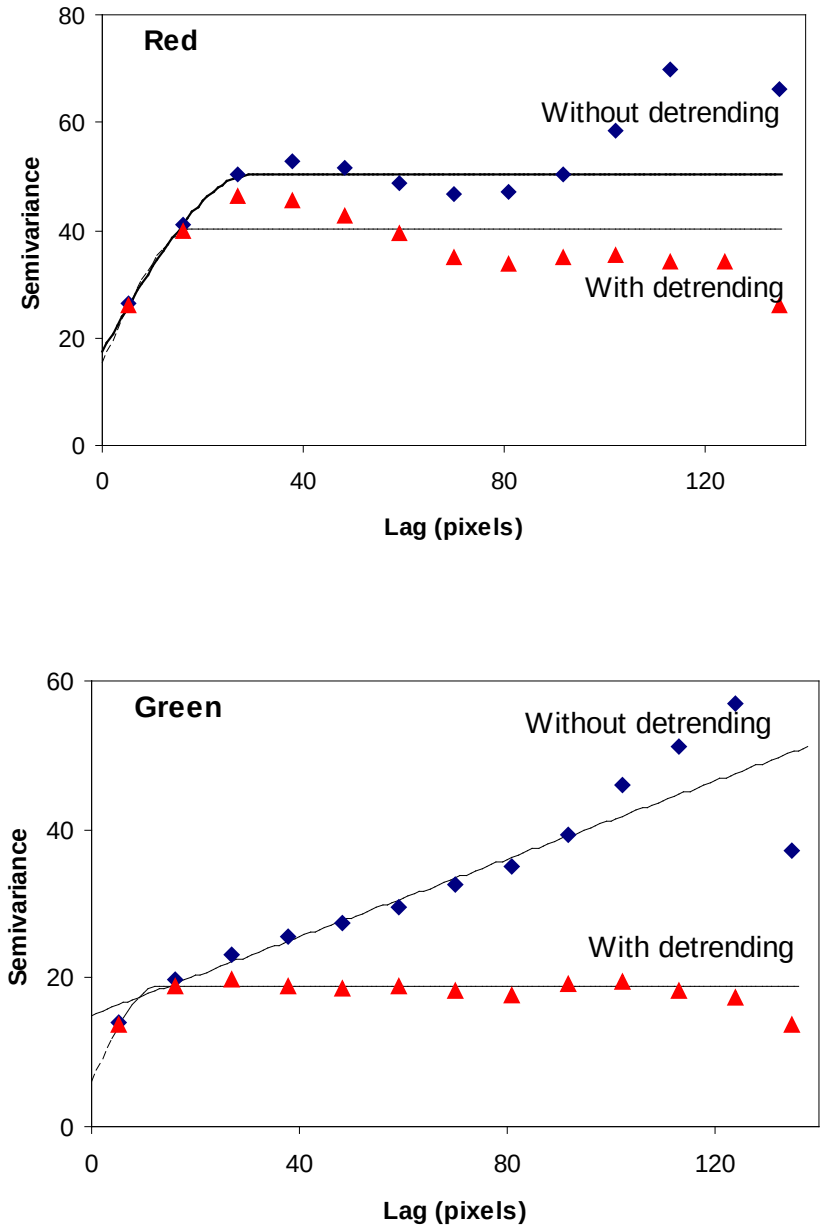

Figure 6.5. Continued

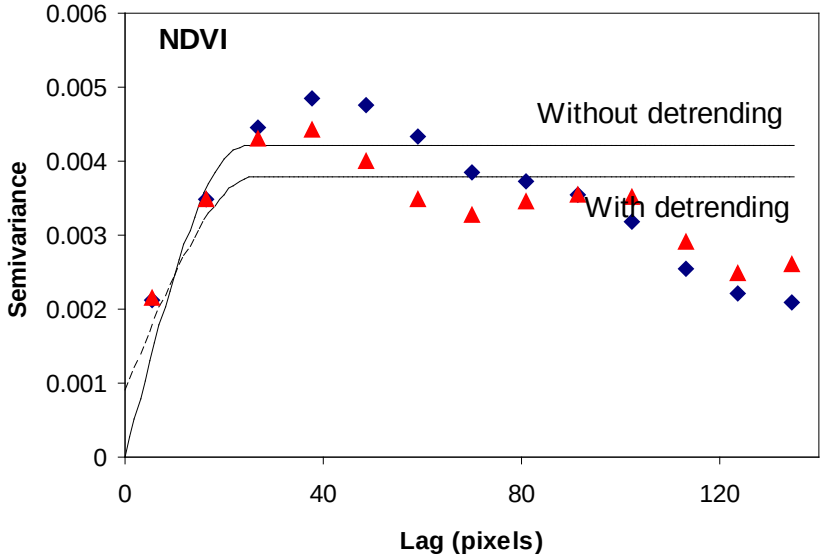

Figure 6.5. Continued

increased slightly. For Green, both range and partial sill of variogram decreased dramatically with detrending. There is no noticeable difference between two variograms for NDVI.

Sub-sampling on the NIR Band

The sample variograms for NIR were computed with samples sizes 50, 100, 300, 500, 1000, 2000, 3000, 4000, 5000, 6000, 7000, 8000, and 9000 pixels (Figure 6.6).

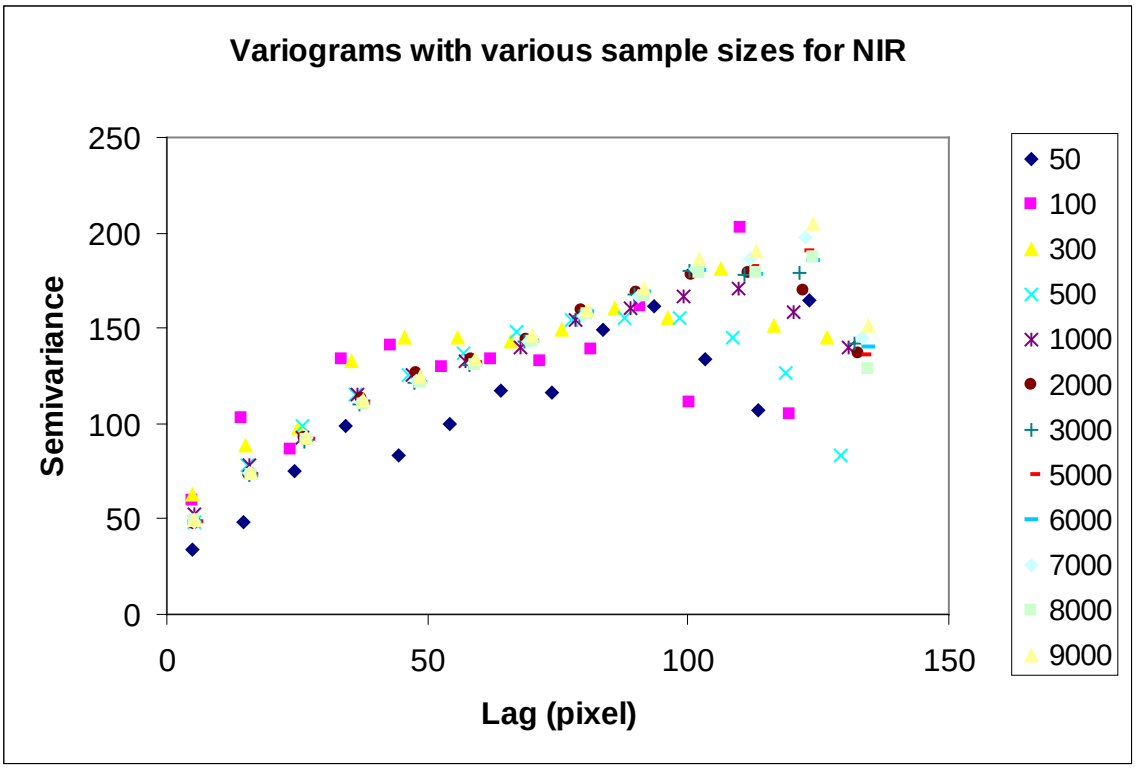

Figure 6.6. Sample variograms with sample sizes from 50 to 9,000 pixels for NIR.

All the parameters of variograms fitted with spherical models for NIR are summarized in Table 6.1. The range and partial sill of the sample size 50 were similar to those of the sample size 10,000. The range was 50 pixels for the sample size 100. The range was increasing until the sample size reaches 5000, which is half of the total sample size. After that, the range became almost stable. The nugget, sill, and nugget to sill ratio became stable after the sample size 1000.

Table 6.1. Parameters of variograms fitted with spherical models with various sample sizes for NIR waveband.

Sample size (pixel)	Rang (pixel)	Nugget	Sill	Nugget/Sill (%)
50	138	35	161	22
100	50	50	138	36
300	60	46	151	30
500	83	48	154	31
1000	107	55	165	33
2000	116	49	177	27
3000	128	49	183	27
4000	118	49	176	28
5000	136	50	187	27
6000	131	48	184	26
7000	136	52	188	27
8000	130	49	182	27
9000	139	51	193	26
10,000	137	51	192	26

Sub-sampling on the Red Band

The sample variograms for Red were computed on samples size 50, 100, 300, 500, 1000, 2000, 3000, 4000, 5000, 6000, 7000, 8000, and 9000 pixels (Figure 6.7).

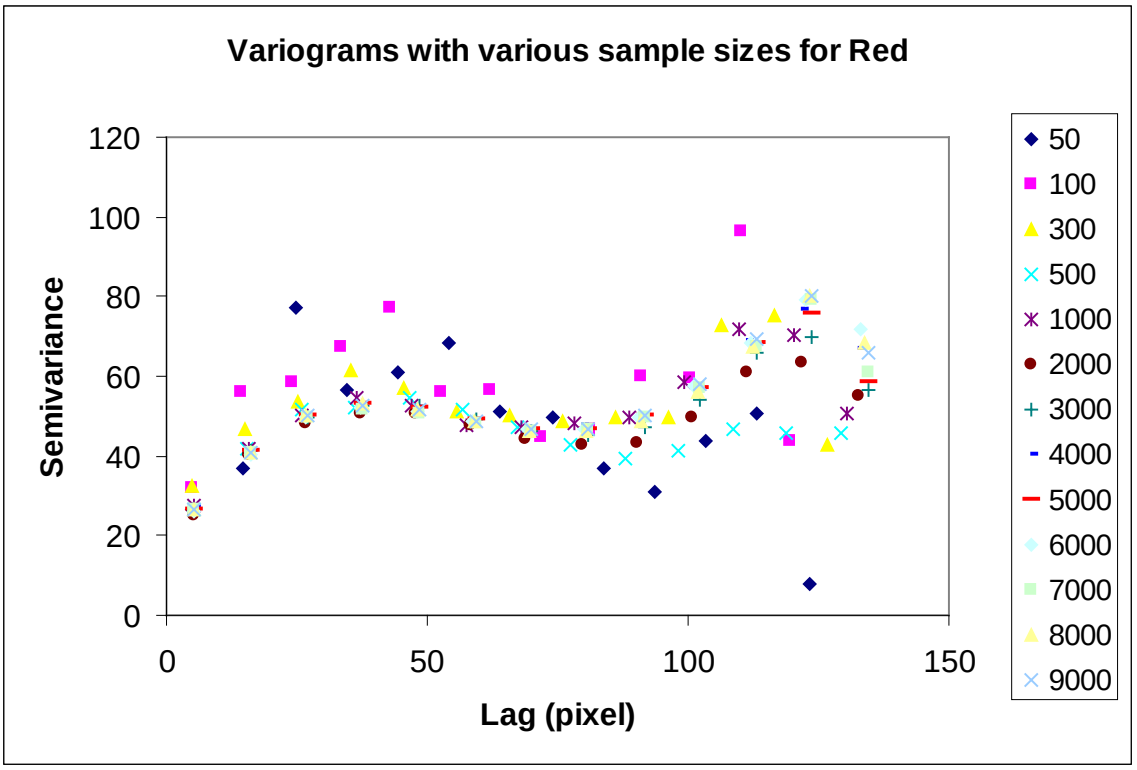

Figure 6.7. Sample variograms with sample sizes from 50 to 9,000 pixels for Red.

All the parameters of variograms fitted with spherical models for Red are presented in Table 6.2. The sample sizes of 50 and 100 appeared to be pure nugget models, which mean there was no spatial dependence in the data. From the sample size 300, the range gradually increased until the sample size 5000 with exception of sample size 1000, which might be caused by the randomly sampling process by the computer. Beyond the sample size 5000, all parameters became stable.

Table 6.2. Parameters of variograms fitted with spherical models with various sample sizes for Red waveband.

Sample size (pixel)	Rang (pixel)	Nugget	Sill	Nugget/ Sill (%)
50	361	54	54	100
100	656	58	58	100
300	14	10	53	19
500	14	10	53	19
1000	505	44	80	55
2000	28	16	48	33
3000	29	17	50	34
4000	31	19	51	37
5000	30	17	50	34
6000	30	17	50	34
7000	30	17	49	35
8000	29	17	50	34
9000	30	17	50	34
10,000	30	17	50	34

Sub-sampling on the Green Band and NDVI

Similar procedures had been undertaken for Green and NDVI. For Green, all variograms computed on all subsample sizes were similar to the variogram without detrending shown in Figure 6.5. For NDVI, all the variograms and model parameters were remarkably consistent. The scale of spatial dependence of the NDVI was 24 pixels, which was about 12 m on the ground.

CONCLUSIONS

In this study, the analysis of variograms computed on various sample sizes of remotely sensed data was conducted. A 100 x 100 - pixel subset was chosen randomly from an aerial multispectral image which contains Green, Red and NIR wavebands over

our weed study field. Green, Red, NIR and NDVI datasets were imported into R software for spatial analysis. By fitting with spherical models, behaviors of the major parameters of those variograms were investigated. In this case, it turned out that half size of the subset image data was enough to reliably estimate the variograms for NIR and Red wavebands. To map the variation on NDVI within the weed field, sampling interval should be smaller than 12 m. The information will be particularly important for kriging and also give a good guide of fieldwork in a future study.

CHAPTER VII

MULTISENSOR FUSION OF CHLOROPHYLL READINGS AND HYPERSPECTRAL MEASUREMENTS AND AIRBORNE IMAGERY IN THE DETECTION OF NITROGEN STATUS ON CROP CANOPY

OVERVIEW

Taking the advantages of airborne multispectral imagery and ground-based remote sensing data, the objective of this work was to investigate whether the multisensor fusion of ground-based SPAD chlorophyll meter readings, hyperspectral reflectance data, and aerial imagery data can improve the performance of remotely sensed data for the discrimination of crop nitrogen status under different treatment levels.

The multispectral imagery was acquired by an airborne imaging system over crop field; at the same period, leaf chlorophyll content and spectral reflectance measurements were gathered with SPAD 502 chlorophyll meter and spectroradiometer at canopy level on the ground, respectively. Statistical analyses were applied on the data from individual sensor for discrimination with respect to the nitrogen treatment levels. Multisensor data fusion was performed at data level. The results of analysis of variance on imagery, SPAD meter readings, and fused data of them showed that extracted first principal

component was able to detect the difference among different nitrogen treatment levels for cotton at the significant level of 0.05 (*p-value* = 0.0307). The results of discriminant analyses on imagery, FieldSpec hyperpectral reflectance data, and fused data with them indicated that the classification accuracy of fused data to detect the difference between N treatment and without N treatment on soybean was 100 % in both calibration and cross-validation steps with DISCRIM procedure in SAS. Fused data had better performance than the imagery for discrimination analysis.

Further research may be conducted to improve the performance of data fusion by using non-parametric classification models, such as neural network. The data fusion method may be extended to other types of data, and other level data fusion.

INTRODUCTION

Remote sensing technologies have been widely used for modern agricultural management. Various types of data have been provided for detecting crop conditions or soil properties by optical sensors or instruments from ground-based, airborne and space borne platforms. However, despite the availabilities of these sensors, few studies have examined multisensor fusion techniques for their data. In this study, the potential of multisensor fusion of ground-based and airborne imagery data was investigated for detecting crop nitrogen status. The method may be extended to other types of data.

Nitrogen (N) fertilizers are effective in driving crop yield improvement. The use of nitrogen fertilizer will be continued to increase substantially as global population and food requirements grow. International Fertilizer Industry Association (IFA) forecasts suggest that under current conditions nitrogen fertilizer applications will be totally 100

million tons per year by 2010-11. However, nitrogen fertilizers also have a negative impact on environment. Stern (2006) pointed out that nitrogen fertilizer accounts for one-third of greenhouse gases produced by agriculture.

Nitrogen is also one of the most expensive nutrients used for cotton production in Texas, and also the most difficult to properly manage because of its reactivity and mobility in the soil environment (Lemon et al., 2009). Inadequate N will cause the reduction of fruit quality and yield, whereas overdosed N will increase problems with disease, insects, and defoliation. Moreover, most plants are only able to utilize less than one-half of the N applied by growers and the remaining will leach into air, soil and water. Therefore, advanced nondestructive methods are needed to detect crop N status in the field and make a timely decision on where and in what amount N fertilizer needs to be applied. Remote sensing has been a promising tool for rapid identification of crop N status.

The presence of chlorophyll pigments in the leaf tissues influences the light reflectance by vegetation in the visible region of the spectrum. Since chlorophyll a and b absorb light in the red (660 and 650 nm) and blue (around 430 and 450 nm) regions of the spectrum (Jensen, 2005), they provide diagnosis of absorption features. The light reflected by vegetation in the NIR region of the spectrum is influenced by internal structure of leaf cell. Healthy green vegetation reflects 70 % light in the NIR region. Therefore, leaf chlorophyll content can be effectively characterized by spectral transmittance or reflectance measurements. The absorption and high reflectance feature

by crop canopy and leaf will provide critical information on leaf chlorophyll content, and subsequently, detect N status.

A positive correlation between leaf N or N fertilization rate and chlorophyll content has been well documented for a large number of plant species. Plants with increased levels of available N typically have greater leaf N concentrations, and more chlorophyll (Wolfe et al., 1988). The positive relationship means it should be possible to assess crop N needs from remotely sensed reflectance measurements of crop canopy and leaves (Walburg et al., 1982; Dwyer et al., 1991). Based on the difference in attenuation of transmitted light through a leaf sample at peak wavelengths of 650 and 940 nm, a hand-held chlorophyll meter, SPAD 502, has been developed by Minolta Co., Ltd. (Osaka, Japan) to measure leaf chlorophyll content. The value determined by the instrument provides an indication of the relatively amount of chlorophyll present in plant leaves. Wu et al. (1998) found highly significant linear relationships between SPAD values and contents of both N and chlorophyll at each growth stages. They also reported that the linear regression between SPAD values and N fertilizer levels were also highly significant. Their data provided evidence that the SPAD meter could be used to determine sidedress N requirements of short-season cotton before boll opening stage. Thompson et al. (1996) observed strong correlation of chlorophyll content with SPAD readings in soybean. Madeira et al. (2000) indicated that SPAD values may be used to determine algorithms to accurately estimate leaf chlorophyll in green beans. Fritschi and Ray (2007) found good correlation between extracted chlorophyll and SPAD readings for two soybean genotypes.

The major limitation of the chlorophyll meter is that readings are generally taken at a limited number of locations in the field. As such, the chlorophyll meter alone is not practical for characterizing crop N status on the whole field based. (Han et al. 2002).

Nowadays, airborne or space borne remote sensing has become important tools to provide time-specific information on crop within a large field or region. Shanahan et al. (2001) collected aerial imagery data with four bands periodically through the growing season. They showed that reflectance in the green and NIR bands in the form of green normalized difference vegetation index (GNDVI) had greater potential for assessing corn canopy variation when collected after tasseling than before tasseling. Han et al. (2002) compared the satellite and aerial imagery for detecting leaf chlorophyll content in corn. They reported that the correlation between SPOT images and SPAD data was similar to that between aerial images and SPAD data and it indicated that SPOT imagery has potential for detecting chlorophyll levels and nitrogen stress in corn. Tilling et al. (2007) reported that the normalized difference red edge (NDRE) index calculated from airborne multispectral imagery accounted for 41% of variability in wheat crop N status. Goel et al (2003a) used airborne hyperspectral data to estimate crop biophysical parameters within corn plots which were treated with combined different levels of weed control and N rates. The incorporation of more spectral reflectance in different wavelengths regions resulted in a better regression model. More than 90 % of the variation could be explained for many crop biophysical variables. However, it should be noticed that both satellite and aerial imagery can be comprised by cloud cover. More time are needed and more works need to be done to process the images, especially,

hyperspectral imagery. Although hyperspectral imagery can provide hundreds of wavebands, they are expensive and needs a lot of work to process a proper image. They are also not always available for farmers.

In precision agriculture practice, although those optical sensors and instruments which are fitted for different platforms have been demonstrated as promising tools for crop spectral reflectance measurements, only a few studies involved with multisensor data fusion for assessment of crop conditions. Bravo et al. (2004) combined hyperspectral reflection information between 450 nm and 900 nm and fluorescence imaging to detect and recognize foliar disease in wheat. Kaleita (2003) developed a methodology for mapping surface soil moisture content across an agriculture field from optical remote sensing data and limited ground sampling data. More efforts need to be made to apply multisensor fusion techniques to fuse data from different sensors and improve the performance of sensing systems.

Multispectral images can be a very useful tool for identifying crop N status and is relatively cheaper than hyperspectral imagery. Taking the advantages of airborne multispectral imagery and ground-based remote sensing data, the objective of this work was to investigate whether the multisensor fusion of ground-based SPAD chlorophyll meter readings, hyperspectral reflectance data, and aerial imagery data can improve the performance of remotely sensed data for the discrimination of crop nitrogen status under different treatment levels.

MATERIALS AND METHODS

Flowchart of Methodology

Figure 7.1 presents the flowchart of the methodology of data fusion. The data was gathered from remote sensing system onboard on aircraft and ground. The data from two platforms were preprocessed individually before being combined together. Different statistical analyses were applied on individual sensor data and fused data. The performance of data fusion was evaluated at last.

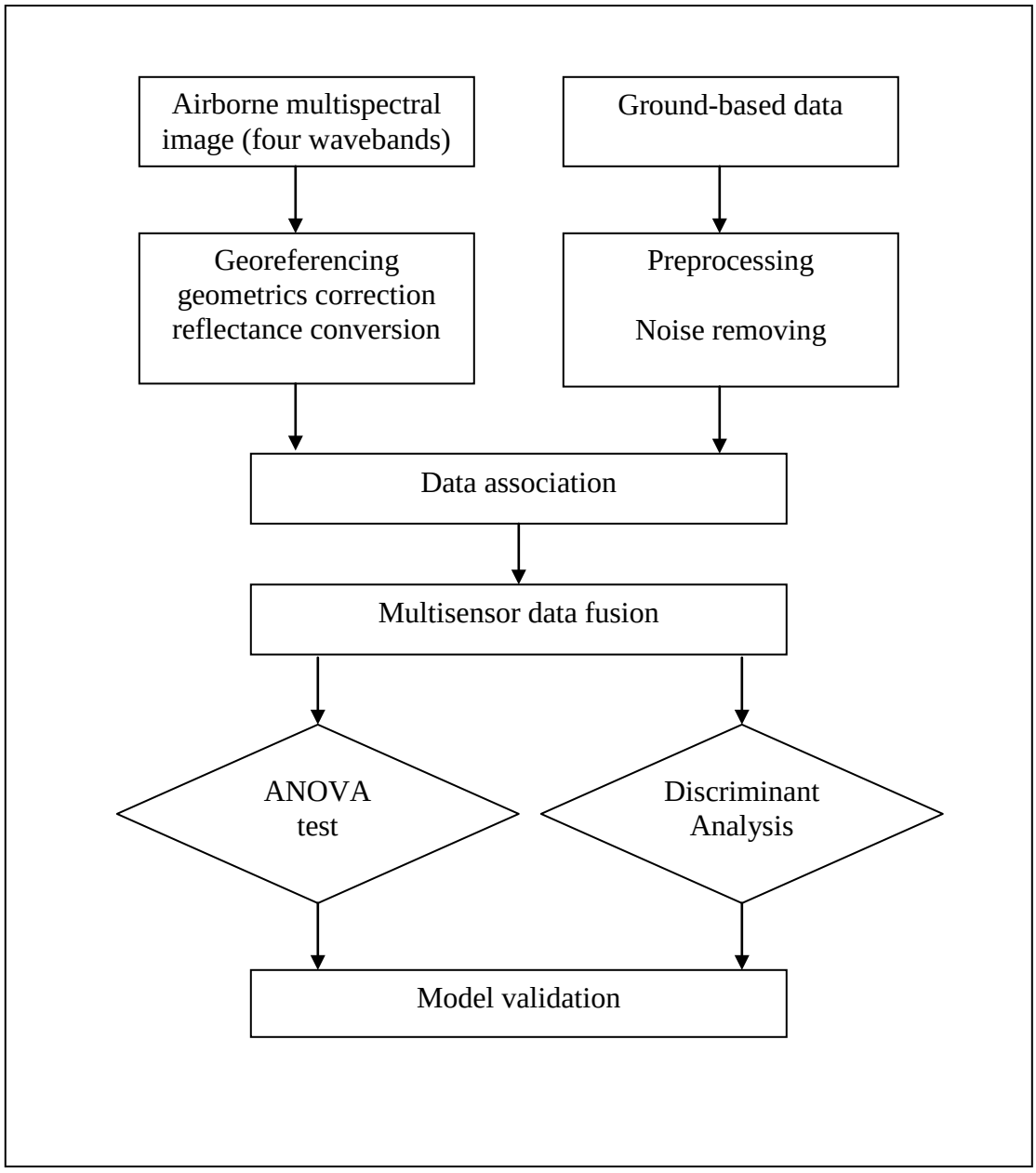

Figure 7.1. Flowchart of methodology.

Experimental Design

Field experiments were conducted at the Texas ArgiLife Farm of Texas A&M University at College Station. The cotton and soybean were planted on April 30, 2010.

Each crop field was divided into three blocks (replicates). Each replicate block was subdivided into three unique randomized nitrogen treatments, control (N0), 70 kg N ha^{-1}, (N1), and 140 kg N ha^{-1} (N2). Nitrogen treatments were supplied at the time of seeding. The plot size was about 9 x 21 m^2 with a 1 m buffer. Each plot consisted of eight rows of crop with a row spacing of 1 m and rows oriented in the east-west direction. The crops were grown under conventional tillage practice, and irrigated throughout the growing season. Plot layout is shown in Figure 7.2.

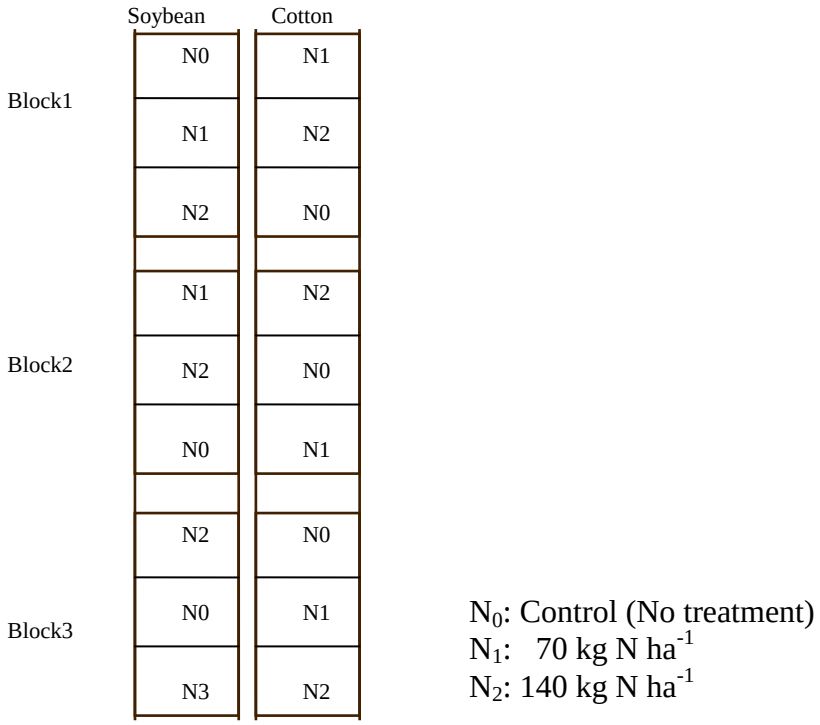

Figure 7.2. Layout of the experimental field.

Data Collection

Airborne Multispectral Image

The airborne imaging system described in Yang (2010) was used to capture aerial image in this study. The system consists of four high resolution charge coupled device (CCD) digital cameras and a ruggedized PC equipped with a frame grabber and image acquisition software. The cameras are sensitive in the 400 to 1000 nm spectral range and provide 2048 × 2048 active pixels with 12-bit data depth. The four cameras are equipped with blue (430-470 nm), green (530-570 nm), red (630-670 nm), and near-infrared (810-850 nm) band pass interference filters, respectively, but has the flexibility to change filters for desired wavelengths and bandwidths.

The multispectral image was acquired on June 18, 2010. The four bands image was georeferenced to the Universal Transverse Mercator (UTM), World Geodetic Survey (WGS 84), Zone 14, coordinate system based on ground control points around the field located with a meter-accuracy GPS unit. Then the image was rectified to a DOQQ image by performing image-to-image rectification. The pixel size for the rectified image was adjusted to 1 m. The total root mean square error (RMSE) was less than 1 m. All the steps were done in ENVI 4.5. Since this study was to evaluate the relationship between imagery data and ground-based reflectance data, the raw digital numbers of the image needs to be converted into reflectance values. For radiometric calibration of the imagery, two 8 m by 8 m tarpaulins were placed near the fields during image acquisition. The actual reflectance values from the tarpaulins were measured using the FieldSpec spectroradiometer. The rectified multispectral image was converted

to reflectance image based on the digital values of pixels and the reflectance data from the spectroradiometer.

Ground-based Data Collection

The sampling locations are shown in Figure 7.3. The five sampling locations (1 m^2 area) were marked within each plot with color flags. The measurements were not taken from the boundary rows of the plots. The coordinates was recorded with a meter-accuracy GPS unit (Thales Navigation, Santa Clara, CA) and later were used to correspond with the pixel data of the image. At each marked location, leaf chlorophyll content (greenness) was measured with SPAD 502 chlorophyll meter. Each recorded observation was the mean of five measurements from the plants within 1 m^2 of each flag. Measurements were taken on the middle of fully developed leaves on the top of the plants. Five measurements were averaged to one value to represent the mean leaf

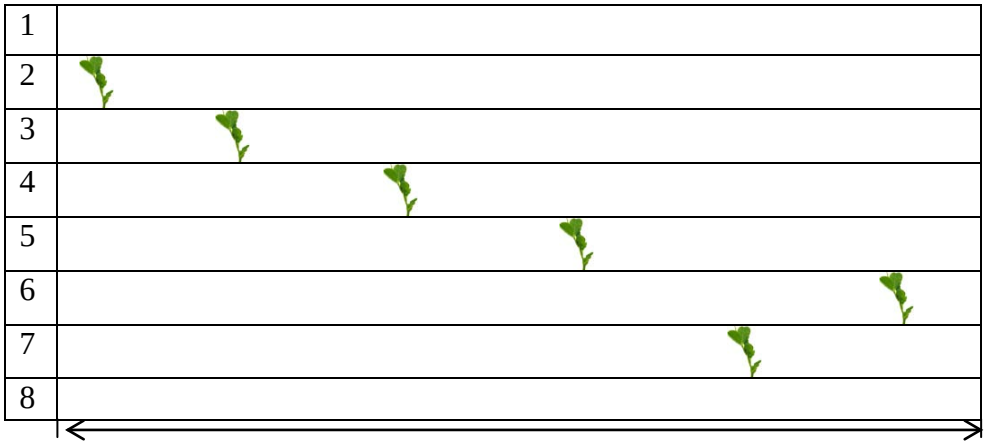

Figure 7.3. Sampling locations within a subplot.

chlorophyll content of the 1 m^2 sampling area. Total 45 data points were obtained from cotton and soybean fields, respectively. FieldSpec hyperspectral data also were collected at each sampling location. By holding it at a height of 2.5 m above the ground, it scanned approximately 1 m^2 of ground area.

Data Association

A shape file was created with the GPS coordinates of 45 ground sampling locations in ArcGIS 9.3.1 (Esri, Redlands, CA, USA). The regions of interest were selected for cotton and soybean plots by eye and the subset image were exported into ArcGIS too. The ground sampling points were overlaid on the image. The four bands values of the image pixels which were collocated with ground sampling points were extracted to be further analyzed.

Data Analysis

Principal Component Analysis

The image datasets and SPAD data were normalized into the same scale. Then they were combined into a matrix and analyzed with principal component analysis (PCA) to extract features. PCA is a multivariate technique used as a tool for reducing high dimensional data. The information content contained in original variables is projected onto a smaller number of principal components (PCs) which are linear combinations of those variables. The process of PCA returns PCA scores which are the estimated values for each principal component and PCA loadings. The PCA score plot can present the clustering of the data and the PCA loading plot can be used to investigate the

contribution of each variable. PCA was performed using proc PRINCOMP in SAS in which a new principal component was created for each wavelength variable in the original data.

Partial Least Square (PLS) Disciminant Analysis

Partial least square (PLS) is a dimension reduction approach that is coupled with a regression model. In PLS regression, the original independent variables (X) is projected onto a set of latent components (LCs). These latent components perform simultaneous decomposition of $\boldsymbol{X}$ and response variables ($\boldsymbol{Y}$) while explain as much as possible of the covariance between X and Y.

PLS regression is to decompose X and Y using model

$$\boldsymbol{Y}=\boldsymbol{T}\boldsymbol{Q}^{\boldsymbol{T}}+\boldsymbol{F} \qquad (7.\ 1)$$

$$\boldsymbol{X}=\boldsymbol{T}\boldsymbol{P}^{\boldsymbol{T}}+\boldsymbol{E} \qquad (7.\ 2)$$

where $\boldsymbol{T}$ is a matrix giving the latent components for the observations; $\boldsymbol{P}$ and $\boldsymbol{Q}$ are matrices of coefficients and often denoted as ‘X loadings’ and ‘Y loading’, respectively; $\boldsymbol{E}$ and $\boldsymbol{F}$ are matrices of random errors.

To investigate whether the fused imagery and ground hyperpsectral data (1-nm bandwidth, 400 to 1000 nm) could improve the performance of the differentiation between the N treatments, the partial least square was applied on the high dimension hyperspectral dataset and the combined imagery and hyperspectral data for compression. Five measurements were taken from each sub-plot. Thus, the dimension of hyperspectral data was 45 by 601, and the dimension of fused data was 45 by 605. Unlike in similar approaches such as principal components regression, the PLS compresses data by

considering the relationship between the independent variable X (reflectance values) and the response variable Y (treatment level).

Data Fusion

There were six datasets for each crop field, the four wavebands data of the extracted image pixels, SPAD data, and first principal component. Five data of each sub treatment plot were averaged for each dataset. The analysis of variance (ANOVA) test was performed on the data (three treatments with three replicates) to determine the differences among the N treatments. Tukey's HSD (Honestly Significant Difference) was used for multiple comparisons between the treatments.

The DISCRIM procedure in SAS (SAS Institute, Cary, NC) was applied on various numbers of derived PCs and band combinations for classification. The parameters being used to develop discriminant function were pooled covariance matrix and prior probability of the groups. The DISCRIM procedure divides the data into two subsets. One subset was used to develop calibration model and the other is used to validate the model. "One data out" method was used for cross-validation in this procedure. The output matrix provided the misclassification rate of calibration and cross-validation.

Image and FieldSpec Data

A 45 by 4 of image data matrix was combined with a 45 by 601 of FieldSpec data matrix (the spectral range was 400-1000 nm). Dummy variables were assigned artificially as 1, 2, and 3, respectively, to represent control, N1 and N2 treatments. There

were 15 measurements for each class level (treatment). The derived principal components by PLS need to be applied by linear discriminant analysis in SAS.

RESULTS AND DISCUSSION

Principal Component Analysis

The first principal components explained 58% and 66% of all variability in the combined image and SPAD data of cotton and soybean, respectively. Although the percentage of explained by the first PCs were not high, the first PCs were further analyzed by ANOVA tests.

ANOVA Tests

ANOVA tests were performed to verify whether the differences among treatments were statistically significant for six datasets, which were the image data of Blue, Green, Red and NIR wavebands, SPAD data, and derived first principal components. Table 7.1 shows the ANOVA table testing the equality of means for each dataset of cotton. None of the Blue, Green, Red, NIR and SPAD data had significant *F* values, which meant all these datasets were equal for the treatments. Only the first principal component derived from data fusion of the image and SPAD data had significant *F* values at significant level 0.05, indicating that the differences did exist among N treatments Although the block effect was only significant for SPAD data, the block was kept in the models. Table 7.2 gives the results of Tukey's HSD multiple comparisons for PC, for which significant *F* value was found. However, the difference between control and the N treatment of 70 kg N ha^{-1} could not be detected.

Table 7.1 Summary of analysis of variance *F* tests for equality of means among N treatments on six datasets for cotton.

Source	DF	Sum of Squares	Mean Squares	F Value	Pr > F
		Blue			
Model	4	0.0161	0.0040	1.47	0.3589
Error	4	0.0110	0.0027		
Corrected Total	8	0.0271			
		Green			
Model	4	0.0085	0.0021	1.4	0.3762
Error	4	0.0061	0.0015		
Corrected Total	8	0.0146			
		Red			
Model	4	0.0336	0.0084	5.83	0.058
Error	4	0.0058	0.0014		
Corrected Total	8	0.0393			
		NIR			
Model	4	0.0376	0.0094	5.25	0.0685
Error	4	0.0072	0.0018		
Corrected Total	8	0.0448			
		SPAD			
Model	4	0.0107	0.0027	6.26	0.0517
Error	4	0.0017	0.0004		
Corrected Total	8	0.0124			
		PC1			
Model	4	0.0831	0.0208	8.53	0.0307*
Error	4	0.0097	0.0024		
Corrected Total	8	0.0928			

*significant at $\alpha = 0.05$ level

Table 7.2. Summary of multiple comparisons on PC1.

Dependent Variable	Mean Treatment	Difference	P-value
PC1	Control vs. N1	-0.060	0.2624
	Control vs. N2	0.14	0.0355*
	N1 vs. N2	0.20	0.0115*

*significant at $\alpha = 0.05$ level

Table 7.3 reports the results of ANOVA test on the datasets for soybean. The Blue, Green, NIR and SPAD data had non-significant *F* values, which meant all these datasets were equal for the treatments. The Red and first principal component were able to detect the treatment differences at the significant level 0.1. However, the first principal component derived from the image and SPAD data did not have better performance than the Red dataset alone.

Table 7.3. Summary of analysis of variance *F* tests for equality of means among N treatments on six datasets for soybean.

Source	DF	Sum of Squares	Mean Squares	F Value	Pr > F
		Blue			
Model	4	0.028	0.0069	2.98	0.1575
Error	4	0.009	0.0023		
Corrected Total	8	0.037			
		Green			
Model	4	0.029	0.007	2.5	0.1981
Error	4	0.012	0.003		
Corrected Total	8	0.041			
		Red			
Model	4	0.056	0.014	5.45	0.0647·
Error	4	0.011	0.0026		
Corrected Total	8	0.067			
		NIR			
Model	4	0.023	0.006	1.86	0.2809
Error	4	0.012	0.003		
Corrected Total	8	0.035			
		SPAD			
Model	4	0.015	0.004	1.59	0.3313
Error	4	0.010	0.002		
Corrected Total	8	0.025			
		PC1			
Model	4	0.110	0.028	4.58	0.085·
Error	4	0.024	0.006		
Corrected Total	8	0.134			

·Significant at $\alpha = 0.1$ level

Table 7.4 shows the multiple comparisons results on the Red and first PC. Neither of them was able to differentiate the treatment N1 from N2.

Table 7.4. Summary of multiple comparisons on soybean.

Dependent Variable	Mean Treatment	Difference	P-value
Red	Control vs. N1	-0.18	0.0120*
	Control vs. N2	-0.12	0.0435*
	N1 vs. N2	0.06	0.2191
PC1	Control vs. N1	-0.22	0.0273*
	Control vs. N2	-0.21	0.0289*
	N1 vs. N2	0.0037	0.9557

*significant at $\alpha = 0.05$ level

The result indicates that the ground SPAD data did not have any contribution in the data fusion procedure.

Discrimination of N Treatments

Table 7.5 gives the proportion of variation explained by each principal component in dependent variables X and dependent variable Y for FieldSpec hyperspectral dataset and the fused imagery and hyperspectral dataset for cotton and soybean. According to the percentages of the explained variation in Y by principal components, nine to twenty PCs were chosen for classification since they accounted for about 90 %, 95 % and 99.8 % of the variance in Y.

Table 7.5. Summary of PLS applied on FieldSpec hyperspectral data and fused imagery and hyperspectral data.

Data Source	No. of PCs	Explained variation in X (%)	Explained variation in Y (%)
		Cotton	
FieldSpec	9	99.94	89.41
	12	99.96	96.74
	20	99.99	99.83
FieldSpec+Image	10	99.92	90.47
	13	99.96	96.28
	20	99.98	99.62
		Soybean	
FieldSpec	10	99.82	91.53
	13	99.90	96.26
	20	99.98	99.78
	9	99.74	89.77
FieldSpec+Image	12	99.85	95.09
	20	99.97	99.72

The classification results are reported in Table 7.6. The results show both the FieldSpec hyperspectral data and the fused imagery and hyperspectral data were able to detect differences between different N treatment levels with different numbers of PCs in calibration step in DISCRIM procedure. The classification accuracy was 100 %. However, using imagery alone, the classification accuracy was only 77.8 % and 82.2 % for different N treatment levels on cotton and soybean, respectively. In cross-validation step, both FieldSpec and fused datasets reduced the misclassification rate compared to that of imagery.

The fused data set did not have better performance than FieldSpec data for classification on N treatment levels on cotton; but it did for soybean with only 6.6 % misclassification rate in cross-validation step.

Table 7.6. Summary of misclassification matrices obtained from DISCRIM procedure (%) for cotton and soybean.

Data Source	No. of PCs	Calibration (%)	Cross-Validation (%)
		Cotton	
Image		22.2	42.2
FieldSpec	9	0	15.6
	10	0	17.8
	20	0	11.1
FieldSpec+Image	9	0	22.2
	10	0	26.7
	13	0	40
	20	0	37.8
		Soybean	
Image		17.8	31.1
FieldSpec	10	0	20
	13	0	44.4
	20	0	13.3
FieldSpec+Image	9	0	24.4
	12	0	35.6
	20	0	6.7

Discrimination of N vs. No N Treatments

Beside the discrimination on three N treatment levels, the classification also was applied on two treatment levels, which were crop with N treatment and without N treatment. Table 7.7 indicates the results. Again, by imagery alone, the misclassification rate was 17.8 % and 15.6 % for cotton and soybean in calibration, respectively. Both

FieldSpec hyperspectral data and fused imagery and hyperspectral data were capable of detecting differences between N and without N treatment in calibration. The fused dataset improved the classification accuracy for N treatment on soybean than FieldSpec dataset. With 10 PCs derived by PLS, the classification accuracy in both calibration and cross-validation steps were 100 %; while FieldSpec dataset still had 2.2 % error rate in cross-validation.

Table 7.7. Summary of misclassification matrices obtained from DISCRIM procedure (%) for N vs. No N. treatment on cotton and soybean.

Data Source	No. of PCs	Calibration (%)	Cross-Validation (%)
		Cotton	
Image		17.8	33.3
FieldSpec	8	0	0
	10	0	4
	20	0	3.3
FieldSpec+Image	9	0	4.4
	12	0	8.9
	20	0	33.3
		Soybean	
Image		15.6	20
FieldSpec	10	0	2.2
	13	0	2.2
	20	0	33.3
FieldSpec+Image	10	0	0
	13	0	4.4
	20	0	33.3

These two procedures of multisensor data fusion were both applied at data level. It combines raw data from different sensors, in our case, multispectral camera (four

sensors) and spectroradiometer (512 detector array). Not only was the multisensor data fusion procedure performed with multiple sensors, but also the fusion process involved with the sensors from different platforms. Aforementioned, the advantage of raw data identity fusion provides the most accurate results only if with proper sensor association and alignment. Although the consistent results were not found for the fused data to detect different N treatment levels on cotton or soybean, no matter ANOVA test on fused data of imagery and SPAD chlorophyll meter readings, or discriminant analysis on fused data of imagery and FieldSpec hyperspectral data, the fused data did have better performance than two original datasets as expected.

A few factors that need to pay more attention during the data fusion process are discussed as follows:

1. The quality of airborne multispectral imagery. The aerial images need to be taken in clear atmospheric conditions, such as cloud free; around noon time; and with high spatial resolution. During the period of image being taken, in situ ground truth spectral reflectance measurements need to be collected with a spectroradiomter. The ground truth measurements can be used to convert the digital number of image pixel into reflectance data.

2. Geometric correction of imagery. Remote sensing systems without stabilization equipment will introduce some geometric error into the remote sensing dataset through variations in roll, pitch, and yaw (Jensen, 2005). The geometric distortion can be corrected using a set of ground control points (GCP). A ground control point is a location on the ground surface that can be identified on the imagery and

located accurately on a map. There are two types of geometric correction, image-to-map rectification and image-to-image rectification. The study site was a poorly mapped region. Global positioning system (GPS) collection of map coordinate information to be used for image rectification is especially effective in this kind of region (Jensen, 2005). A sub-meter GPS unit needs to be used to collect at least 20 GCPs around the study area. The total root mean square error (RMSE) of all ground control points needs to be minimized, in this case, 1 pixel (1 m).

3. Ground data and imagery pixel association. The spatial coordinates of sampling locations within field should be recorded with a differential GPS unit with high accuracy, meter or sub-meter. Around each sampling point, a 1 m^2 square of ground area was marked. Leaf chlorophyll content needs to be taken from all the plants within the 1 m^2 area with SPAD chlorophyll meter to get an average value for the location. FieldSpec should be held at the height of 2.5 m to scan about 1 m^2 spot size on the ground. The size of image pixel should be resampled to 1 m also. All the ground data need to be collected within one hour when the image was taken.

CONCLUSIONS

In this study, the potential of multisensor fusion of ground-based and airborne imagery data was investigated for detecting nitrogen status on cotton and soybean crops. The multispectral imagery was acquired by an airborne imaging system over crop field; at the same period, leaf chlorophyll content and spectral reflectance measurements were gathered with SPAD 502 chlorophyll meter and FieldSpec spectroradiometer at canopy level on the ground. Three datasets were preprocessed individually. Then the image

pixels were associated with ground sampling location according to their spatial coordinates. The raw data of imagery and SPAD meter readings, imagery and FieldSpec hyperspectral reflectance measurements were combined. Principal component analysis was applied on the combination of imagery and SPAD data for fusion. Partial least square compression technique was carried out on the combination of imagery and Fieldspec hyperspectral data to reduce the dimension of data and extract features.

The results of analysis of variance on imagery, SPAD meter readings, and fused data of them showed that extracted first principal component was able to detect the difference among different nitrogen treatment levels for cotton at the significant level of 0.05 (*p-value* = 0.0307). The results of discriminant analyses on imagery, FieldSpec hyperpectral reflectance data, and fused data with them indicated that the classification accuracy of fused data to detect the difference between N treatment and without N treatment on soybean was 100 % in both calibration and cross-validation steps with DISCRIM procedure in SAS. Fused data had better performance than the imagery for discrimination analysis.

Further research may be conducted to improve the performance of data fusion by using non-parametric classification models, such as neural network. The method may be extended to other types of data, and the data fusion can be performed at feature or decision level.

CHAPTER VIII

CONCLUSIONS AND SUMMARY

The overall goal of this dissertation was to evaluate the performances of optical sensors and instruments which were carried on both ground-based and airborne platforms for monitoring crop or vegetation growing status. Six individual studies addressed several aspects of applying remote sensing technology for agricultural applications. The major conclusions regarding these studies are as follows:

1. a). The proposed integrated sensor and instrumentation system was able to gather spectral information by various sensors simultaneously at ground level. The collected spectral information was real-time, multi-source, multi-form, and crop related data.

   b). Spectral reflectance, NDVI, multispectral image, and crop height data showed good repeatability of measurements.

2. a). Ground-based hyperspectral data was able to distinguish four agricultural crops, cotton, corn, soybean, and sorghum at their different growth stages of development.

   b). Selected narrowbands which carried significant information on the discrimination of crop types were between 548-556 nm, 679-682 nm, 756-764 nm, and 928-940 nm.

c). Using the first derivative of the spectral reflectance, the red-edge position of cotton crop was found at the shorter wavelength than those of other crops. The red-edge position of cotton, soybean and sorghum shifted to longer wavelength with later crop development.

3. a). Ground-based remote sensing was a promising tool for evaluating glyphosate herbicide applied using agricultural aircraft fitted with different aerial nozzle technologies.

   b). Spectral reflectance data showed that all the glyphosate treatments provided effective weed control as compared to untreated check areas at day 17 after treatments were applied.

   c). Based on hyperspectral data, conventional flat-fan nozzles and rotary atomizers had better performance than the electrostatic nozzles with charging off.

   d). No evidence showed that the electrostatic nozzles with charging on performed better than the electrostatic nozzles with charging off.

   e). Glyphosate herbicidal efficacy under different aerial spray treatments could be differentiated from spectral response over visible regions of the spectrum.

4. Spatial structure of canopy NDVI was characterized by variogram analysis with different sampling density. It was possible to decrease data density without influencing the field's NDVI spatial structure.

5. The analyses of variograms computed on various sample sizes taken from a multispectral image were conducted. Half size of the subset image data was enough to reliably estimate the variogram for NIR and Red wavebands data.

6. a). Data level multisensor data fusion was applied to combine the chlorophyll meter readings and airborne imagery; and hyperspectral data and airborne imagery, to achieve better performance on crop nitrogen status detection compared to using single sensor alone.

   b). None of individual multispectral wavebands and chlorophyll readings was able to detect different nitrogen treatments. However, first principal component derived from combined chlorophyll readings and airborne imagery was able to detect the difference among different nitrogen treatment level for cotton crop at the significant level of 0.05 (*p-value* = 0.0307).

   c). Multisensor data fusion of hyperspectral data and imagery indicated that the classification accuracy with fused data to detect the difference between nitrogen treatment and without nitrogen treatment on soybean crop was 100 % in both calibration and cross-validation steps with DISCRIM procedure in SAS. Fused data had better performance on crop nitrogen status detection than single sensor data alone.

REFERENCES

Akaike, H. 1973. Information theory and an extension of maximum likelihood principle. In: *Second International Symposium on Information Theory* (Eds. B. N. Petrov and F. Coaki). 267-281. Akademia Kiado, Budapest.

Ahlrichs, J. S., and M. E. Bauer. 1983. Relation of agronomic and multispectral reflectance characteristics of spring wheat canopies. *Agron. J.* 75: 987-993.

Aparicio, N., D. Villegas, J. L. Araus, J. Casades´us, and C. Royo. 2002. Relationship between growth traits and spectral vegetation indices in durum wheat. *Crop Sci.* 42:1547–1555.

Atkinson, P. M., and D. R. Emery. 1999. Exploring the relation between spatial structure and wavelength: Implications for sampling reflectance in the field. *Int'l J.Remote Sens.* 20(13): 2663-2678.

Atkinson, P. M., and P. J. Curran. 1995. Defining an optimal size of support for remote sensing investigations. *Geosci. & Remote Sens. IEEE Trans.* 33(3): 768-776.

Bechtel, A., W. Puttmann, T. N. Carlson, and D. A. Ripley. 1997. On the relation between NDVI, fractional vegetation cover, and leaf area index. *Remote Sens. Environ.* 62(3): 241-252.

Blackmer, T. M., J. S. Schepers, and C. E. Varvel. 1994. Light reflectance compared With other nitrogen stress measurements in corn leaves. *Agron. J.* 86: 934-938.

Boegh, E., H. Soegaard, N. Broge, C. B. Hasager, N. O. Jensen, K. Schelde, and A. Thomsen. (2002). Airborne multispectral data for quantifying leaf area index, nitrogen concentration, and photosynthetic efficiency in agriculture. *Remote Sens. Environ.* 81(2-3): 179-193.

Bouse, L. F., S. G. Whisenant, and J. B. Carlton.1992. Aerial spray deposition on mesquite. *Trans. ASAE* 35:51-59.

Bravo, C., D. Moshou, R. Oberti, J. West, A. McCartney, L. Bodria, and H. Ramon. 2004. Foliar disease detection in the field using optical sensor fusion. A*gri. Eng. Int'l: The CIGR EJournal.* Manuscript FP 04 008, Vol. VI.

Bronson, K. F., J. D. Booker, W. J. Keeling, R. K. Boman, T. A. Wheeler, R. J. Lascano, and R. L. Nichols. 2005. Cotton canopy reflectance at landscape scale as affected by nitrogen fertilization. *Agron. J.* 97(3): 654-660.

Brus, D. J., and J. De Gruijter. Estimation on non-ergodic variograms and their sampling variance by design-based sampling strategies. *Mathematical Geology* 26(4): 437-454.

Cambardella, C. A., and D. L. Karlen. 1999. Spatial analysis of soil fertility parameters. *Precision Agri.* 1: 5-14.

Castro-Esau, K. L., G. A. Sanchez-Azofeifa, and B. Rivard. 2006. Comparison of spectral indices obtained using multiple spectroradiometers. *Remote Sens. Environ.* 103:276-288.

Cohen, W. B., T. A. Spies, and G. A. Bradshaw. 1990. Semivariograms of digital imagery for analysis of conifer canopy structure. *Remote Sens. Environ.* 34(3): 167-178.

Cressie, N.A.C. 1993. *Statistics for Spatial Data.* New York: John Wiley & Sons.

Curran, P. J. 1988. The semivariogram in remote sensing: An introduction. *Remote Sens. Environ.* 24(3): 493-507.

Curran, P. J. 1989. Remote sensing of foliar chemistry. *Remote Sens. Environ.* 30: 271-278.

Curran, P. J., and P. M. Atkinson. 1998. Geostatistics and remote sensing. *Prog. in Physi. Geography* 22(1): 61-78.

Curran, P. J., J. L. Dungan, B. A. Macler, and S. E. Plummer. 1991. The effect of a red leaf pigment on the relationship between red edge and chlorophyll concentration. *Remote Sens. Environ.* 35(1): 69–76.

Danson, F. M., and S. E. Plummer. 1995. Red edge response to forest leaf area index. *Int'l J. Remote Sens.* 16 (1): 183–188.

Darvishzadeh, R., A. Skidmore, M. Schlerf, C. Atzberger, F. Corsi, and M. Cho. 2008. LAI and chlorophyll estimation for a heterogeneous grassland using hyperspectral measurements. *ISPRS J. Photogrammetry & Remote Sens.* 63(4): 409- 426.

Demetriades-Shah, T., M. D. Steven, and J. A. Clark. 1990. High resolution derivative spectra in remote sensing. *Remote Sens. Environ.* 33: 55-64.

Dobermann, A., and J. L. Ping. 2004. Geostatistical integration of yield monitor data and remote sensing improves yield maps. *Agron J.* 96: 285-297.

Dwyer, L. M., M. Tollenaar, and L. Houwing. 1991. A nondestructive method to monitor leaf greenness in corn. *Can. J. Plant Sci.* 71: 505–509.

El-Shikha, D. M., P. Waller, D. Hunsaker, T. Clarke, and E. Barnes. 2007. Ground-based remote sensing for assessing water and nitrogen status of broccoli. *Agri. Water Management* 92: 183-193.

Fillella, I., and J. Peñuelas. 1994. The red edge position and shape as indicators of plant chlorophyll content, biomass and hydric status. *Int'l J. Remote Sens.* 15(7): 1459-1470.

Flynn, S. E., C. T. Dougherty, and O. Wendroth. 2008. Assessment of pasture biomass with the normalized difference vegetation index from active ground-Based sensors. *Agron. J.* 100(1): 114-121.

Freeman, K. W., K. Girma, D. B. Arnall, R. W. Mullen, K. L. Martin, R. K. Teal, and W. R. Raun. 2007. By-plant prediction of corn forage biomass and nitrogen uptake at various growth stages using remote sensing and plant height. *Agron. J.* 99(2): 530-536.

Fritschi, F. B., and J. D. Ray. 2007. Soybean leaf nitrogen, chlorophyll content, and chlorophyll a/b ratio. *Photosynthetica* 45(1): 92-98.

Gascuel-Odoux, C., and P. Boivin. 1994. Variability of variograms and spatial estimates due to soil sampling: a case study. *Geoderma* 62: 165-182.

Ge, Y., J. A. Thomasson, C. L. Morgan, S. W. Searcy. 2007. VNIR diffuse reflectance spectroscopy for agricultural soil determination based on regression-kriging. *Trans. ASABE* 50: 1081-1092.

Ge, Y., J. A. Thomasson, R. Sui, C. L. Morgan, S. W. Searcy, C. B. Parnell. 2008. Spatial variation of fiber quality and associated loan rate in a dryland cotton field. *Precision Agri.* 9: 181-194.

Goel, P. K., S. O. Prasher, J. A. Landry, R. M. Patel, R. B. Bonnell, A. A. Viau, and J. R. Miller. 2003a. Potential of airborne hyperspectral remote sensing to detect nitrogen deficiency and weed infestation in corn. *Comput. & Electron. Agri.* 38(2):99-124.

Goel, P. K., S. O. Prasher, J. A. Landry, R. M. Patel, and A. A. Viau. 2003b. Estimation

of crop biophysical parameters through airborne and field hyperspectral remote sensing. *Trans. ASAE* 46(4): 1235–1246.

Gray, C. J., D. R. Shaw, and L. M. Bruce. 2009. Utility of hyperspectral reflectance for differentiating soybean (*Glycine max*) and six weed species. *Weed Technol*. 23: 108 -119.

Haboudane, D., J. R. Miller, N. Tremblay, P. J. Zarco-Tejada, and L. Dextraze. 2002. Integrated narrow-band vegetation indices for prediction of crop chlorophyll content for application to precision agriculture. *Remote Sens. Environ.* 81(2): 416-426.

Hall, D., and J. Llinas. 1997. An introduction to multisensory data fusion. *Proceedings of the IEEE* 85(1): 6-23.

Hall, D.L., and S.A.H. McMullen. 2004. *Mathematical Techniques in Multi-sensor Data Fusion* (2nd ed). Boston: Artech House.

Han, S., L. L. Hendrickson, and B. Ni. 2002. Comparison of satellite and aerial imagery for detecting leaf chlorophyll content in corn. *Trans. ASABE.* 45(4): 1229–1236.

Hengl, T. G., B. M. Heuvelink, and A. Stein. 2004. A generic framework for spatial prediction of soil variables based on regression-kriging. *Geoderma.* 120: 75-93.

Heisel, T., C. Andersen, and A.K. Ersboll. 1996. Annual weed distributions can be mapped with kriging. *Weed Research*. 36: 325-337.

Hoffmann, W. C., P. S. Lingren, J. R. Coppedge, and I. W. Kirk. 1998. Application parameter effects on efficacy of a semiochemical-based insecticide. *Applied Eng. Agric*. 14: 459-463.

Horler, D. N. H., M. Dockray, and J. Barber. 1983. The red edge of plant leaf reflectance. *Int'l J. Remote Sens.* 4: 273–288.

Huang, Y., Y. Lan, and W. C. Hoffmann. 2008. Use of airborne multi-spectral imagery in pest management systems. *Agri. Eng. Int'l: The CIGR Ejournal*. Manuscript IT 07010. Vol. X. February.

Huang, Y., S. J. Thomson, Y. Lan, and S. J. Maas. 2009. Multispectral imaging system for Airborne remote sensing to support site-specific agricultural management. In: Proceedings of the 3rd Asian Conference on Precision Agriculture (ACPA), Beijing, China, 14–17 October, 2009.

Inoue, Y., S. Morinaga, and A. Tomita. 2000. A blimp–based remote sensing system for

low–altitude monitoring of plant variables: A preliminary experiment for agriculture and ecological applications. *Int'l J. Remote Sens.* 21(2): 379–385.

Iqbal, J., J. A. Thomasson, J. N. Jenkins, P. O. Owens, F. D. Whisler. 2005. Spatial variability of soil physical properties of alluvial soils. *Soil Sci. Soc. Am. J.* 69: 1338-1350.

Jensen, J. R. 2005. *Introductory Digital Image Processing: A Remote Sensing Perspective* (3rd ed). New York: Pearson Prentice Hall.

Johnson, R. M., and E. P. Richard, Jr. 2005. Sugarcane yield, sugarcane quality, and soil variability in Louisiana. *Agron. J.* 97: 760-771.

Jones, C. L., P. R. Weckler, N. O. Maness, R. Jayasekara, M. L. Stone, and D. Chrz. 2007. Remote sensing to estimate chlorophyll concentration in spinach using multi-spectral plant reflectance. *Trans. ASAE* 50(6): 2267-2273.

Jones, C. L., N. O. Maness, M. L. Stone, R. Jayasekara, M. L. Stone, and D. Chrz. 2007. Chlorophyll estimation using multispectral reflectance and height sensing. *Trans. ASABE* 50(5): 1867-1872.

Jordan, T. N. 1981. Effects of diluents volumes and surfactants on the phytotoxicity of glyphosate to bermudagrass. *Weed Sci.* 29: 79–83.

Jupp, D. L. B., A. H. Strahler, and C. E. Woodcock. 1988a. Autocorrelation and regularization in digital images. I. Basic theory. *Geosci. & Remote Sens., IEEE Trans.* 26(4): 463-473.

Jupp, D. L. B., A. H. Strahler, and C. E. Woodcock. 1988b. Autocorrelation and regularization in digital images. II. Simple image models. *Geosci. & Remote Sens. IEEE Trans.* 27: 247-258.

Kaleita, A. (2003). Fusion of remotely sensed imagery and minimal ground sampling for soil moisture mapping. ASABE Paper No. 061137. Portland, OR.: ASABE.

Kataoka, T., H. Okamoto, T. Kaneko, and S. Hata. 2002. Performance of crop height sensing using ultra sonic sensor and laser beam sensor. ASAE Paper No. 021184. Chicago, IL.: ASABE.

Kerry, R., and M.A. Oliver. 2007. Comparing sampling needs for variograms of soil properties computed by the methods of moments and residual maximum likelihood. *Geoderma.* 140: 383–396.

Klein., L. A. 2004. *Sensor and Data Fusion: A Tool for Information Assessment and*

Decision Making. Bellingham, Washington: SPIE Press.

Kirk, I. W. 2007. Measurement and prediction of atomization parameters from fixed-wing aircraft spray nozzles. *Trans. ASABE* 50(3): 693-703.

Kirk, I. W., L. F. Bouse, J. B. Carlton, E. Frans, and R. A. Stermer.1992. Aerial spray deposition in cotton. *Trans. ASAE* 35: 1393-1399.

Kirk, I. W., J. F. Esquivel, D. J. Porteous, and W. H. Hendrix. 1998. Aerial application of tracer to control bollworm/budworm in cotton. *Down to Earth* 53: 13-17.

Kirk, I. W., W. C. Hoffmann, and J. B. Carlton. 2001. Aerial electrostatic spray system performance. *Trans. ASAE* 44: 1089-1092.

Koger, C. H., L. M. Bruce, D. R. Shaw, and K. N. Reddy. 2003. Wavelet analysis of hyperspectral reflectance data for detecting pitted morningglory (*Ipomoea lacunosa*) in soybean (*Glycine max*). *Remote Sens. Environ.* 86 (1): 108-119.

Kravchenko, A. N., and D. G. Bullock. 2002. Spatial variability of soybean quality data as a function of field topography: I. Spatial data analysis. *Crop Sci.* 42: 804-815.

Lamb, D. W. and R. B. Brown. 2001. Remote-sensing and mapping of weeds in crops, a Review. *J. Agric. Eng. Research* 78(2): 117-125.

Lan, Y., Y. Huang, D. E. Martin, and W. C. Hoffmann. 2007a. Crop pest management with an aerial imaging system. ASABE Paper No. AA07-005. Reno, NV.: ASABE

Lan, Y., Y. Huang, and W. C. Hoffmann. 2007b. Airborne multispectral remote sensing with ground truth for areawide pest management. ASABE Paper No. 07-3004. Minneapolis, MN.: ASABE.

Lan, Y., Y. Huang, D. E. Martin, and W. C. Hoffmann. 2009a. Development of an airborne remote sensing system for crop pest management: system integration and verification. *Trans. ASABE* 25 (4): 607–615.

Lan, Y., H. Zhang, R. Lacey, W. C. Hoffmann, and W. Wu. 2009b. Development of an integrated sensor and instrumentation system for measuring crop conditions. *Agric. Eng. Int'l: The CIGR EJournal.* Manuscript IT 08 1115. Vol. XI. April.

Lark, R. M. 2000. Estimating variograms of soil properties by the method-of-moments and maximum likelihood. *Eur. J. Soil Sci*. 51: 717-728.

Latheef, M. A., J. B. Carlton, I. K. Kirk, and W. C. Hoffmann. 2009. Aerial electrostatic-

charged sprays for deposition and efficacy against sweet potato whitefly (*Bemisia tabaci*) on cotton. *Pest Management Sci.* 65 (7): 744-752.

Laudien, R, G. Bareth, and R. Doluschitz. 2003. Analysis of hyperspectral field data for detection of sugar beet diseases. In Proceedings 4th Conference of the European Federation for Information Technology in Agriculture, Food and the Environment, pp. 375-381, Debrecen, Hungary.

Lee, K. S., W. B. Cohen, R. E. Kennedy, T. K. Maiersperger, and S. T. Gower. 2004 Hyperspectral versus multispectral data for estimating leaf area index in four different biomes. *Remote Sens. Environ.* 91(3-4): 508–520.

Legg, B. J., and J. V. Stafford. 1998. Precision agriculture-new technologies. In Proceedings of the Brighton Crop Protection Conference-Pest and Disease. pp. 1143-1150. Farnham, UK: British Crop Protection Council.

Lemon, R., R. Boman, M. McFarland, B. Bean, T. Provin, and F. Hons. 2009. Nitrogen management in cotton. Available at: http://lubbock.tamu.edu/cotton/pdf/NitrogenManagementCottonSCS-2009-2.pdf. Accessed 22 September 2010.

Leon, C. T., D. R. Shaw, M. S. Cox, M. J. Abshire, B. Ward, and M. C. Wardlaw. 2003. Utility of remote sensing in predicting crop and soil characteristics. *Precision Agric.* 4: 359–384.

Madeira, A. C., A. Mendonca, M. E. Ferreira, and M. Taborda. 2000. Relationship between spectroradiometric and chlorophyll measurements in green beans. *Comm. Soil Sci. Plant Anal.* 31(5-6): 631-643.

Martin, K. L., P. J. Hodgen, K. W. Freeman, R. Melchiori, D. B. Arnall, R. K. Teal, R. W. Mullen, K. Desta, S. B. Phillips, J. B. Solie, M. L. Stone, O. Caviglia, F. Solari, A. Bianchini, D. D. Francis, J. S. Schepers, J. L. Hatfield, and W. R. Raun. 2005. Plant-to-Plant variability in corn production. *Agron. J.* 97(6): 1603-1611.

Martin, K. L., K. Girma, K. W. Freeman, R. K. Teal, B. Tubafia, D. B. Arnall, B. Chung, O. Walsh, J. B. Solie, M .J. Stone, and W. R. Raun. 2007. Expression of variability in corn as influenced by growth stage using optical sensor measurements. *Agron. J.* 99(2): 384-389.

Matheron, G. 1963. Principles of geostatistics. *Economic Geology* 58(8): 1246-1266.

Matheron, G. 1965. Les variables re´gionalise´es et leur estimation: une application de la the´orie defonctions ale´atoires aux sciences de la nature. Paris: Masson et Cie,

1965.

Miao, Y., D. J. Mulla, and P. C. Robert. 2006. Spatial variability of soil properties, corn quality and yield in two Illinois, USA fields: implications for precision corn management. *Precision Agri.* 7: 5-20.

Muhammed, H. H. 2005. Hyperspectral crop reflectance data for characterizing and estimating fungal disease severity in wheat. *Biosyst. Eng.* 91(1): 9-20.

Mutanga, O., and A. K. Skidmore. 2007. Red edge shift and biochemical content in grass canopies. *ISPRS J. Photogrammetry & Remote Sens.* 62(1): 34- 42.

Nowak, P. 1997. A sociological analysis of site-specific management. In: The State of Site-specific Management for Agriculture. Am. Soc. Agron. Miscellaneous publication, pp. 397-422, Madison, WI.

Oliver, M. A., and R. Webster. 1991. How geostatistics can help you. *Soil Use & Management* 7(14): 206-217.

Oliver, M. A., and R. Webster, and K. Slocum. 2000. Filtering SPOT imagery by kriging analysis. *Int'l J. Remote Sens.* 21(4): 735-752.

Osborne, S. L., J. S., Schepers, D. D. Francis, and M. R. Schlemmer. 2002. Detection of phosphorus and nitrogen deficiencies in corn using spectral radiance measurements. *Agron. J.* 94: 1215-1221.

Panagopoulos, T., J. Jesus, M. D.C. Antunes, and J. Beltrão. 2006. Analysis of spatial interpolation for optimizing management of a salinized field cultivated with lettuce. *Eur. J. Agron.* 24: 1-10.

Plant, R. E. 2001. Site-specific management: the application of information technology to crop production. *Comput. & Electron. Agri.* 30: 9-29.

Plant, R. E., D. S. Munk, B. R. Robert, R. L. Vargas, D. W. Rains, R. L. Travis, and R. B. Hutmacher. 2000. Relationships between remotely sensed reflectance data and cotton growth and yield. *Trans. ASAE*. 43(3):535–546.

Railyan, V. Y., and R. M. Korobov. 1993. Red edge structure of canopy reflectance spectra of triticale. *Remote Sens. Environ*. 46(2): 173-182.

Reyniers, M., E. Vrindts, and J.D. Baerdemaeker. 2006. Comparison of an aerial-based system and an on the ground continuous measuring device to predict yield of winter wheat. *Eur. J. Agron.* 24: 87-94.

Rouse, J. W., R. H. Haas, J. A. Schell, and D. W. Deering. 1973. Monitoring vegetation systems in the Great Plains with ERTS. *Third ERTS Symposium*, NASA SP-351 I, 309-317.

SAS. 2004. *Base SAS® 9.1 Procedure Guide: Statistics*. Cary, N.C.: SAS Institute, Inc.

Scotford, I. M., and P. C. H. Miller. 2004. Combination of spectral reflectance and ultrasonic sensing to monitor the growth of winter wheat. *Biosyst. Eng.* 87(1): 27- 38.

Sembiring, H, W. R. Raun, G. V. Johnson, M. L. Stone, J. B. Solie, and S. B. Phillips. 1998. Detection of nitrogen and phosphorus nutrient status in winter wheat using spectral radiance. *J. Plant Nutrition*. 21(6): 1207-1232.

Serrano, L., I. Filella, and J. Penuelas. 2000. Remote sensing of biomass and yield of winter wheat under different nitrogen supplies. *Crop Sci.* 40: 723-731.

Shanahan, J. F., J. S. Schepers, D. D. Francis, G. E. Varvel, W. W. Wilhelm, J. M. Tringe, M. R. Schlemmer, and D. J. Major. 2001. Use of remote sensing imagery to estimate corn grain yield. *Agron. J.* 93: 583-589.

Stein, A., J. Brouwer, and J. Bouma. 1997. Methods for comparing spatial variability patterns of millet yield and soil data. *Soil Sci. Soc. Am. J.* 61: 861–870.

Stein, A., and L. C. A. Corsten. 1991. Universal kriging and cokriging as a regression procedure. *Biometrics* 47(2): 575-588.

Stein, A., and F. D. Van Der Meer, and B. Gorte. 1999. *Spatial Statistics for Remote Sensing.* The Netherlands: Kluwer Academic Publishers.

Stern, N. 2006. *Stern Review on the Economics of Climate Change.* New York: Cambridge Univeristy Press.

Stewart, C. M., A. B. McBratney, and J. H. Skerritt. 2002. Site-specific durum wheat quality and its relationship to soil properties in a single field in Northern New South Wales. *Precision Agri.* 3(2):155-168.

Taiz, L. and E. Zeiger. 2006. *Plant Physiology* (4th ed). Sunderland, MA: Sinauer Associates, Inc.

Thenkabail, P. S. 2002. Optimal hyperspectral narrowbands for discrimination agricultural crops. *Remote Sens. Review* 20: 257-291.

Thenkabail, P. S., R. B. Smith, and E. De. Pauw. 2000. Hyperspectral vegetation indices and their relationships with agricultural crop characteristics. *Remote Sens. Environ.* 71(2): 158-182.

Thompson, J. A., L. E. Schweitzer, and R. L. Nelson. 1996. Association of specific leaf weight, an estimate of chlorophyll, and chlorophyll content with apparent photosynthesis in soybean. *Photosynth. Res.* 49: 1-10.

Tilling, A. K., G. J. O'Leary, J. G. Ferwerda, S. D. Jones, G. J. Fitzgerald, D. Rodriguez, And R. Belford. 2007. Remote sensing of nitrogen and water stress in wheat. *Field Crop Res.* 104: 77-85.

Tucker, C. J. 1979. Red and photographic infrared linear combinations for monitoring vegetation. *Remote Sens. Environ*. 8 (2): 127-150.

Tumbo, S. D., D. G. Wagner, and P. H. Heinemann. 2002. On-the-go sensing of chlorophyll status in corn. *Trans. ASAE* 45(4): 1207-1215.

Van Meirvenne, M., and G. Hofman. 1991. Sampling strategy for quantitative soil mapping. *Pedology* 41: 263-275.

Walburg, G., M. E. Bauer, C. S. T. Daughtry, and T. L. Housley. 1982. Effects of nitrogen nutrition on growth, yield and reflectance characteristics of corn canopies. *Agron. J.* 74: 677-683.

Webster, R., and M. A. Oliver. 1992. Sample adequately to estimate variogram of soil properties. *J. Soil Sci.* 43: 177-192.

Webster, R., and M. A. Oliver. 2007. *Geostatistics for Environmental Scientists* (2nd ed). Chichester, England: John Wiley & Sons Ltd.

Wolfe, D.W., D.W. Henderson, T. C. Hsiao, and A. Alvino. 1988. Interactive water and nitrogen effects on senescence of maize. II. Photosynthetic decline and longevity of individual leaves. *Agron. J.* 80: 865-870.

Woodcock, C. E., A. H. Strahler, and D. L. B. Jupp. 1988a. The use of variograms in remote sensing: I. Scene models and simulated images. *Remote Sens. Environ.* 25(3): 323-348.

Woodcock C. E., A. H. Strahler, and D. L. B. Jupp. 1988b.The use of variograms in remote sensing: II. Real digital images. *Remote Sens. Environ.* 25(3): 349-379.

Wu, F. B., L. H. Wu, and F. H. Xu. 1998. Chlorophyll meter to predict nitrogen sidedress requirements for short-season cotton (*Gossypium hirsutum* L.). *Field*

Crop Res. 56(3): 309-314.

Xue, L. H., W. X. Cao, W. H. Luo, T. B. Dai, and Y. Zhu. 2004. Monitoring leaf nitrogen status in rice with canopy spectral reflectance. *Agron. J.* 96: 135-142.

Yamagishi, J., T. Nakamoto, and W. Richner. 2003. Stability of spatial variability of wheat and maize biomass in a small field managed under two contrasting tillage systems over 3 years. *Field Crops Research*. 81(2-3): 95-108.

Yang, C. 2010. An airborne four-camera imaging system for agricultural applications. ASABE paper No. 1008855. Pittsburgh, PA, USA.

Yang, C., and J. H. Everitt. 2002. Relationships between yield monitor data and airborne multidate multispectral digital imagery for grain sorghum. *Precision Agri.* 3: 373-388.

Yoder, B. J., and R. E. Pettigrew-Crosby. 1995. Predicting nitrogen and chlorophyll content and concentrations from reflectance spectral (400-2500 nm) at leaf and canopy scales. *Remote Sens. Environ.* 53: 199-211.

Zhang, H., Y. Lan, R. Lacey, H. C. Hoffmann, and J. K. Westbrook. 2009. Spatial analysis of hyperspectral vegetation index. ASABE Paper No. 095982. Reno, NV.: ASABE.

Zhao, D. H., J. L. Li, and J. G. Qi. 2005a. Identification of red and NIR spectral regions and vegetative indices for discrimination of cotton nitrogen stress and growth stage. *Comput. & Electron. Agric*. 48(2): 155-169.

Zhao, D., K. R. Reddy, V. G. Kakani, and V. R. Reddy. 2005b. Nitrogen deficiency effects on plant growth, leaf photosynthesis, and hyperspectral reflectance properties of sorghum. *Eur. J. Agron.* 22(4): 391-403.

VITA

Name:	Huihui Zhang
Address:	2771 F&B Road, College Station, TX 77845 c/o Dr. Yubin Lan
Email Address:	zhh815@tamu.edu
Education:	B.S., Electrical Engineering, Tongji University, Shanghai, China, 1998
	M.S., Electrical Engineering, San Francisco State University, 2005
	Ph.D., Biological and Agricultural Engineering, Texas A&M University, 2010